

## **Pedestrian fundamental diagrams: Comparative analysis of experiments in different geometries**

Jun Zhang





Forschungszentrum Jülich GmbH  
Institute for Advanced Simulation (IAS)  
Jülich Supercomputing Centre (JSC)

# **Pedestrian fundamental diagrams: Comparative analysis of experiments in different geometries**

Jun Zhang

Schriften des Forschungszentrums Jülich

IAS Series

Volume 14

---

ISSN 1868-8489

ISBN 978-3-89336-825-9



Bibliographic information published by the Deutsche Nationalbibliothek.  
The Deutsche Nationalbibliothek lists this publication in the Deutsche  
Nationalbibliografie; detailed bibliographic data are available in the  
Internet at <http://dnb.d-nb.de>.

Publisher and  
Distributor: Forschungszentrum Jülich GmbH  
Zentralbibliothek  
52425 Jülich  
Phone +49 (0) 24 61 61-53 68 · Fax +49 (0) 24 61 61-61 03  
e-mail: [zb-publikation@fz-juelich.de](mailto:zb-publikation@fz-juelich.de)  
Internet: <http://www.fz-juelich.de/zb>

Cover Design: Jülich Supercomputing Centre, Forschungszentrum Jülich GmbH

Printer: Grafische Medien, Forschungszentrum Jülich GmbH

Copyright: Forschungszentrum Jülich 2012

Schriften des Forschungszentrums Jülich  
IAS Series Volume 14

D 468 (Diss., Wuppertal, Univ., 2012)

ISSN 1868-8489  
ISBN 978-3-89336-825-9

The complete volume is freely available on the Internet on the Jülicher Open Access Server (JUWEL) at  
<http://www.fz-juelich.de/zb/juwel>

Persistent Identifier: [urn:nbn:de:0001-2012102405](http://nbn-resolving.org/urn:nbn:de:0001-2012102405)  
Resolving URL: <http://www.persistent-identifier.de/?link=610>

Neither this book nor any part of it may be reproduced or transmitted in any form or by any  
means, electronic or mechanical, including photocopying, microfilming, and recording, or by any  
information storage and retrieval system, without permission in writing from the publisher.

---

## **Abstract**

Over the last few decades, several approaches for modeling of pedestrian traffic have been proposed and developed. However, the existing empirical data are insufficient and have large discrepancies, which makes difficult for the quantitative validation of models, design and safety assessment of facilities.

This thesis mainly analyze the pedestrian fundamental diagram describing the relation between crowd density, velocity and flow based on series of well-controlled laboratory experiments. The second chapter reviews the commonly used fundamental diagrams in handbooks. The differences and influence of them on facility designs are compared. Then the existing empirical studies on pedestrian fundamental diagrams are discussed especially for uni- and bidirectional pedestrian streams.

In the third chapter, the experiment setup and the extraction of the pedestrian trajectories from video recordings are described. Four different measurement methods are taken to calculate the crowd density, velocity and specific flow. Their influences on the fundamental diagram are tested with the data obtained from the experiment of unidirectional flow. For the density ranges achieved in the experiment, minor effects are observed but the Voronoi method is able to resolve a finer structure of the diagram and to reveal a discontinuity.

The fourth chapter deals with the analysis of experiments of uni-, bi-directional and merging flow based on the Voronoi method. The first two experiments were carried out in a straight corridor, whereas the third one were performed in a T-junction. The topographical information for density, velocity and specific flow, from which the boundary effect are observed, are extracted with Voronoi method. The specific concept is applicable to all types of flows in the density ranges observed in the experiments. Surprisingly, no difference is found for the fundamental diagrams of bidirectional flow with different modes of order. However, there is a sharp distinction between the fundamental diagrams of uni- and bidirectional flow. For the merging flow in a T-junction, the fundamental diagrams measured in front and behind the merging show also significant differences.

---

## **Zusammenfassung**

In den letzten Jahrzehnten wurden verschiedene Ansätze zur Modellierung von Fußgängerverkehr entwickelt und vorgeschlagen. Die bestehende Datenbasis ist jedoch unzureichend und weist große Abweichungen auf. Das erschwert die quantitative Validierung von Modellen sowie die Sicherheitsbeurteilung für Rettungswege in Gebäuden.

Schwerpunkt dieser Dissertation ist die Analyse des Fundamentaldiagramms für Fußgänger, welches die Beziehung von Personendichte zu Geschwindigkeit und Personenfluss beschreibt, auf Basis von Experimenten unter Laborbedingungen. Im zweiten Kapitel werden die üblich genutzten Fundamentaldiagramme aus Handbüchern zusammengefasst. Der Einfluss von unterschiedlichen Fundamentaldiagrammen auf die Auslegung von Rettungswegen in Gebäuden wird verglichen. Anschließend werden existierende empirische Studien, insbesondere bezogen auf das Fundamentaldiagramm für uni- und bidirektionale Personenströme, diskutiert.

Das dritte Kapitel beschreibt die durchgeführten Experimente und die Extraktion von Trajektorien aus Videoaufnahmen. Vier verschiedene Messmethoden werden genutzt um Personendichte, Geschwindigkeit und spezifischen Fluss zu berechnen. Deren Einfluss auf das Fundamentaldiagramm wird anhand der Experimente mit unidirektionalem Personenfluss geprüft. Für den in den Experimenten auftretenden Dichtebereich sind nur minimale Unterschiede festzustellen. Die Voronoi Messmethode ermöglicht eine feinere Auflösung wodurch eine Diskontinuität im Fundamentaldiagramm festgestellt werden konnte.

Im vierten Kapitel wird die Analyse der Experimente mit uni-, bidirektionalen und sich vereinigenden Personenströmen anhand der Voronoi Messmethode vorgestellt. Die ersten beiden Experimente wurden in einem geraden Korridor und das dritte Experiment in einer T-Kreuzung durchgeführt. Topographische Informationen von Dichte, Geschwindigkeit und spezifischen Fluss wurden mit der Voronoi Methode ermittelt und veranschaulichen Randeffekte. Das spezifische Fluss Konzept ist für alle Arten von Personenströmen im Dichtebereich der durchgeführten Experimente anwendbar. Überraschender Weise wurden keine Unterschiede für bidirektionalen Personenfluss mit unterschiedlichen Ordnungs-

---

graden festgestellt. Deutlich ist jedoch der Unterschied zwischen dem Fundamentaldiagramm für uni- und bidirektionalen Personenfluss. Die Vereinigung von Personenströmen an einer T-Kreuzung wurde durch Messungen des Fundamentaldiagramms vor und hinter der Vereinigung untersucht. Hier konnten signifikante Unterschiede festgestellt werden.

---

## Acknowledgements

I would like to express my deepest gratitude especially to Prof. Dr. Armin Seyfried for his invaluable support, generous help, kind encouragement throughout the course of my PhD studies at Bergische Universität Wuppertal. During these three years, he always help me kindly not only on my work but also on my daily life in Germany. From him I learned to become more rigorous and patient especially in addressing and resolving scientific problems. Without his consideration and support this work would not have been possible.

I appreciate Univ.-Prof. Dr.-Ing. Wolfram Klingsch and Prof. Weiguo Song in China for offering me the chance to pursuit PhD degree in Germany and giving me suggestions in research. Many thanks Prof. Klingsch for his understanding and support on my work.

I would also thank Prof. Dr. Andreas Schadschneider for important discussions and suggestions on my research. He was always ready for a fruitful discussion and timely feedback. His insights into physics and enthusiasm in academical research helped me to improve the thesis and also to train my scientific literacy.

Special thanks also go to all my colleagues both in Bergische Universität Wuppertal and Jülich Supercomputer centre for their company during my time in Germany, in particular: Many thanks Stefan Holl and Sabine Mehring for their kindly help on the daily affair related to my study and giving me useful advice. Sebastian Burghardt for helping me to deal with daily things both in study and life concerning German. Mike Boltes for developing *PeTrack* which made high precision trajectory-extraction possible; Ulrich Kemloh for helping me to correct the language of my thesis; Mohcine Chraïbi and Jack Liddle for discussing and improving my program for experiment analysis;

Acknowledgements also go to my family and relatives for their understanding and support for my study in Germany, especially when I prepared to apply the Visa at the beginning. Many thanks my girlfriend for her unwavering support and reliance. Many thanks Dr. Jian Ma and Dr. Zhiming Fang for useful discussion and encouragement. I would like to thank all my friends who accompany and care about me these years.

---

I fully acknowledge the support I received from the China Scholarship Council. Any opinion, findings, and conclusions or recommendations expressed in this study are those of the writer and do not necessarily reflect the views of the China Scholarship Council.

# Contents

<b>Declaration</b>	<b>i</b>
<b>Abstract</b>	<b>ii</b>
<b>Zusammenfassung</b>	<b>iii</b>
<b>Acknowledgements</b>	<b>v</b>
<b>List of tables</b>	<b>x</b>
<b>List of figures</b>	<b>xi</b>
<b>1 Introduction</b>	<b>1</b>
1.1 Background . . . . .	1
1.2 Aim and objective . . . . .	4
1.3 Methodology . . . . .	5
1.4 Thesis outline . . . . .	6
<b>2 Literature review on the fundamental diagram</b>	<b>7</b>
2.1 Design of escape routes . . . . .	7
2.1.1 Prescriptive method . . . . .	8
2.1.2 Performance-based method . . . . .	9
2.1.2.1 Handbooks . . . . .	10
2.1.2.2 Simulations . . . . .	22



## CONTENTS

---

2.2	Empirical studies . . . . .	25
<b>3</b>	<b>Experiments and methodology</b>	<b>32</b>
3.1	Experiment setup . . . . .	33
3.1.1	Unidirectional flow in corridor . . . . .	34
3.1.2	Bidirectional flow in corridor . . . . .	36
3.1.3	Merging flows in T-junction . . . . .	40
3.2	Extraction of pedestrian trajectories . . . . .	41
3.2.1	Extraction method . . . . .	41
3.2.2	Trajectories . . . . .	43
3.3	Measurement methodology . . . . .	47
3.3.1	Method A . . . . .	48
3.3.2	Method B . . . . .	49
3.3.3	Method C . . . . .	49
3.3.4	Method D . . . . .	51
3.3.5	Effect of measurement methods . . . . .	51
<b>4</b>	<b>Fundamental diagram analysis</b>	<b>57</b>
4.1	Unidirectional flow . . . . .	57
4.1.1	Spatiotemporal profile . . . . .	57
4.1.2	Size and position of the measurement area . . . . .	62
4.1.3	Specific flow concept . . . . .	65
4.1.4	Interpretation in terms of boundary-induced phase transitions . . . . .	69
4.2	Bidirectional flow . . . . .	72
4.2.1	Spatiotemporal profile . . . . .	73
4.2.2	Lane formation . . . . .	73
4.2.3	Specific flow concept . . . . .	75
4.2.4	Comparison of SSL and DML flow . . . . .	76
4.2.5	Comparison of BFR and UFR flow . . . . .	76

## *CONTENTS*

---

4.3	Merging flow . . . . .	77
4.3.1	Spatiotemporal profile . . . . .	78
4.3.2	Branch and main stream . . . . .	80
4.3.3	Specific flow concept . . . . .	82
4.4	Comparison of different types of flows . . . . .	84
4.4.1	Uni- and bidirectional flows . . . . .	84
4.4.2	Unidirectional and merging flows . . . . .	86
<b>5</b>	<b>Conclusion and outlook</b>	<b>88</b>
5.1	Conclusion . . . . .	88
5.2	Outlook . . . . .	90
	<b>Bibliography</b>	<b>93</b>
	<b>Publications</b>	<b>102</b>
	<b>Curriculum Vitae</b>	<b>103</b>

## List of Tables

2.1	Mean dimensions of a person for computations . . . . .	11
2.2	The Level of Service standards for walkways . . . . .	15
2.3	Main design parameters in handbooks . . . . .	17
2.4	Calculated movement time for Testcase1 . . . . .	18
2.5	Calculated results for Testcase2 . . . . .	20
3.1	Parameters for the unidirectional flow experiments in straight corridor . . . .	35
3.2	The related parameters in BFR-SSL experiments . . . . .	38
3.3	The related parameters in BFR-DML experiments . . . . .	38
3.4	The related parameters in UFR-DML experiments . . . . .	38
3.5	Parameters for the T-junction experiments . . . . .	41
3.6	Standard deviation of velocities for different methods . . . . .	54
4.1	Density and velocity distribution along x-direction . . . . .	63
4.2	Density and velocity distribution along y-direction . . . . .	64
4.3	Comparison of flow rate for congestion conditions . . . . .	67
4.4	The location of measurement area in T-junction. . . . .	82

# List of Figures

1.1	Crowd scenarios in different occasions. . . . .	2
1.2	Differences of fundamental diagram of corridor from various handbooks. . .	4
2.1	Fundamental diagrams given by Predtechenskii and Milinskii . . . . .	13
2.2	Relationship between pedestrian flow and density on walkways . . . . .	14
2.3	Relationship between pedestrian flow, velocity and density . . . . .	16
2.4	Testcase 1, pedestrian movement in a straight corridor. . . . .	18
2.5	Testcase 2, pedestrian movement through a bottleneck. . . . .	19
2.6	Testcase 3, pedestrian movement through bottlenecks. . . . .	21
2.7	The calculated opening widths from the handbook of SFPE and PM. . . . .	21
2.8	Simulation results from 4 different commercial softwares . . . . .	23
2.9	Comparison of the results from egress softwares and experiment . . . . .	24
2.10	Comparison of fundamental diagrams of unidirectional pedestrian flow . . .	27
2.11	Comparison of fundamental diagrams of bidirectional pedestrian flow . . .	28
2.12	Methods for recognition and representation of lanes. . . . .	29
2.13	Comparison of fundamental diagrams between uni- and bidirectional flow .	30
3.1	Schematic illustration and snapshots of the unidirectional experiment . . . .	34
3.2	Schematic illustration and snapshots of the bidirectional experiment . . . .	37
3.3	Sketch and snapshots of the pedestrian experiment in T-junction . . . . .	39
3.4	Snapshot of <i>PeTrack</i> . . . . .	42
3.5	Pedestrian trajectories from unidirectional flow experiments . . . . .	44

## LIST OF FIGURES

---

3.6	Pedestrian Trajectories from bidirectional flow experiments. . . . .	45
3.7	Pedestrian Trajectories from merging flow experiments. . . . .	46
3.8	Illustration of different measurement methods. . . . .	48
3.9	Space distribution of density and velocity from Voronoi method . . . . .	50
3.10	Time series of density and velocity . . . . .	52
3.11	The density-velocity relationship from different methods . . . . .	53
3.12	The density-flow relationship from different methods . . . . .	55
4.1	Spatiotemporal profiles of unidirectional flow for different density interval .	58
4.2	Spatiotemporal profiles of unidirectional flow for different exit widths . . .	59
4.3	Spatiotemporal profiles of unidirectional flow for different corridor widths .	61
4.4	Effect of the size of the measurement area on the fundamental diagram. . .	62
4.5	Density and velocity distribution along transverse direction in corridor. . . .	65
4.6	Comparison of the fundamental diagram for different corridor widths. . . .	66
4.7	Comparison of flow rate through the corridor and the exit . . . . .	67
4.8	Relationship between flow rate $J_{\text{exit}}$ and width $b_{\text{exit}}$ . . . . .	68
4.9	Open system with particle input and output at left and right boundary . . . .	70
4.10	Generic form of the phase diagram for an open system . . . . .	71
4.11	Spatiotemporal profiles of bidirectional flow . . . . .	72
4.12	Recognition of lane formation with velocity profile . . . . .	74
4.13	Fundamental diagram of DML flow at different width of corridors . . . . .	75
4.14	Comparison of the fundamental diagram of SSL and DML flow. . . . .	77
4.15	Comparison of the fundamental diagram of BFR and UFR flow. . . . .	78
4.16	Spatiotemporal profiles of T-junction flow . . . . .	79
4.17	Fundamental diagram of T-junction stream in different branches . . . . .	81
4.18	Fundamental diagram of T-junction with different corridor width . . . . .	83
4.19	Fundamental diagrams of unidirectional flow and bidirectional flow . . . .	85
4.20	Fundamental diagrams of unidirectional and merging flow . . . . .	86

*LIST OF FIGURES*

---

5.1	The probable fundamental diagram of unidirectional flow . . . . .	91
-----	---	----

# Chapter 1

## Introduction

### 1.1 Background

In recent years, more and more crowd scenes appear with the increasing population and economy, especially in modern cities. During the rush-hours, a large number of people gather in public places including train stations and shopping malls (see Figure 1.1(a)). Meanwhile, more large events related to sports, entertainment, cultural or religious activities are held all over the world on a regular basis (see Figure 1.1(b)). In these occasions, the crowd densities can be extremely high which make movement of pedestrians difficult and possibly dangerous. In the case of an emergency, it is difficult to quickly escape in such high densities and this increases the probability of casualties. For example, a stampede at the 2010 Love Parade electronic dance music festival in Duisburg in Germany caused the death of 21 people and at least 510 more were injured [4]. In the same year, at least 347 people were killed in a stampede as millions of Cambodians were celebrating the last day of the annual Water Festival. Those unfortunate events raise serious safety and security issues not only for the participants but also for the organizers and designers of such events. How to design optimal escape routes for any case of emergency or critical situation? Facing incidents, how to guide the participants away from the dangerous areas as quickly as possible to reduce casualties? Without deep understanding of the crowd dynamics, it is not





(a) Rush-hour in Beijing subway station [3]

(b) Love parade in Duisburg 2010 [4]

Figure 1.1: Crowd scenarios in different occasions.

possible to provide answers to these questions.

Facing such situations, research on pedestrian and traffic flow became popular and attracted a lot of attention during the last decades [7, 8, 31, 57, 56]. A large number of models have been developed. Most of them are able to qualitatively reproduce some phenomena observed. Nevertheless, it is important to calibrate them with empirical data before using in practice. Some empirical data including field and well-controlled experiments studies on pedestrian dynamics have been collected in these years. These results promote the understanding of pedestrian traffic and also enrich the laws, standards and regulations related to the buildings. Unfortunately, compared to modeling, empirical studies are rare currently and there is a lack of empirical data to calibrate models and to guide the facility design.

The long-accepted beliefs, data and formulas in regulations, standards and handbooks are foundations of design and affect the safety in existing and proposed facilities. However, much of the data used in current egress calculations and performance-based predictions were collected about 40 years ago. Therefore, they should not be assumed to apply generally to building evacuation everywhere. In the United States for example, prime sources for data are Fruin's Dissertation, *Designing for Pedestrians: A Level of Service Concept*, (1970) and subsequent books, *Pedestrian Planning and Design*, (Fruin, 1971, 1987). In Canada, prime sources for data related particularly to high-rise office buildings and large public areas are Pauls and his colleagues, beginning especially in 1969 [6]. There are also

many examples of poor, and even hazardous, human environments resulting from a lack of understanding of traffic flow relationships and space requirements of pedestrians. A number of authorities have been using maximum pedestrian capacity as a basis for design. Yet, analysis of time-lapse photography of pedestrian traffic flow on walkways and stairs has shown that the capacity is reached when there is a dense crowding of pedestrians, causing restricted and uncomfortable locomotion. Insufficient consideration of human space requirements has resulted in inadequate design of many areas where pedestrians may be obliged to accumulate in large groups [17]. Furthermore the movement of pedestrians is influenced by many factors including cultural and regional differences [11], the characteristics of the pedestrians (gender, age, size, health, mood, stress, baggage,...), the surrounding environment (trip purpose/length/steepness/safety, time of the day, period of the year) [62], the differences between uni- and multidirectional flow [46, 51]. Along with the ongoing changes of times, the demographics such as body size and mass, and behavioral pattern are also changing and influencing the characteristics of pedestrian movement.

Besides, a number of available datasets from different handbooks and researchers show surprisingly large differences [55, 59]. One of these differences is the fundamental diagram which denotes the relation between pedestrian flow and density and is associated with many qualitative self organization phenomena such as lane formation and jams. Specifications of various experimental studies, guidelines, and handbooks display substantial differences in maximal flow values and the corresponding densities, as well as the density where the flow vanishes due to overcrowding [55], as shown in Figure 1.2. Facing such discrepancies, it is not sure whether they arise from the specific properties of pedestrian flow or other external factors. According to [58], even the measurement methodologies applied on the datasets have large influence on the fundamental diagram. To overcome the afore mentioned discrepancies, it is crucial to develop not only better data capture methods but also better data analysis methods.

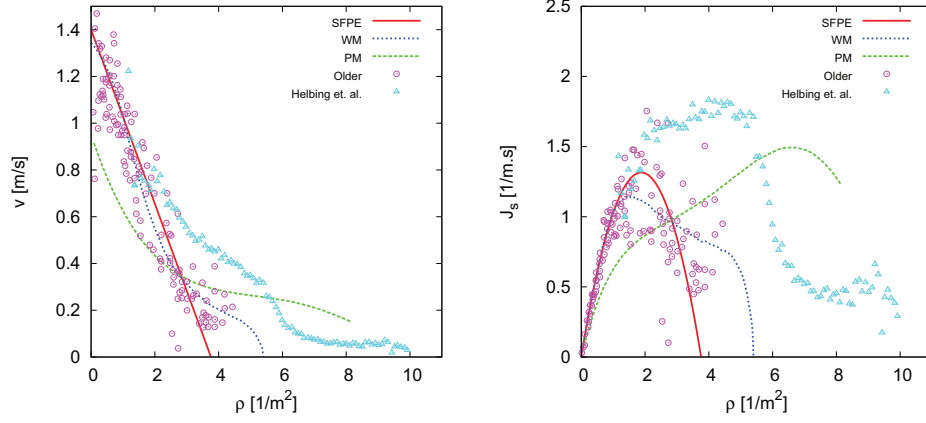


Figure 1.2: Differences of fundamental diagram of corridor from various handbooks.

## 1.2 Aim and objective

In the view of the above conditions, a thorough investigation of the laws of crowd motion and the factors that may influence the datasets, e.g., the measurement methodology or the types of the facilities, is required. In this study, we focus on the pedestrian movement in straight corridors and T-junction. The characteristics of uni-, bidirectional and merging pedestrian flow will be studied systematically. This thesis aims at studying basic laws of pedestrian dynamics, supplying methodologies for analyzing the empirical pedestrian data, investigating the factors that influence fundamental diagram and providing pedestrian data for facility design, model calibration and validation. To achieve this aim, we plan:

- To systematically review the current design basis of escape route including regulations and handbooks, the empirical studies on pedestrian dynamics especially for the movement in straight corridors and T-junction.
- To explore the methodologies for pedestrian data extraction and analysis.
- To study the factors that influence crowd quantities such as density, velocity and flow and determine the effects of them on the fundamental diagram.

- To compare the characteristics for various types of pedestrian flows including uni- and bidirectional flows in straight corridor and merging flows in a T-junction.
- To formulate some suggestions for improving current facility design and crowd management based on our empirical results.

### 1.3 Methodology

In order to achieve the objectives mentioned earlier, the following methodology is adopted:

Firstly, we conduct a comprehensive literature review to scrutinize the current used design basis and methods for pedestrian facilities. Aiming at the design requirement, the empirical research on pedestrian at the present stage will be discussed. Based on this discussion, we will study the advantages and disadvantages of existing theories, data and approaches. Thereafter the scientific question and methods approach of the thesis will be proposed

As one of the important tasks of this thesis, we investigate the characteristics of pedestrian movement in straight corridors and T-junctions. A series of well-controlled laboratory experiments with up to 350 participants is performed. The trajectories of each participant are automatically extracted from the video recordings of experiments using the software *PeTrack* [9] with high accuracy in space and time. From these trajectories microscopic pedestrian characteristics such as personal space and instant velocity and macroscopic quantities including flow and densities can be obtained.

To analyze the data from the experiment as precise as possible, four different measurement methods are proposed and their effects on the fundamental diagrams are compared. At the end, the Voronoi method is chosen as the best method for pedestrian flow analysis for its small scatter and high resolution in space and time. With this analysis method, the basic parameters for facility design and some spatiotemporal characteristics of pedestrian dynamics are studied in detail.

## **1.4 Thesis outline**

The structure of the thesis is arranged as follows:

Chapter 2 of this thesis presents a review of current basis of escape route design, including building regulations, handbooks and simulations, and studies concerning the empirically studies on pedestrian dynamics.

In chapter 3, the setups of experiments and the extraction of pedestrian trajectories from video recordings are described. Then the measurement methodologies for analyzing the fundamental diagram of pedestrian flow and their effects on the results are investigated.

Chapter 4 demonstrates the main results of the pedestrian flow in straight corridors and T-junction quantitatively and qualitatively. The fundamental diagram of unidirectional flow and the factors that influence it are studied in section 4.1. The ordering in bidirectional flow and its effect on the fundamental diagram is studied in section 4.2. The investigation of pedestrian flow in a T-junction is shown in section 4.3 and we compare the fundamental diagram of different kind of pedestrian flows in section 4.4.

Chapter 5 summarizes the main results of the thesis and presents ideas of further studies.

## **Chapter 2**

# **Literature review on the fundamental diagram**

Studies performed in the area of pedestrian dynamics have provided valuable knowledge to facility designers, to building safety agencies and well as to crowds managers. The requirements for a better understanding of factors ruling pedestrian dynamics increase with the appearance of super high and large buildings such as skyscrapers. In this chapter, the current studies on pedestrian dynamics are briefly reviewed from the aspects of practical application and empirical research. In the first section, the commonly used methods and related data for facility design are compared. Thereafter, the empirical studies especially on fundamental diagrams are discussed.

### **2.1 Design of escape routes**

Escape routes are important components of buildings and are the main paths for the occupants exposed to the danger to an area free from danger. Reasonable design of escape routes is significant for effective evacuation and ensuring the safety of occupants especially in emergency such as fire or earthquake etc.. Otherwise, narrow, insufficient, hard-to-find or blocked escape routes would lead to problems in evacuation.

At present, the fire safety design on building facility can mainly be divided into two categories: prescriptive method and performance-based method [72]. The former is based on the prescription codes, regulations and guidelines, while the latter is performed according to handbooks and simulation results. Crowd movement in buildings generally consists of three general motions [41]: i) movement along corridors; ii) movement up and/or down staircases; iii) movement through exits. In this thesis, we review these approaches mainly on pedestrian movement along corridors.

### **2.1.1 Prescriptive method**

Prescriptive approaches exist usually in the form of law, codes, standards and regulations. The content is mainly based on past experience and consolidated know-how, such as a consequence of an accident with casualties which requires remedy to avoid a repeat, a consequence of some hazardous situations, or a consequence of some recognized social needs [65].

In prescriptive regulations, buildings are classified into different types including residential buildings, school buildings, high-rise buildings and plant buildings. For each type of building, some features that must be designed, e.g, the minimal width of exit, the maximal length of corridors etc., are prescribed. For example, in Chinese regulations [1], the minimum clear widths of egress corridors and exits are 1.1 *m* and 0.9 *m* for residential buildings, respectively. For public places, the clear width of the exit should not be smaller than 1.4 *m*, the minimum width of outdoor passageways is 3 *m*. For aisles in theaters, cinemas and stadiums, the widths of them should be calculated according to the lanes and flow. The width of each lane is 0.55 *m* and the flow rates on the horizontal ground and stairs are 43 and 37 persons per minute separately. Some of these parameters are determined based on fire resistance rating (from I to IV) of buildings. For building with fire resistance rating of I or II, the maximal evacuation time should be within 2 *minutes*, while for that of III it should be within 1.5 *minnutes*. In this way, it is simple to use and can make direct analysis based on various of requirements. Fire safety engineers with more specific qualifications



and/or skills are not required. The architects or designers have to follow them and choose corresponding parameters to satisfy the requirements of the codes.

However, the structures and functions of various buildings are not the same. The number and the distribution of combustibles in each building is also different. In this case, the design based on prescriptive methods would have some disadvantages. It is impossible to consider the environmental and social factors, as well as other fire protection systems related to a certain building. Consequently, it is difficult to develop safe design with reduced costs and overall considerations. Besides, with the development of modern building technologies, materials and design concept, the constructions, shapes and functions of buildings change a lot. The risks and hazards of modern buildings also increase along with these changes. In this situation, it becomes insufficient to dimension escape routes for more complicated buildings such as indoor arenas, shopping malls, or underground railway stations with prescriptive methods.

### **2.1.2 Performance-based method**

As a response to architects and designers who want more flexibility, performance-based codes have been developed in many parts of the world, for example, New Zealand, Australia and Japan. The main steps in a performance based building design process include [65]: 1) identifying and formulating the relevant user requirements. 2) transforming the user requirements identified into performance requirements and quantitative performance criteria. 3) using reliable design and evaluation tools to access whether proposed solutions meet the stated criteria at a satisfactory level.

In the performance-based building approach, it is essential to match the performance requirement and compare demand with supply. Prediction of the pedestrian movement is an important aspect of fire safety design in this method. Comparison of required safe egress time (RSET) with available safe egress time (ASET) has been generally accepted as the basis of life safety assessment. Here, the ASET, which is always evaluated using fire models, is defined as the time when fire-induced conditions within an occupied space or

building become untenable. While the RSET is the sum of the time from fire ignition to detection, the time from detection to notification of occupants, the time from notification until occupants decide to take action, the time from decision to take action until evacuation commences, as well as the occupant movement time (from the start of evacuation until it is completed) [15]. The escape route design of walking facilities should guarantee  $RSET > ASET$ . In this thesis, we primarily discuss the determination of occupant movement time in RSET. The main methods used for predicting this time include hydraulic flow calculations based on handbooks and simulation results based on egress models. Nearly all the handbook methods are based on fundamental diagrams, the relationship between the density, velocity and flow rate, which are also basic input for most egress models. However, the fundamental diagrams in various handbooks have differences not only in quantity but also in quality. We will discuss some of these methods and their discrepancies on planar facilities like sidewalks or corridors in the following sections.

### **2.1.2.1 Handbooks**

In this section, we list some researches on fundamental diagrams of pedestrian movement from common used handbooks.

1) Weidmann [69]

Weidmann described the fundamental diagram of pedestrian flow on flat areas through the Kladek formula by collecting 25 data sets.

$$v(\rho) = v_0 \cdot [1 - e^{-1.913 \cdot [\frac{1}{\rho} - \frac{1}{\rho_{jam}}]}] \quad (2.1)$$

$$J_s = v(\rho) \cdot \rho \quad (2.2)$$

where  $v$  is the velocity of crowd [m/s]

$v_0$  is the free-flow walking speed,  $1.34 \text{ m/s}$

$\rho$  is pedestrian density [ $\text{m}^{-2}$ ],  $\rho_{jam} = 5.4 \text{ m}^{-2}$

$J_s$  is the specific flow

Weidmann neglected differences between uni- and multidirectional flows. An examination of the data which were included in his analysis shows that most measurements with densities larger than  $\rho = 1.8 \text{ m}^{-2}$  are performed on multidirectional flows. According to this fundamental diagram, the maximum pedestrian flow rate  $J_{s,max} = 1.22 \text{ (m} \cdot \text{s)}^{-1}$ , while the corresponding walking speed and density are  $0.70 \text{ m/s}$  and  $1.75 \text{ m}^{-2}$  separately.

2) Predtechenskii and Milinskii (PM) [50]

*Planning for Foot Traffic Flow in Buildings* by Predtechenskii and Milinskii is one of the often referenced books in facility design. In the handbook, pedestrian density ( $D \text{ [m}^2/\text{m}^2]$ ) is expressed by the ratio of the sum of horizontal projections of people to the floor area occupied by the flow. The density  $D$  can be converted into  $\rho \text{ [m}^{-2}]$  according to the pedestrian dimensions. The mean dimensions of an adult person in different seasons given in the handbook range from  $0.1 \sim 0.125 \text{ m}^2$ , see Table 2.1 for details.

Age and dress of person	Width, m	Thickness, m	Area, $\text{m}^2$
Adult:			
In summer dress	0.46	0.28	0.1
In mid-season street dress	0.48	0.3	0.113
In winter street dress	0.5	0.32	0.125
Youth	0.43-0.38	0.27-0.22	0.09-0.067
Child	0.34-0.3	0.21-0.17	0.056-0.04
Adult:			
With child in arms	0.75	0.48	0.285
With baggage in hand	0.9-1.1	0.75	0.35-0.825
With knapsack	0.5	0.8	0.315
With light package	0.75	0.4	0.235

Table 2.1: Mean dimensions of a person for computations [50]

The relationship between density  $D$  and velocity  $v_H$  for horizontal paths are given as

the following empirical expression:

$$v_H(D) = 112D^4 - 380D^3 + 434D^2 - 217D + 57 \text{ [m/min]} \quad (2.3)$$

Note that the equation is valid for the interval of densities  $D \in [0, 0.92]$ . Taking it as the fundamental function, the fundamental diagram for other forms of paths (stairs, doorways for example) is given by introducing empirical coefficients (see Figure 2.1(a)). The velocity  $v_O$  for movement passing through doorways or openings is:

$$v_O(D) = (1.17 + 0.13 \sin(6.03D - 0.12)) \cdot v_H(D) \text{ [m/min]} \quad (2.4)$$

Besides, the influence of the state of pedestrians on the velocity is also considered and is determined with the help of the so-called coefficients ( $\mu_e$ ,  $\mu$  and  $\mu_c$ ) of movement conditions (emergency, normal and comfortable), as seen in Figure 2.1(b). Correspondingly, for horizontal paths and doorways with density varying from 0 to 0.92, the coefficients are given as:

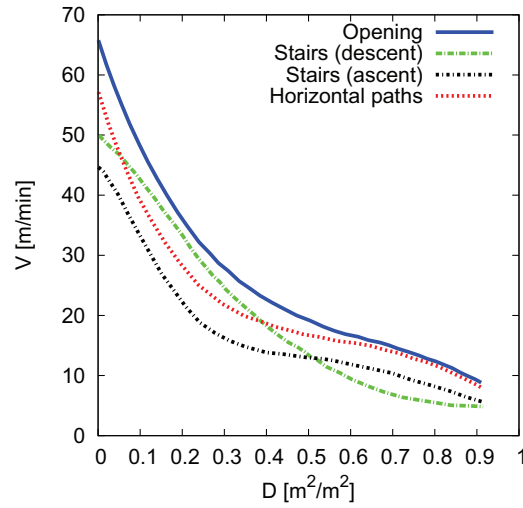
$$\mu_e = 1.49 - 0.36D \quad (2.5)$$

$$\mu = 1 \quad (2.6)$$

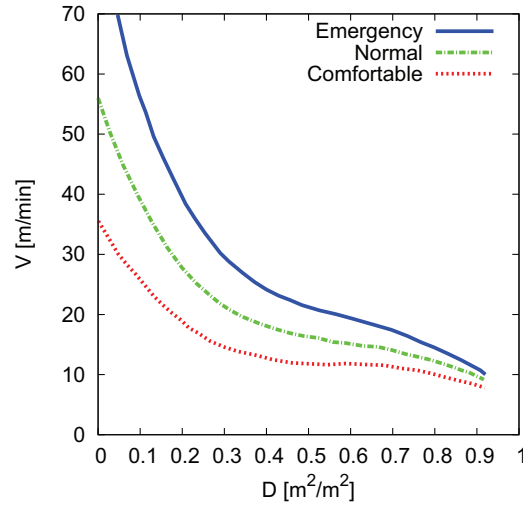
$$\mu_c = 0.63 + 0.25D \quad (2.7)$$

In this handbook, the capacity, the maximum specific flow  $J_{s,m}$ , of horizontal paths is somewhat lower than equivalent doorways, which are made narrower than the corresponding horizontal path. It is explained that this is mainly due to the coordination of movement, which forces pedestrians to adjust their psychological states in order to pass through a narrower segment of the path quickly.

As for jamming or congestions in front of the boundary of adjacent sectors, it is thought that they happen when the inflow is larger than the outflow. When jamming occurs, the



(a) For horizontal paths, stairs and openings.



(b) For horizontal paths in normal, comfortable and emergency conditions

Figure 2.1: Speed of movement as function of density in different type of facilities and conditions [50]

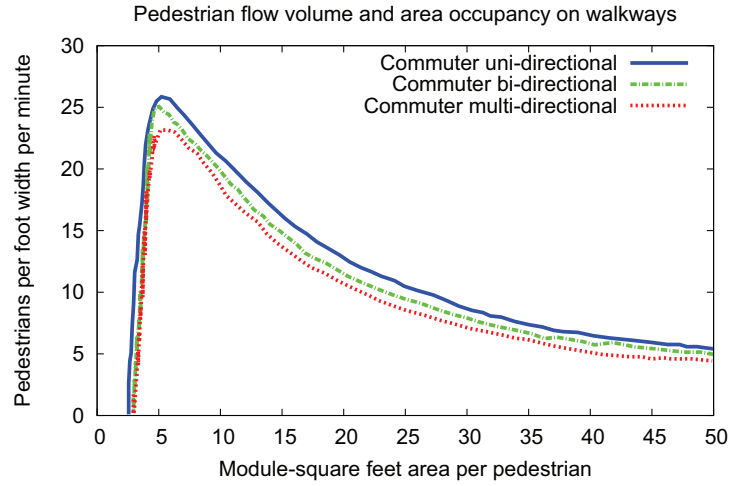


Figure 2.2: Relationship between pedestrian flow and density on walkways [17].

calculated specific flow based on conservation law could be larger than  $J_{s,m}$  for the corresponding form of the path. In this case, it is assumed that the flow rate at the following sector should be taken equal to that for  $D_{max} = 0.92$ . Consequently, this value is not the capacity  $J_{s,m}$  of facility.

### 3) Fruin [17]

*Pedestrian Planning and Design* by Fruin is a further comprehensive reference handbook on crowd movement. In this book, human characteristics related pedestrian design and the movement properties on different facilities such as walkways, stairs, escalators etc. are described. The concept of Pedestrian Area Module ( $M$  [square feet area per pedestrian]), the reciprocal of density  $\rho$ , is used to represent the pedestrian density.

Figure 2.2 shows the empirical flow-density relationships for three categories of pedestrian flows on walkways. These relationships, representing the average conditions of three

Level of Service	Average pedestrian area occupancy (Square feet per person)	Average Flow rate (Pedestrians per foot per minute)
A	35 or more	7 or less
B	25-35	7-10
C	15-25	10-15
D	10-15	15-20
E	5-10	20-25
F	5 or less	up to 25

Table 2.2: The Level of Service standards for walkways [17]

distinctive types of pedestrian traffic, show a relative small range of variation. It is thought that reverse and cross-flow traffic conflicts do not drastically reduce either pedestrian velocity or flow rate. A minor traffic flow ratio of 10 percent of the total flow results in only a 14.5 percent reduction in potential sidewalk capacity. As the minor traffic flow ratio increases, its detrimental effect on the capacity is actually reduced. With a 50/50 traffic-flow mix, the two-way traffic capacity of sidewalks is about equal to its one-way capacity.

The capacity of walkways in Figure 2.2 are 26.2, 24.7 and 23.3 persons per foot of walkway width per minute ( $PFM$ ), corresponding to 1.43, 1.35 and 1.27 ( $m \cdot s$ )<sup>-1</sup>, for uni-, bi- and multi-directional flow respectively. They are the design values in use by a number of authorities. However, Fruin states that using the maximum flow rate as a basis for design produces a limited walkway section that restricts normal movement. Consequently, the concept of Level-of-Service (A-F) and the Level-of-Service design standards for different building facilities are recommended in this handbook. For example, the standard for walkways is as shown in Table 2.2. The facilities in different environments are asked to be designed based on different standards according to the requirements.



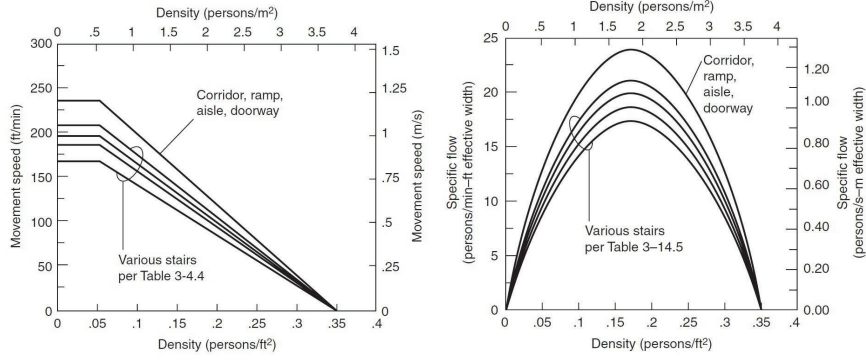


Figure 2.3: Relationship between pedestrian flow, velocity and density [15].

#### 4) SFPE Handbook [15]

Figure 2.3 shows the fundamental diagram of pedestrian flows in the SFPE handbook. When the pedestrian density is less than about  $0.54 \text{ m}^{-2}$ , people are able to move along walkways at about  $1.25 \text{ m/s}$ , an average unrestricted walking speed. If the density exceeds about  $3.8 \text{ m}^{-2}$ , no movement will take place. The speed decreases linearly with increasing density from  $0.54$  to  $3.8 \text{ m}^{-2}$ . The equation is

$$v(\rho) = k - ak\rho \quad (2.8)$$

where  $k = 1.4$  and  $a = 0.266$  for density in  $\text{m}^{-2}$  and velocity in  $\text{m/s}$  for corridors, aisles, ramps and doorways.

The specific flow  $J_s$  is

$$J_s = \rho \cdot v \quad (2.9)$$

Compared with the values given by Predtechenskii and Milinskii, there are some different relationships and assumptions in the SFPE handbook. First, the fundamental diagrams for corridors, ramps, aisles and doorways are not distinguished and unified into one equa-

tion. Second, when congestions occur in front of transitions, any points in the exit system where the character or dimension of a route changes or where routes merge, it is assumed that the flow after the transition will be the capacity of facility. Further, it is believed in the book that people should not be expected to react faster or move more efficiently in a fire emergency than they do normally.

	Weidmann PM		Fruin	SFPE
Maximum density $\rho$ [ $m^{-2}$ ]	5.4	8.14	5.4	3.8
Free velocity $v$ [ $m/s$ ]	1.34	$\approx 0.95$	$\approx 1.27$	1.19
$J_{s,m}$ [ $(m \cdot s)^{-1}$ ] and the corresponding $\rho, v$	1.22	1.49	1.43	1.30
	$1.75 m^{-2}$	$6.64 m^{-2}$	$2.16 m^{-2}$	$1.88 m^{-2}$
	$0.7 m/s$	$0.2 m/s$	$0.7 m/s$	$0.7 m/s$
Distinguish corridor and doorway	NO	YES	NO	NO
Distinguish uni- and multi-directional flow	NO		YES	NO
Outflow during jamming	-	$J_s(D_{max})$	-	$J_{s,m}$

Table 2.3: Main design parameters in Handbooks

From the above discussion, nearly all the handbooks need fundamental diagrams for design of facilities. But the fundamental diagrams and corresponding assumptions given in various handbooks are different, for details of the differences see Table 2.3. Next, three simple scenarios will be discussed to show problems appearing in applications.

**Test case 1** As shown in Figure 2.4, the movement time of pedestrians in a corridor will be determined. The width and length of the corridor are  $2 m$  and  $20 m$  separately. And there are  $N = 150$  pedestrians with density  $\rho = 1.6 m^{-2}$  in front of the corridor.

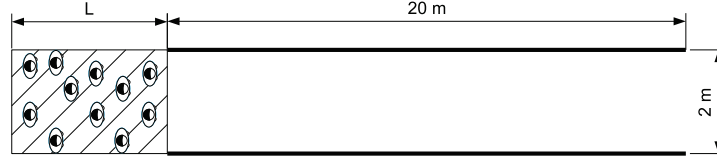


Figure 2.4: Testcase 1, pedestrian movement in a straight corridor.

**Solution** Under the given condition, the density,  $\rho = 1.6 \text{ m}^{-2}$ , is smaller than the critical densities where the maximum flow is reached for all of the above handbooks. Thus, the movement time only depends on the speed of the crowd. Table 2.4 shows the results obtained from different handbooks. Note that, the average dimension  $0.113 \text{ m}^2$  per person is used for transforming density  $D$  to  $\rho$ . In such a simple scenario, the movement time ranges from  $73.5 \text{ s}$  to  $142.9 \text{ s}$ . The most conservative time, which is nearly twice of the others, is from handbook of PM.

Handbooks	density [ $\text{m}^{-2}$ ]	velocity [ $\text{m/s}$ ]	time [ $\text{s}$ ]
Weidmann	1.6	0.762	87.8
PM	1.6	0.498	134.3
Fruin	1.6	0.930	71.9
SFPE	1.6	0.804	83.2

Table 2.4: Calculated movement time for Testcase1

**Test case 2** As shown in Figure 2.5, the minimum width of bottleneck will be determined when the width of the wider is  $4 \text{ m}$  and the density is  $3.5 \text{ m}^{-2}$ .

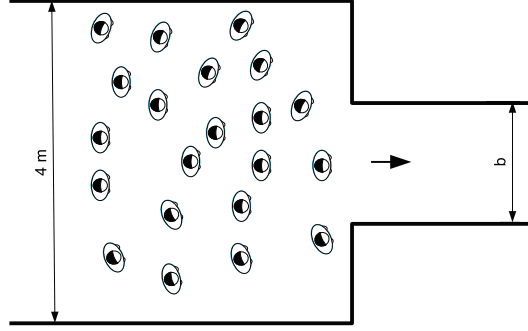


Figure 2.5: Testcase 2, pedestrian movement through a bottleneck.

**Solution** In this case, the supposed density exceeds the critical densities in all the above handbooks except PM. According to these handbooks, it is important to adjust whether the inflow through the bottleneck is larger than its capacity. It is believed that jamming and clogging typically occur for high densities at locations where the inflow exceeds the capacity [55]. Besides in front of the bottleneck [22, 60, 59], it is also possible to observe the jamming effect in counterflow [16, 10, 25], merging stream [63, 45] where two groups of pedestrians meet each other where the outflow is limited. For this effect, there is different assumptions in these handbooks. In the SFPE handbook, the outflow in this case is the capacity of the bottleneck, while it is the flow rate corresponding to the maximum density  $D = 0.92$  but not the capacity in PM. Further, the fundamental diagrams of the flow through corridors, doorways and ramps are discriminated in PM, however, they are regarded as the same in other handbooks.

The results from different handbooks are shown in Table 2.5. Compared to others, the minimum width of the bottleneck obtained from SFPE is less than half of them. The handbook of PM is still the most conservative one. Besides, the assumption for the occurrence

Handbook	$\rho [m^{-2}]$	$v [m/s]$	$J_s(in) [(m \cdot s)^{-1}]$	$J_s(out) [(m \cdot s)^{-1}]$	$b_{min} [m]$
Weidmann	3.5	0.23	0.81	1.22	2.57
PM	3.5	0.30	1.05	1.34	3.13
Fruin	3.5	0.27	0.93	1.43	2.60
SFPE	3.5	0.10	0.35	1.30	1.08

Table 2.5: Calculated results for Testcase2

of jamming that inflow is larger than the capacity of facility should be noticed. Nearly in all the fundamental diagrams, the density-flow relationships can be divided into two parts from a density  $J_c$  where the specific flow reaches the maximum. When the density is smaller than  $J_c$ , the density-flow relation is a monotonic increasing function. However, it becomes a monotonic decreasing function in the second part when the density exceeds  $J_c$ . In the second situation, for the same bottleneck the jamming may be detected in lower densities but not in higher densities according to the assumption. However, this seems unreasonable.

**Testcase 3** For the geometry shown in Figure 2.6, we regulate the width of the two openings A and B to change the location of congestions. As discussed above, the definition for the occurrence of jamming seems to have some problems especially at high densities. To make it simple, we suppose that the inflows through A and B are both  $1 (m \cdot s)^{-1}$  at low density. The widths of all corridors are 3 m.

**Solution** From the last two cases, we found the influence of fundamental diagrams in different handbooks on calculation of movement time and facility widths. The most and the least conservative results are obtained from handbooks of PM and SFPE. For the solution of this case, we are only with these two handbooks. In the handbook of PM, the capacities

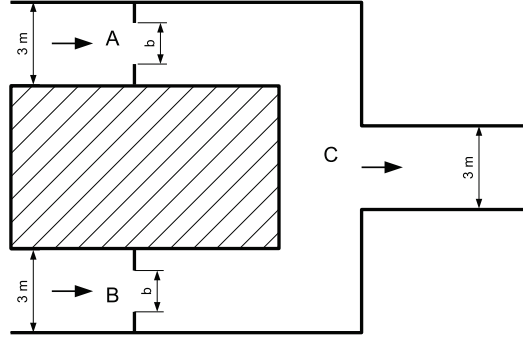


Figure 2.6: Testcase 3, pedestrian movement through bottlenecks.

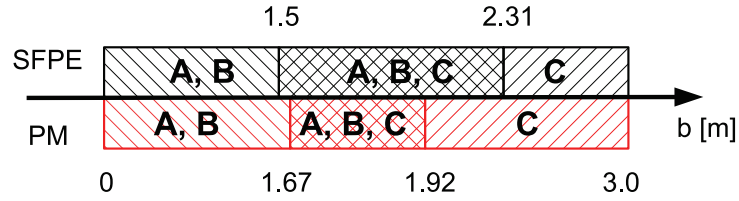


Figure 2.7: The calculated opening widths from the handbook of SFPE and PM.

for the horizontal paths and the opening are 10.13 and 10.59  $m/min$ , corresponding to 1.49 and 1.56  $(m \cdot s)^{-1}$  if the area of a pedestrian is chosen as 0.113  $m^2$ . Whereas both of them are 1.30  $(m \cdot s)^{-1}$  in SFPE handbook.

Figure 2.7 shows the width of the openings and the corresponding distribution of jams. If a congestion is wanted in front of the two openings, the width  $b$  should be smaller than 1.5  $m$  according to SFPE and 1.67  $m$  according to the handbook PM. On contrary, the widths should be larger than 2.31  $m$  and 1.92  $m$  according to them if the jam occurs in front of the bottleneck  $C$  but not the opening. Between the two widths, the jams will take place in all

of the three transitions.

From these three examples, it is shown that large discrepancies are obtained using different handbooks. Not only the values of the capacities, but also the other characteristic of fundamental diagrams and the assumptions on jamming or congestion have large influences on the facility design. In some extent, it is not possible to use only one handbook to make designs. In this case, two approaches are adopted to develop the facility design. In one hand, researchers go on investigating the reasonable and reliable fundamental diagram empirically. On the other hand, the engineers try to develop some simulation tools to assist the facility design.

#### **2.1.2.2 Simulations**

Although it is possible to design facilities and assess their safety using the macroscopic models in handbooks, it is not sufficient and has difficulties especially for the safety design of complex buildings. In these models the crowd is regarded as an homogeneous ensemble while their individual characteristics are unable to be considered. By comparison, the inhomogeneity of crowd could be considered by setting the parameters of each individuals in microscopic models. The influences of the environment on pedestrian behavior and decision-making can be reflected. Further, they are able to model the dynamic processes of pedestrian traffic and pedestrian flows in complicated areas and different scenarios, which was not possible with conventional macroscopic models. In this case, in addition with the development of computer technology and building techniques, a number of microscopic models have been developed to calculate pedestrian movement times. These models include force-based models, such as the social force model [20], the centrifugal-force model [12], the magnetic force model [47], rule-based models (CA models [55, 30, 64, 44] for

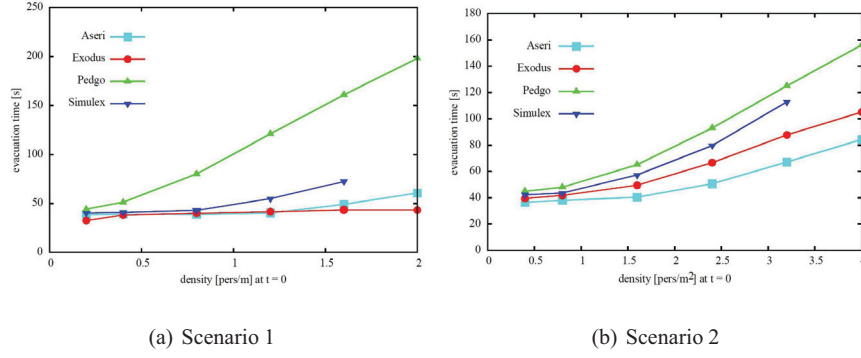


Figure 2.8: Simulation results from 4 different commercial softwares [53].

example) and so on.

Based on these basic models, some commercial and open-source software tools, e.g., *buildingEXODUS*, *Simulex*, *STEPS*, *pathfinder*, *FDS + Evac*, *Aseri*, *PedGo* etc., have been developed and are used for pedestrian movement simulations in practical engineering applications. However, there still have discrepancies among the simulation results from different tools even for very simple scenario like narrow corridor. Rogsch et al. tested some software tools based on simple scenarios and the results are presented in [53]. As shown in Figure 2.8, (a) is the simulation results of a 50 m long narrow floor without possibility to overtake, while (b) is that of a 2 m wide and 50 m long floor with possibility to overtake using 4 commercial softwares: *Aseri*, *BuildingExodus*, *PedGo* and *Simulex*. It is obvious that the differences of the evacuation time from various softwares become larger and larger with the increase of initial densities. In scenario 1, for example, the longest evacuation time is nearly four times of the shortest time when the density is 2 persons per meter. Besides, Thomas studied the pedestrian streams merging and passing through an exit in a stadium by simulation and experiments in [66]. Figure 2.9 shows the relationship between the number of pedestrians passing the exit over time. The differences of results from these tools are



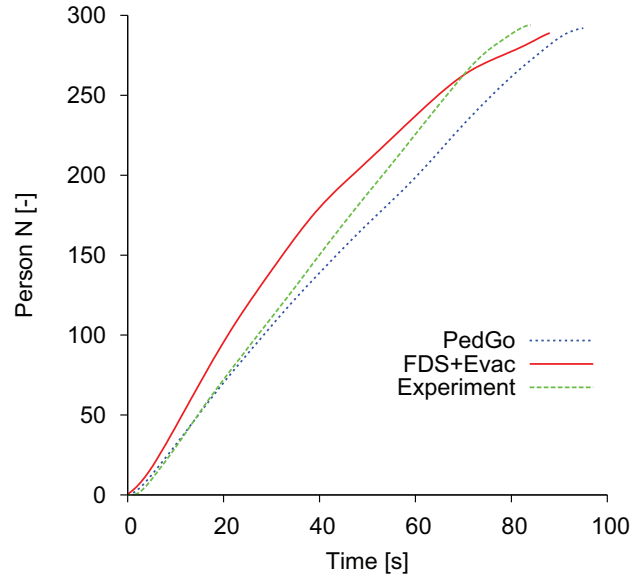


Figure 2.9: Comparison of the results from egress softwares and experiment [66].

obvious. Facing such disagreements, it is not easy to say which result is more realistic or reliable. It's difficult to make decisions for facility design and crowd management based on models without calibration.

Validation of computer models is not a "once and forget" task. It usually involves component testing, functional validation, qualitative and quantitative validations. While the first three components of the validation protocol are not so difficult, the task of quantitative validation poses a number of challenges because of the shortage of suitable experimental data. The simulation tools mentioned above are calibrated more or less in different ways. The fundamental diagram, as one of common-used principles concerning pedestrian dynamics, is closely associated with these tools. In some models, it is used as input parameters to adjust the travel speed of pedestrians. For example in *Simulex*, the walking velocity for

a person is dependant on the forward linear distance (proximity) to people ahead. While the algorithms for the movement of individuals are based on real-life data collected by using computer-based techniques for the analysis of human movement, observed in real-life videos [5]. Whereas, Davidich et al. presented methods to automatically calibrate pedestrian simulations to the socio-cultural parameters captured through measured fundamental diagrams [14]. Most of behavior-based tools like FDS+Evac, PedGo and buildingEXODUS reproduce the fundamental diagrams and compare it with empirical data to set parameters or make calibration. Even if they have been calibrated well to some extent, however, the results from different tools vary largely, which causes a lot of troubles and uncertainties in practical applications as well as in safety analysis.

No matter the fundamental diagrams are used as input parameters or criterion of models, their uncertainties and diversities are significant. If the presented diversities are ignored, the simple comparison of fundamental diagrams between simulation and experiments is meaningless.

## **2.2 Empirical studies**

From the above review, the fundamental diagram plays an important role in fire safety design but has uncertainties not only in handbooks but also in simulation softwares. In this situation, empirical studies become significant to obtain some latest, reliable and more detailed data in both qualitative and quantitative. The characteristics of pedestrian dynamics and the reasons for the uncertainties of fundamental diagrams can be investigated. In this section, we review the main outcomes from both well-controlled pedestrian experiments [24, 34, 35, 43, 40] and field studies [26, 27, 71] in the past years.

As discussed before, nearly all the fundamental diagrams in use come from empirical studies. But there is still no consensus among them except that pedestrian velocity decreases with increasing density. Pedestrian movement requires sufficient area for unrestricted pacing, and for sensory recognition and reaction to potential obstacles [17]. As the density increases, the available clear area for locomotion reduces for single pedestrians, and then the ability to bypass slower-moving pedestrians and to select their desired walking speed is also restricted. In this way, it is always true that the crowd velocity will decrease. However, this consensus is not enough and the specific equations are expected in facility design and safety assessments. However, pedestrian dynamics is quite complex due to the large number of pedestrians and their interactions, as well as some other external factors like the environment. The factors that could affect the fundamental diagrams may refer to physiological, psychological and social aspects. In [32], it is concluded that age, gender, and site environment have significant impact on pedestrian walking speed and start-up time at crosswalks. Psychological factors, reactions to environment, traffic composition, and trip purpose could all contribute to each pedestrian's selection of his unimpeded free-flow speed. Correspondingly, the dimensions of pedestrians, which influence the calculation of densities, are also various in different countries, times and so on.

Several researchers, in particular Fruin and Pauls [17], Predtechenskii and Milinskii [50], Weidmann [69], Helbing [21] have collected information about the relation between density and velocity. Different empirical equations are also given by different researchers as listed in section 2.1.2.1. For various facilities like corridors, stairs and ramps the shapes of the diagrams differ, but the equations are also different for the same type of facilities or movement.

Figure 2.10 shows the fundamental diagrams of unidirectional pedestrian flow in liter-

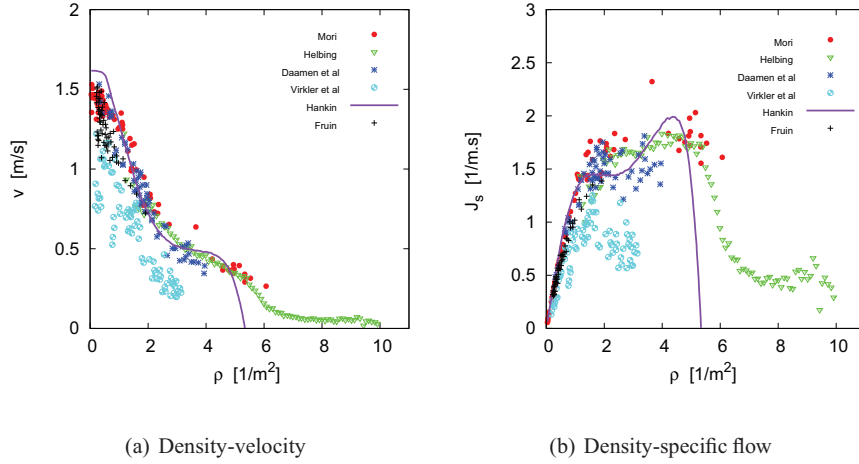


Figure 2.10: Comparison of fundamental diagrams of unidirectional pedestrian flow.

atures. The data of Mori et al. was for the flows of commuters in sidewalk sections, which ranged from 2.2 m to 4.5 m in width and 20 m in length in the central business district of Osaka in Japan [42]. Helbing et al. extracted the data from video recording of a crowd disaster, the Muslim pilgrimage in Mina/Makkah, in a 27.7 m × 22.5 m large area [21]. The maximum density in this study reaches about 10 m<sup>-2</sup> and stop-and-go waves are observed. The data of Virkler were collected over 12 m length of walkway after a football game in the USA. It's worth noticing that the width of the walkway changes from 14 m to 8.5 m along the movement direction of the pedestrian stream. While Daamen et al. collected the data from well-controlled laboratory experiments. Although all of these data are for unidirectional flow, the discrepancies can still be observed not only for the maximum densities but also the capacities. Since they are collected in different geometries in different countries, different situations and also different methods, it is not easy to distinguish the dominating reasons for these differences.

In this situation, it is a good way to make single factor analysis by carrying out some

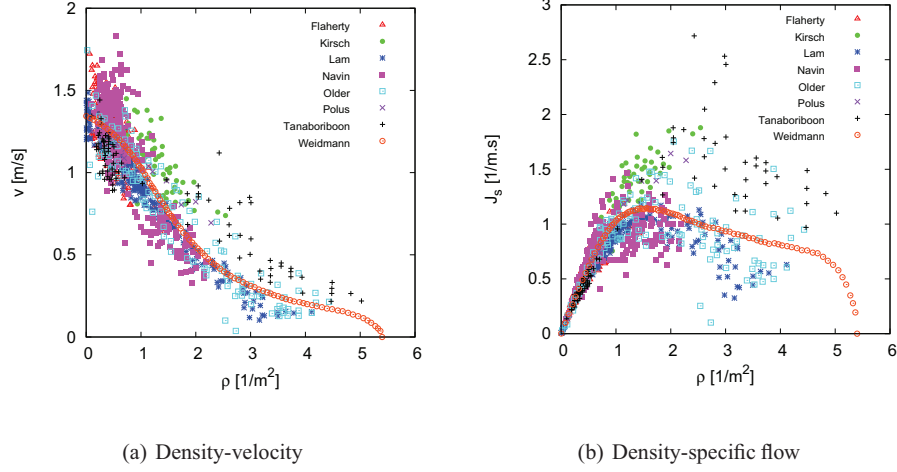


Figure 2.11: Comparison of fundamental diagrams of bidirectional pedestrian flow. Note that the fundamental diagram given by Weidmann [69] is obtained from the collection of 25 data sets.

well-controlled laboratory experiments. In [58], the single file movement experiments was performed in a closed narrow corridor. It is found that the measurement methods used to extract dataset lead to different fundamental diagrams. The same experiments were also conducted in India [11], China [40] and Japan, the culture difference is thought as a source of these discrepancies. However, it was a one dimensional stream and stop-and-go waves occurred in this experiment. We are not sure whether the same results can be found in two dimensional streams without stop-and-go wave. The influences of the corridor width, the geometries of corridor, the location of the measurement area on the fundamental diagrams are still unclear.

Figure 2.11 assembles the fundamental diagrams of bidirectional flow from some empirical studies. From the density-velocity relationship in Figure 2.11(a) it can be seen that they follow nearly the same trend. We also compare the relationship between density and

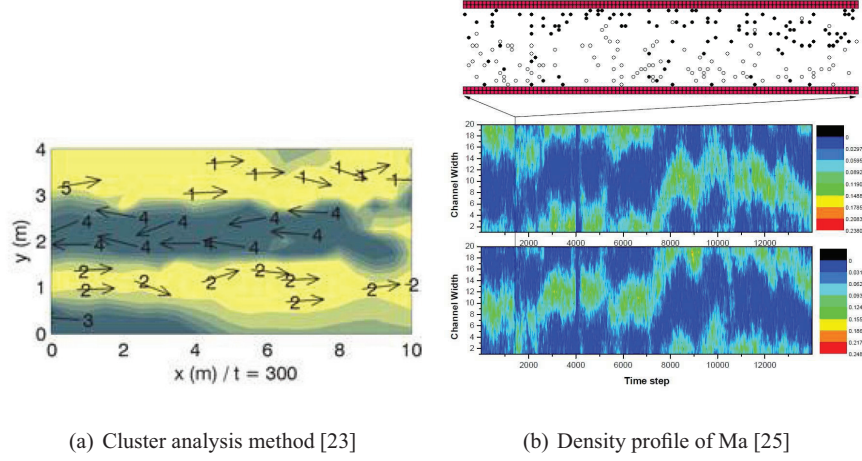


Figure 2.12: Methods for recognition and representation of lanes.

specific flow  $J_s$ , as shown in Figure 2.11(b), using the hydrodynamic relation  $J_s = \rho \cdot v$ . In this graph, differences can be observed especially for densities  $\rho > 2.0 \text{ m}^{-2}$ . The density values where the specific flows reach the maximum range from about  $1.3 \text{ m}^{-2}$  to  $2.3 \text{ m}^{-2}$ . Also the maximum specific flows from different studies range from about  $1.0 (\text{m} \cdot \text{s})^{-1}$  to  $2.0 (\text{m} \cdot \text{s})^{-1}$ .

Referring to bidirectional pedestrian stream, it is necessary to discuss the "Lane Formation" effect [10, 34]. Although it also occurs in unidirectional flow [59], its effect on pedestrian movement is different. In unidirectional streams, the formation of lanes could reduce the lateral conflicts and usually occurs in relative lower densities. While in bidirectional flows, lane formation occurs when pedestrians follow closely behind some other person who moves in the same direction to minimize head-on conflicts with persons moving in the opposite direction. The recognition and representation of the lanes has been investigated in different ways. As shown in Figure 2.12, for example, the cluster analysis method has been developed by Hoogendoorn et al. [23], while Yamori [70] et al. use a bond

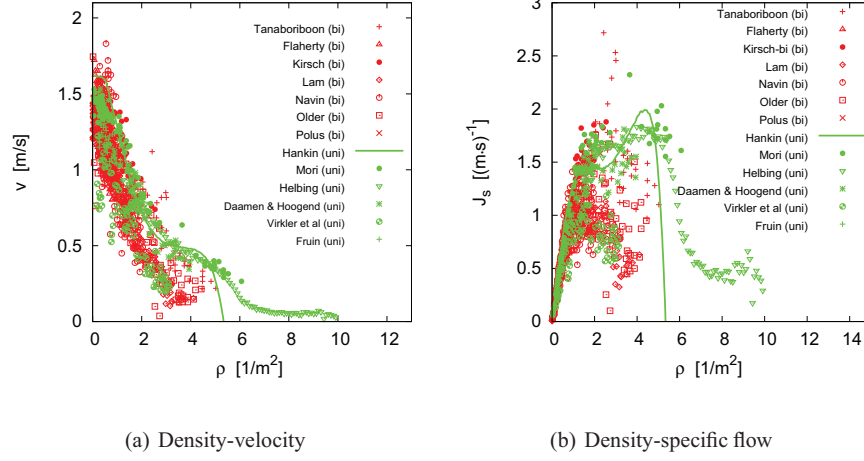


Figure 2.13: The fundamental diagram of uni- and bidirectional pedestrian flow from different previous studies.

index to express lanes from time-lapse photographic records. Ma et al. [25] and Christiani [13] plot density profiles to display lanes. In [52] an order parameter  $\phi = \frac{1}{N} < \sum_{j=1}^N \phi_j >$  is defined to detect lanes in colloidal systems driven by external fields. Lanes that emerge in this way could be either stable or unstable. That means that the number and distribution of lanes could be static or dynamic over time. However, it is still not known which pattern is more efficient for pedestrian movement and what is their effects on fundamental diagrams. Besides, the ratio of the opposing pedestrian stream is another factor that need to be considered in bidirectional flows. If the counterflow is unbalanced, the dominated stream may restrain the movement of the weak stream. It is necessary to investigate its influence on fundamental diagram.

Furthermore, there is up to now no consensus whether or not the fundamental diagrams for uni- and bidirectional flows differ from each other. Predtechenskii and Milinksii [50] and Weidmann [69] neglected the differences in accordance with Fruin, who stated that

the fundamental diagrams of multi- and uni-directional flow differ only slightly [17]. This disagrees with results of Navin and Wheeler [46] who found a reduction of the flow in dependence of directional imbalances. Pushkarev et al. [51] and Lam et al. [37, 38] assume that bidirectional flows are not substantially different from unidirectional flow as long as the densities of the opposite streams are not too different. However, Older et al. stated that different ratios of flows in bidirectional stream do not show any consistent effect on the walking speed [48]. Besides, Helbing et al. [19] concluded that counterflows are significantly more efficient than unidirectional flows. However, they compare average flow values without considering the influence of the density. Kretz et al. [34] have reported similar findings, but the influence of density and variations in time on the flow are not considered in this study. Figure 2.13 shows the fundamental diagrams of unidirectional [18, 21, 42, 67] and bidirectional flow. It seems that the fundamental diagrams of unidirectional flow lie above those of bidirectional flow, especially for  $\rho > 1.0 m^{-2}$ . The actual characteristics and differences between them are not clear and need further analysis. In addition, as one of the most common types of pedestrian flow, there is only little studies on merging flows.



## Chapter 3

### Experiments and methodology

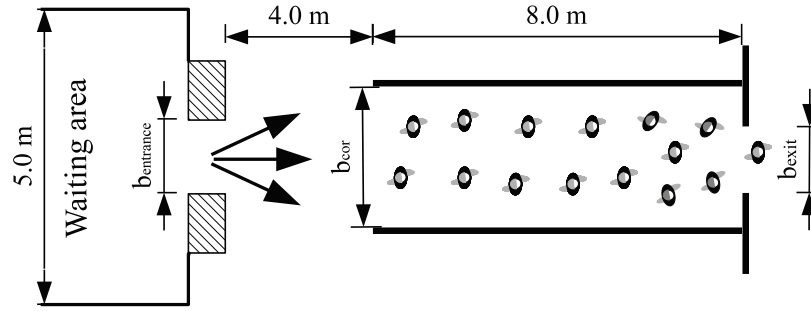
Better understanding of the pedestrian characteristics is particularly important for the planning of walking facilities. Researchers have conducted both well-controlled laboratory experiments and field observations to study pedestrian dynamics in detail. Meanwhile, different measurement methods are proposed to obtain quantitative data from these empirical researches. According to the discussion in the last chapter, however, discrepancies still exist among previous studies and there is no consensus on their origins. To resolve these discrepancies series of experiments under laboratory conditions were carried out in this study. In this chapter, we mainly introduce the setup of uni- and bidirectional pedestrian experiments in straight corridors and merging flow experiments in a T-junction. Then high-precision extraction of pedestrian trajectories from video recordings are described. Lastly, we present four different measurement methods for calculating pedestrian density, velocity and flow and compare their effect on the fundamental diagrams of different kind of flows.

### **3.1 Experiment setup**

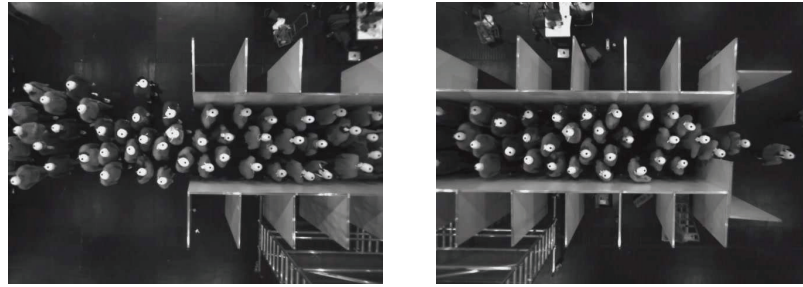
As outlined in the previous chapters, there are plenty of potential factors that may influence the characteristics of crowd movement. To minimize uncontrollable factors, we perform the experiments under well-controlled laboratory conditions with the same group of test persons. Data obtained from very specific conditions may be unsuitable for design of escape routes. However, such types of experiments make it possible to study the influence of single parameters and basic characteristics of pedestrian dynamics.

The experiments were performed in hall 2 of the fairground Düsseldorf (Germany) in May 2009. They were part of the Hermes project [2], in which the data resulted from the experiments were used to calibrate and test pedestrian movement models. The experiments were conducted with up to 400 participants. They were composed mostly of students and each of them was paid 50 € per day. The mean age and height of the participants were  $25 \pm 5.7$  years old and  $1.76 \pm 0.09$  m, respectively. The free velocity  $v_0 = 1.55 \pm 0.18$  m/s was obtained by measuring 42 participants' free movement.

All runs of the experiments were recorded by two synchronized stereo cameras of type Bumblebee XB3 (manufactured by Point Grey). They were mounted on the rack of the ceiling 784 cm above the floor with the viewing direction perpendicular to the floor. The cameras have a resolution of  $1280 \times 960$  pixels and a frame rate of 16 fps (corresponding to 0.0625 second per frame). To increase the region of observation, the left and the right part of the scenario were recorded by the two cameras separately. The overlapping field of view of the stereo system is  $\alpha = 64^\circ$  at the average head distance of about 6 m from the cameras. With the above-mentioned height range, all pedestrians can be seen without occlusion at any time. The geometrical variations of the boundaries and moving directions



(a) Schematic illustration



(b) Snapshots from experiment U-180-180-070

Figure 3.1: Schematic illustration and snapshots of the unidirectional pedestrian experiment in corridor

of pedestrians in each experiment will be introduced in the following sections.

### 3.1.1 Unidirectional flow in corridor

Figure 3.1 shows the sketch of the setup and two snapshots of the unidirectional experiments. Three straight corridors with the widths of 1.8 m, 2.4 m and 3.0 m were chosen and 28 runs of unidirectional pedestrian experiments were carried out. To regulate the pedestrian density in corridor, the widths of the entrance  $b_{entrance}$  and the exit  $b_{exit}$  were changed

---

Experiments and methodology

---

	Runs	Name	$b_{\text{entrance}}$ [m]	$b_{\text{exit}}$ [m]	N
$b_{\text{cor}} = 1.80 \text{ m}$	1	U-050-180-180	0.50	1.80	61
	2	U-060-180-180	0.60	1.80	66
	3	U-070-180-180	0.70	1.80	111
	4	U-100-180-180	1.00	1.80	121
	5	U-145-180-180	1.45	1.80	175
	6	U-180-180-180	1.80	1.80	220
	7	U-180-180-120	1.80	1.20	170
	8	U-180-180-095	1.80	0.95	159
	9	U-180-180-070	1.80	0.70	148
$b_{\text{cor}} = 2.40 \text{ m}$	10	U-065-240-240	0.65	2.40	70
	11	U-080-240-240	0.80	2.40	118
	12	U-095-240-240	0.95	2.40	108
	13	U-145-240-240	1.45	2.40	155
	14	U-190-240-240	1.90	2.40	218
	15	U-240-240-240	2.40	2.40	246
	16	U-240-240-160	2.40	1.60	276
	17	U-240-240-130	2.40	1.30	247
	18	U-240-240-100	2.40	1.00	254
$b_{\text{cor}} = 3.00 \text{ m}$	19	U-080-300-300	0.80	3.00	119
	20	U-100-300-300	1.00	3.00	100
	21	U-120-300-300	1.20	3.00	163
	22	U-180-300-300	1.80	3.00	208
	23	U-240-300-300	2.40	3.00	296
	24	U-300-300-300	3.00	3.00	349
	25	U-300-300-200	3.00	2.00	351
	26	U-300-300-160	3.00	1.60	349
	27	U-300-300-120	3.00	1.20	348
	28	U-300-300-080	3.00	0.80	270

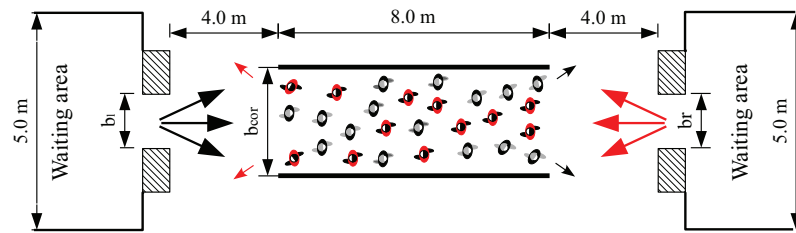
Table 3.1: Parameters for the unidirectional flow experiments in straight corridor

in each run. For overview of all these variables, see Figure 3.1 and Table 4.1. At the beginning of each run, the participants were held within a waiting area. Equal initial densities for different runs were arranged by partitioning the waiting area and counting the number of people in the partitions. Standing at the waiting area, they passed through a 4 m passage into the corridor. The passage was used as a buffer to minimize the effect of the entrance. In this way, the pedestrian flow in the corridor was nearly homogeneous over its entire width. When a pedestrian leaves through the exit, he or she returned to the waiting area for the next run.

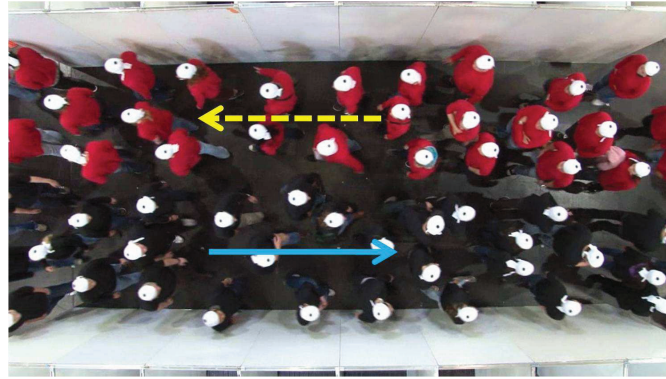
### 3.1.2 Bidirectional flow in corridor

Figure 3.2 shows the sketch of the experiment setup. 22 runs of bidirectional pedestrian streams (see Table 3.2 ~ 3.4) were performed in straight corridors with widths of 3.0 m and 3.6 m respectively. To regulate the density in the corridor and the ratio of the opposing streams, the width of the left entrance  $b_l$  and the right entrance  $b_r$  were changed in each run. At the beginning, the participants were arranged within the waiting areas at the left and right side of the corridor. When the experiment starts, the pedestrians enter the corridor passing through a 4 m passage. The passage was used as a buffer to minimize the effect of the entrance. In this way, the flow in the corridor was nearly homogeneous over the entire width of the corridor. When a pedestrian arrived at the other side of the corridor, he or she left the corridor from the passage and returned to the waiting area for the next run.

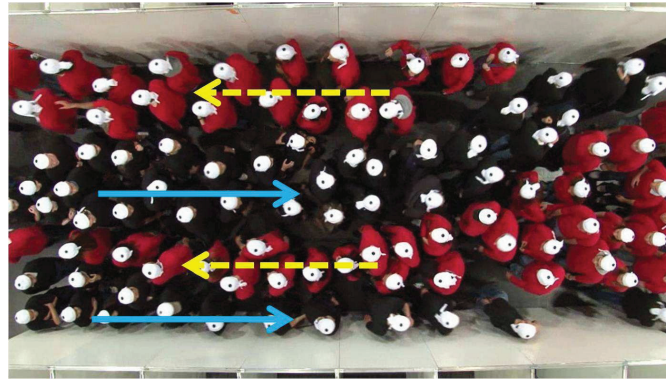
To vary the degree of disorder, the participants get different instructions and the width of entrances is changed each run. Three different types of setting were adopted among these experiments:



(a) Schematic illustration



(b)  $b_l = b_r$ , with instruction



(c)  $b_l = b_r$ , without instruction

Figure 3.2: Schematic illustration and snapshots of the bidirectional pedestrian experiment in corridor

## Experiments and methodology

$b_{\text{cor}}$ [m]	Index	Name	$b_l = b_r$ [m]	$N_l$	$N_r$
3.60	1	BFR – SSL-360-050-050	0.50	57	61
	2	BFR – SSL-360-075-075	0.75	56	80
	3	BFR – SSL-360-090-090	0.90	109	105
	4	BFR – SSL-360-120-120	1.20	143	164
	5	BFR – SSL-360-160-160	1.60	143	166

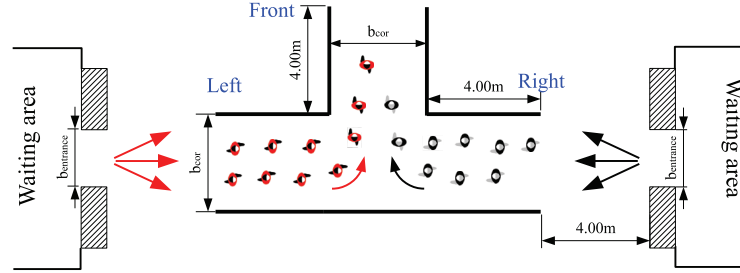
Table 3.2: The related parameters in BFR-SSL experiments

$b_{\text{cor}}$ [m]	Index	Name	$b_l = b_r$ [m]	$N_l$	$N_r$
3.00	1	BFR – DML-300-050-050	0.50	54	71
	2	BFR – DML-300-065-065	0.65	64	83
	3	BFR – DML-300-075-075	0.75	61	86
	4	BFR – DML-300-085-085	0.85	119	97
	5	BFR – DML-300-100-100	1.00	125	105
3.60	6	BFR – DML-360-050-050	0.50	56	74
	7	BFR – DML-360-075-075	0.75	62	65
	8	BFR – DML-360-090-090	0.90	110	102
	9	BFR – DML-360-120-120	1.20	115	106
	10	BFR – DML-360-160-160	1.60	140	166
	11	BFR – DML-360-200-200	2.00	143	166
	12	BFR – DML-360-250-250	2.50	141	163

Table 3.3: The related parameters in BFR-DML experiments

$b_{\text{cor}}$ [m]	Index	Name	$b_l$ [m]	$b_r$ [m]	$N_l$	$N_r$
3.00	1	UFR – DML-300-050-070	0.50	0.70	72	63
	2	UFR – DML-300-050-085	0.50	0.85	61	64
	3	UFR – DML-300-055-095	0.55	0.95	58	70
	4	UFR – DML-300-065-105	0.65	1.05	117	112
	5	UFR – DML-300-080-120	0.80	1.20	116	103

Table 3.4: The related parameters in UFR-DML experiments



(a) Schematic illustration



(b) Snapshots from experiment T-240-050

Figure 3.3: Sketch and snapshots of the pedestrian experiment in T-junction

$b_l = b_r$ , **without instruction**: In this type of experiment, the widths of entrance  $b_l$  and  $b_r$  were the same. The test persons were not given any instruction about the choice of exit and so were free to choose whatever exit they wanted. Five runs of experiments were carried out with this conditions in a corridor with width of 3.6 m. The related parameters are presented in Table 3.2.

$b_l = b_r$ , **with instruction**: Again the same width  $b_l$  and  $b_r$  were chosen in the experiments. But the instruction to the test persons at the beginning of the experiments were changed. The participants were asked to choose an exit at the end of the corridor according



to a number given to them in advance. The persons with odd numbers should choose the left exit in the end, while the ones with even numbers were asked to choose the exit in the right side. All 12 runs of experiments were performed with this setting in corridor with widths of 3.0 and 3.6 m separately, as given in Table 3.3.

**$b_l \neq b_r$ , with instruction:** In this case the widths of entrances  $b_l$  and  $b_r$  are different and the participants are instructed to choose an exit at the end of the corridor according to a number as the last experiment. Also 5 runs of experiments are performed in a corridor with width of 3.0 m, see Table 3.4.

### 3.1.3 Merging flows in T-junction

12 runs of merging flow experiments were carried out in a T-junction with corridor widths of 2.4 m and 3.0 m respectively. Figure 3.3 shows the sketch of the experiment setup and snapshots from one run of the experiments. Two pedestrian streams from the opposite sides of a T-shaped corridor join together into the junction and form a single stream. In these experiments, all these three parts of the corridor had the same width  $b_{cor}$ . To regulate the pedestrian density in the corridor, the width of the entrance was changed in each run. The left and right entrances always had the same width  $b_{entrance}$ . In this way, we guarantee the symmetry of the two branch streams. The number of pedestrians,  $N = N_l + N_r$ , in the left and right branch of the T-junction was approximately equal. The number was set to a value so that the overall duration of all experiments was similar and was long enough to assure a stationary state. The detailed settings for each run of experiment are listed in Table 3.5.

At the beginning, the participants were held within the waiting areas. When the ex-

---

## Experiments and methodology

---

Experiment index	Name	$b_{\text{cor}}$ [m]	$b_{\text{entrance}}$ [m]	$N_l + N_r$
1	T-240-050	2.40	0.50	67 + 67
2	T-240-060	2.40	0.60	66 + 66
3	T-240-080	2.40	0.80	114 + 114
4	T-240-100	2.40	1.00	104 + 104
5	T-240-120	2.40	1.20	152 + 153
6	T-240-150	2.40	1.50	153 + 152
7	T-240-240	2.40	2.40	151 + 152
8	T-300-050	3.00	0.50	73 + 73
9	T-300-080	3.00	0.80	103 + 103
11	T-300-120	3.00	1.20	153 + 153
12	T-300-150	3.00	1.50	153 + 154

Table 3.5: Parameters for the T-junction experiments

periment started, they passed through a 4 m passage into the corridor simultaneously and merged into single stream at the T-junction. The passage was used as a buffer to minimize the effect of the entrance. In this way, the pedestrian flow in the corridor was nearly homogeneous over its entire width. When a pedestrian left the main corridor, he or she returned to the waiting area for the next run.

## 3.2 Extraction of pedestrian trajectories

### 3.2.1 Extraction method

Manual procedures for collecting empirical data are very time-consuming and usually do not supply sufficient accuracy in space and time. In this study, accurate pedestrian trajectories are extracted from video recordings using the software **PTrack** [9]. Figure 3.4 shows a snapshot of **PTrack** with the main tabs corresponding to the steps of the process-

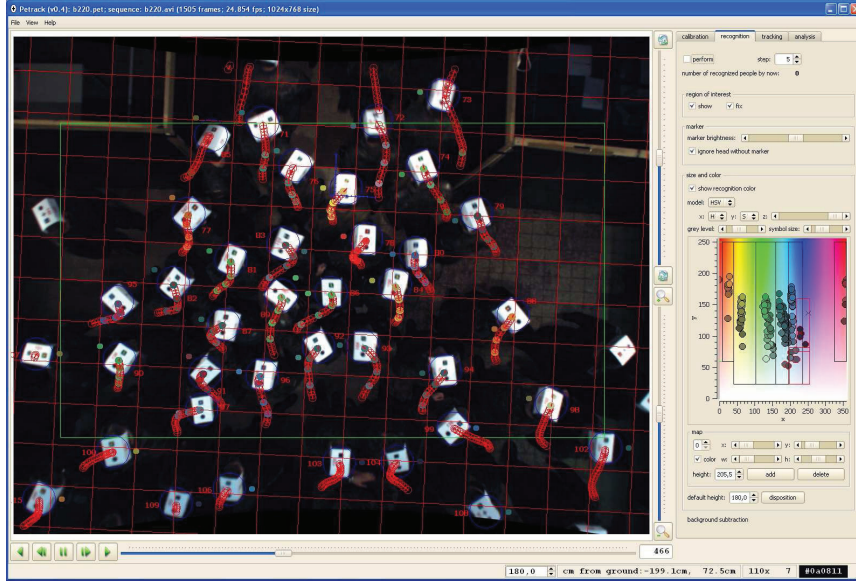


Figure 3.4: Snapshot of **PeTrack** [9].

ing pipeline: calibration, recognition, tracking and height detection. In this software, Lens distortion and perspective views are taken into account. The coordinates of each pedestrian in real space can be calculated and outputted directly from video recording. More information for **PeTrack** can be found in [9].

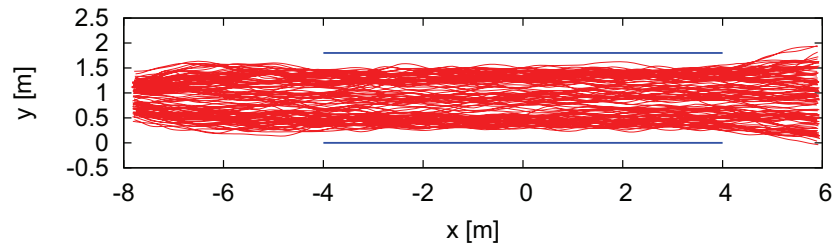
In the experiments, all pedestrians wear a white bandana with a centered black dot of 4 cm diameter which is used to mark their position. The coordinates of each tested person is extracted by detecting the marker from the video recordings. The precision of the trajectories is so high that combination of trajectory sets is allowed with overlapping camera views. At the end, the trajectories from different cameras are combined automatically using a algorithm which searches for the time where the trajectory sets fit best.

### 3.2.2 Trajectories

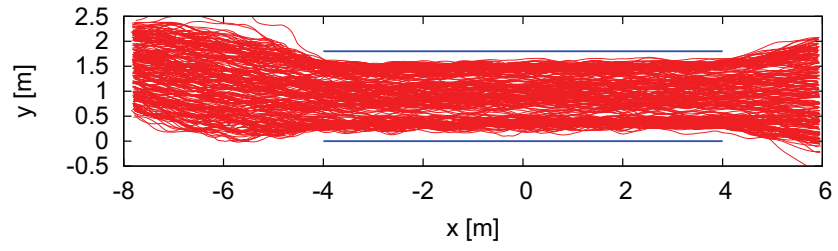
Pedestrian characteristics including flow, density, velocity and individual distances at any time and position can be determined from trajectories. All the results in the following chapters are obtained by analyzing pedestrian trajectories from video recordings of the experiments.

Figure 3.5 shows pedestrian trajectories from three runs of experiment in a straight corridor with a width of 1.8 m. In the experiment, the crowd density in corridor is changed mainly by regulating the values of  $b_{\text{entrance}}$  and  $b_{\text{exit}}$ . Widening the entrance or narrowing the exit could both increase the crowd density in the corridor. In Figure 3.5, the crowd densities increase from (a) to (c). The occupied width of the corridor in low density condition is a little bit smaller than that in higher density. In the corridor, the distribution of trajectories is nearly uniform along the movement direction when  $b_{\text{exit}} = b_{\text{cor}}$ . Whereas it is not the same if  $b_{\text{exit}} < b_{\text{cor}}$  due to the congestions near the exit.

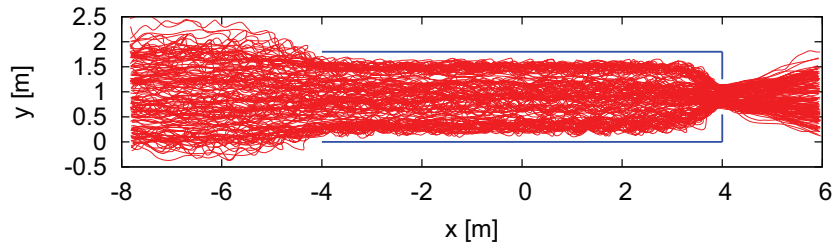
Figure 3.6 shows the pedestrian trajectories from bidirectional flow experiments. In the figure, the solid lines represent the paths of left moving pedestrians, while the dash lines represent the paths of right moving pedestrians. Lane formation is a typical characteristics of bidirectional flow. The formation of lanes, which depends on time as well as space, can be stable or unstable. To categorize these types, we classify the bidirectional streams into **Stable Separated Lanes (SSL)** and **Dynamical Multi-Lanes (DML) flow**. Besides, the opposing flows in bidirectional streams can be balanced or unbalanced. According to the typical densities in the opposing streams we introduce the types **Balanced Flow Ratio (BFR)** and **Unbalanced Flow Ratio (UFR)**. In the experiments, the different type of lanes are observed in the runs with and without instructions. While the different flow ratios are realized by reg-



(a) U-070-180-180



(b) U-180-180-180



(c) U-180-180-070

Figure 3.5: Pedestrian trajectories from unidirectional flow experiments

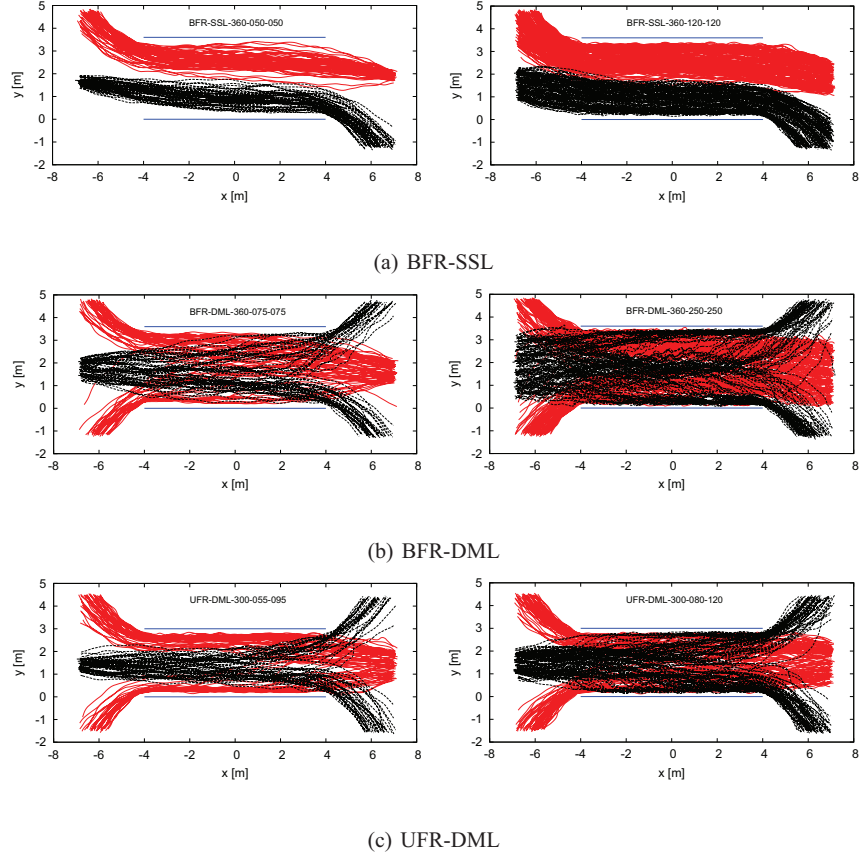


Figure 3.6: Pedestrian Trajectories from bidirectional flow experiments.

ulating the entrance width  $b_l$  and  $b_r$  of opposite sides. These variations result in different types of bidirectional flow:

**BFR-SSL flow**, see Figure 3.6(a): These trajectories are from the runs for  $b_l = b_r$  but without instructions. The opposing flows segregate and occupy proportional shares of the corridor. Stable lanes and interface formed autonomously. The gap between the opposing streams is larger for the situation with low crowd density in the corridor.

**BFR-DML flow**, see Figure 3.6(b): They are obtained from runs of experiment for

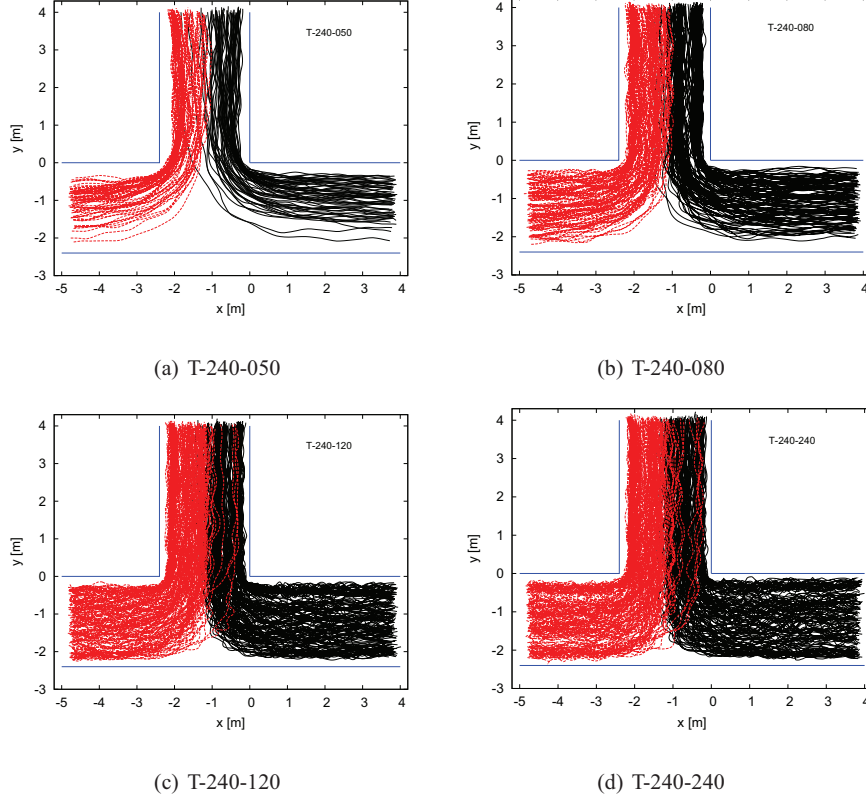


Figure 3.7: Pedestrian Trajectories from merging flow experiments.

$\mathbf{b}_l = \mathbf{b}_r$  with instruction. With this initial condition again lane formation is observable, but the lanes are unstable and vary in time and space. This type of flow is comparable with two streams crossing at a small angle. In this type of flow, the location of different lanes seems more stable at high density conditions.

**UFR-DML flow**, see Figure 3.6(c): These trajectories are obtained from runs of experiment for  $\mathbf{b}_l \neq \mathbf{b}_r$  with instructions. Again lanes are unstable and vary in time and space. The cumulated trajectories indicate that the flow ratio of the opposing streams is unbalanced.

Figure 3.7 shows pedestrian trajectories from merging flow experiments in the T-junction.

The crowd densities increase and the unoccupied space of the junction decreases from (a) to (d). Pedestrians prefer to shortest path since the trajectories tend to the inner side of the junction in (a) and (b). At high density conditions, the congestion in front of the corner can be also observed from the trajectories. The trajectories in (a) and (b) are quite smooth, while in (c) and (d) lateral sways are obvious especially in front of the corner.

### 3.3 Measurement methodology

For vehicular traffic it is well known that different measurement methods lead to different fundamental diagrams [29, 39]. The results obtained from pedestrian trajectories of single file movement in [58] have also shown how large variations induced by different measurement methods could be. In previous studies of pedestrian streams, different measurement methods were used limiting the comparability of the data. E.G. Helbing et al. proposed a Gaussian, distance-dependent weight function [21] to measure the local density and local velocity. Predtechenskii and Milinskii [50] used a dimensionless definition to consider different body sizes and Fruin introduced the "Pedestrian Area Module" [17]. All of these definitions have their advantages and disadvantages. To enable a detailed analysis, we study the influence of several measurement methods on the fundamental diagram and analyze which methods lead to the smallest fluctuations.

In this study four measurement methods were used to calculate the basic quantities: flow, density and velocity. The terminology refers to [58] and [61].



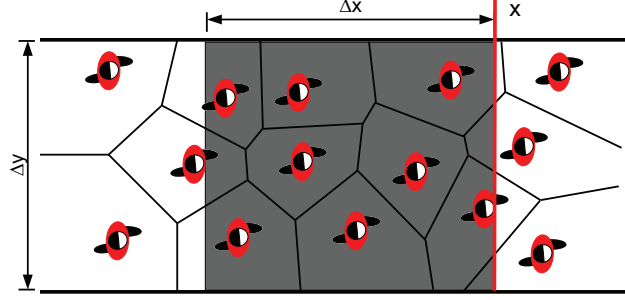


Figure 3.8: Illustration of different measurement methods. **Method A** is a kind of local measurement at cross-section with position  $x$  averaged over a time interval  $\Delta t$ , while **Methods B–D** measure at a certain time and average the results over space  $\Delta x$ . Note that for **Method D**, the Voronoi diagrams are generated according to the spatial distributions of pedestrians at a certain time.

### 3.3.1 Method A

For **Method A**, a reference location  $x$  in the corridor is taken and studied over a fixed period of time  $\Delta t$  (as shown in Figure 3.8). Mean values of flow and velocity are calculated over time. We refer to this average by  $\langle \rangle_{\Delta t}$ . Using this method we obtain the time  $t_i$  and the velocity  $v_i$  of each pedestrian passing  $x$  directly. Thus, the flow over time  $\langle J \rangle_{\Delta t}$  and the time mean velocity  $\langle v \rangle_{\Delta t}$  can be calculated as

$$\langle J \rangle_{\Delta t} = \frac{N_{\Delta t}}{t_{N_{\Delta t}} - t_{1_{\Delta t}}} \quad \text{and} \quad \langle v \rangle_{\Delta t} = \frac{1}{N_{\Delta t}} \sum_{i=1}^{N_{\Delta t}} v_i(t) \quad (3.1)$$

where  $N_{\Delta t}$  is the number of persons passing the location  $x$  during the time interval  $\Delta t$ .  $t_{1_{\Delta t}}$  and  $t_{N_{\Delta t}}$  are the times when the first and last pedestrians pass the location in  $\Delta t$ . They could be different from  $\Delta t$ . The time mean velocity  $\langle v \rangle_{\Delta t}$  is defined as the mean value of the instantaneous velocities  $v_i(t)$  of the  $N_{\Delta t}$  persons according to equation (4.2). We calculate

$v_i(t)$  by using the displacement of pedestrian  $i$  in a small time interval  $\Delta t'$  around  $t$ :

$$v_i(t) = \frac{\|\vec{x}_i(t + \Delta t'/2) - \vec{x}_i(t - \Delta t'/2)\|}{\Delta t'} \quad (3.2)$$

### 3.3.2 Method B

The second method measures the mean value of velocity and density over space and time. The spatial mean velocity and density are calculated by taking a segment with length  $\Delta x$  in the corridor as the measurement area. The velocity  $\langle v \rangle_i$  of each person is defined as the length  $\Delta x$  of the measurement area divided by the time he or she needs to cross the area (see equation (3.3)),

$$\langle v \rangle_i = \frac{\Delta x}{t_{i,out} - t_{i,in}} \quad (3.3)$$

where  $t_{i,in}$  and  $t_{i,out}$  are the times a person  $i$  enters and exits the measurement area, respectively. The density  $\rho_i$  for each person is calculated with equation (3.4):

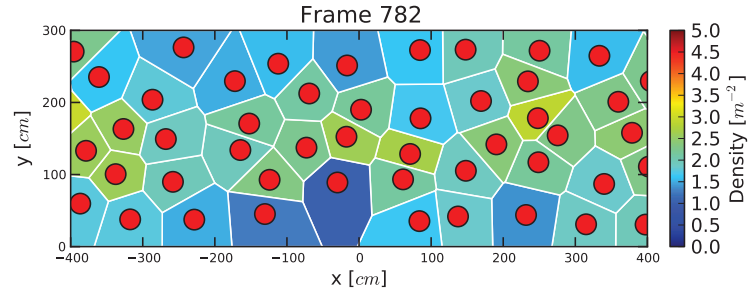
$$\langle \rho \rangle_i = \frac{1}{t_{i,out} - t_{i,in}} \cdot \int_{t_{i,in}}^{t_{i,out}} \frac{N'(t)}{\Delta x \cdot \Delta y} dt \quad (3.4)$$

$\Delta y$  is the width of the measurement area while  $N'(t)$  is the number of person in this area at a time  $t$ .

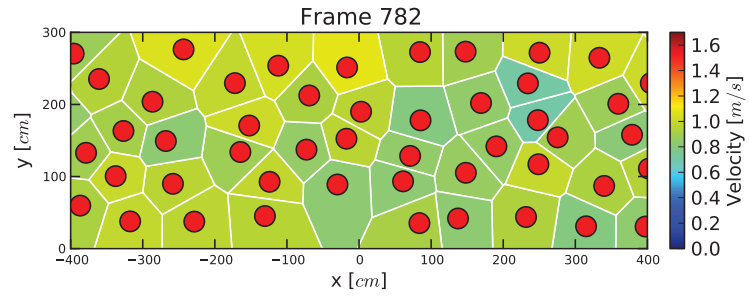
### 3.3.3 Method C

We call the third measurement method classical method. The density  $\langle \rho \rangle_{\Delta x}$  is defined as the number of pedestrians divided by the area of the measurement section:

$$\langle \rho \rangle_{\Delta x} = \frac{N}{\Delta x \cdot \Delta y} \quad (3.5)$$



(a) Density



(b) Velocity

Figure 3.9: Distribution of density and velocity over space obtained from Voronoi method for experiment U-300-300-300.

The spatial mean velocity is the average of the instantaneous velocities  $\mathbf{v}_i(\mathbf{t})$  for all pedestrians in the measurement area at time  $\mathbf{t}$ :

$$\langle \mathbf{v} \rangle_{\Delta x} = \frac{1}{N} \sum_{i=1}^N \mathbf{v}_i(\mathbf{t}) \quad (3.6)$$

### 3.3.4 Method D

This method is based on Voronoi diagrams [68] which are a special kind of decomposition of a metric space determined by distances to a specified discrete set of objects in the space. At any time the positions of the pedestrians can be represented as a set of points, from which the Voronoi diagrams (see Figure 3.8) are generated. The Voronoi cell area,  $A_i$ , for each person  $i$  can be obtained. Then, the density and velocity distribution of the space  $\rho_{xy}$  and  $\mathbf{v}_{xy}$  (see Figure 3.9) are defined as

$$\rho_{xy} = 1/A_i \quad \text{and} \quad \mathbf{v}_{xy} = \mathbf{v}_i(t) \quad \text{if } (x, y) \in A_i \quad (3.7)$$

where  $\mathbf{v}_i(t)$  is the instantaneous velocity of each person, see equation (4.2). The Voronoi density and velocity for the measurement area is then defined as [61]

$$\langle \rho \rangle_v = \frac{\iint \rho_{xy} dxdy}{\Delta x \cdot \Delta y} \quad (3.8)$$

$$\langle \mathbf{v} \rangle_v = \frac{\iint \mathbf{v}_{xy} dxdy}{\Delta x \cdot \Delta y} \quad (3.9)$$

### 3.3.5 Effect of measurement methods

To analyze the effects of measurement methods, we calculate the fundamental diagram from unidirectional experiments with corridor width  $b_{\text{cor}} = 1.8 \text{ m}$ . For **Method A** we choose the time interval  $\Delta t = 10 \text{ s}$ ,  $\Delta t' = 0.625 \text{ s}$  (corresponding to 10 frames) and the measurement position at  $x = 0$  (see Figure 3.5(a)~(c)). For the other three methods a rectangle with a length of  $2 \text{ m}$  from  $x = -2 \text{ m}$  to  $x = 0$  and a width of the corridor is chosen as the measurement area. We calculate the densities and velocities every frame with a frame rate of 16 fps. All data presented below are obtained from the same sets

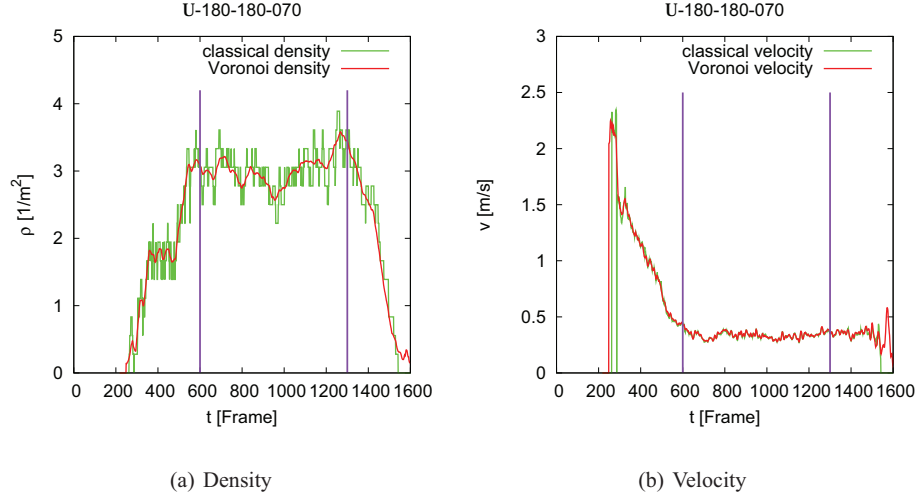


Figure 3.10: Time series of density and velocity using Method C and D. The two vertical lines indicate the beginning and the end of the stationary state.

of trajectories. To determine the fundamental diagram only data at the stationary state, which were selected manually by analyzing the time series of density and velocity (see Figure 3.10), were considered. For **Method D** we use one frame per second to decrease the number of data points and to represent the data more clearly.

Figure 3.11 shows the relationship between density and velocity obtained from different methods. Using **Method A** the flow and mean velocity can be obtained directly. To get the relationship between density and flow, the equation  $\rho = \langle \mathbf{J} \rangle_{\Delta t} / (\langle \mathbf{v} \rangle_{\Delta t} \cdot \mathbf{b}_{\text{cor}})$  was adopted to calculate the density. For the **Method B, C and D** the mean density and velocity can be obtained directly since they are mean values over space. There exists a similar trend of the fundamental diagram obtained using the different methods. However, their influence on the scatter of the results is obvious. Table 3.6 shows the standard deviation of velocities in certain density intervals for different measurement methods. Compared to the other

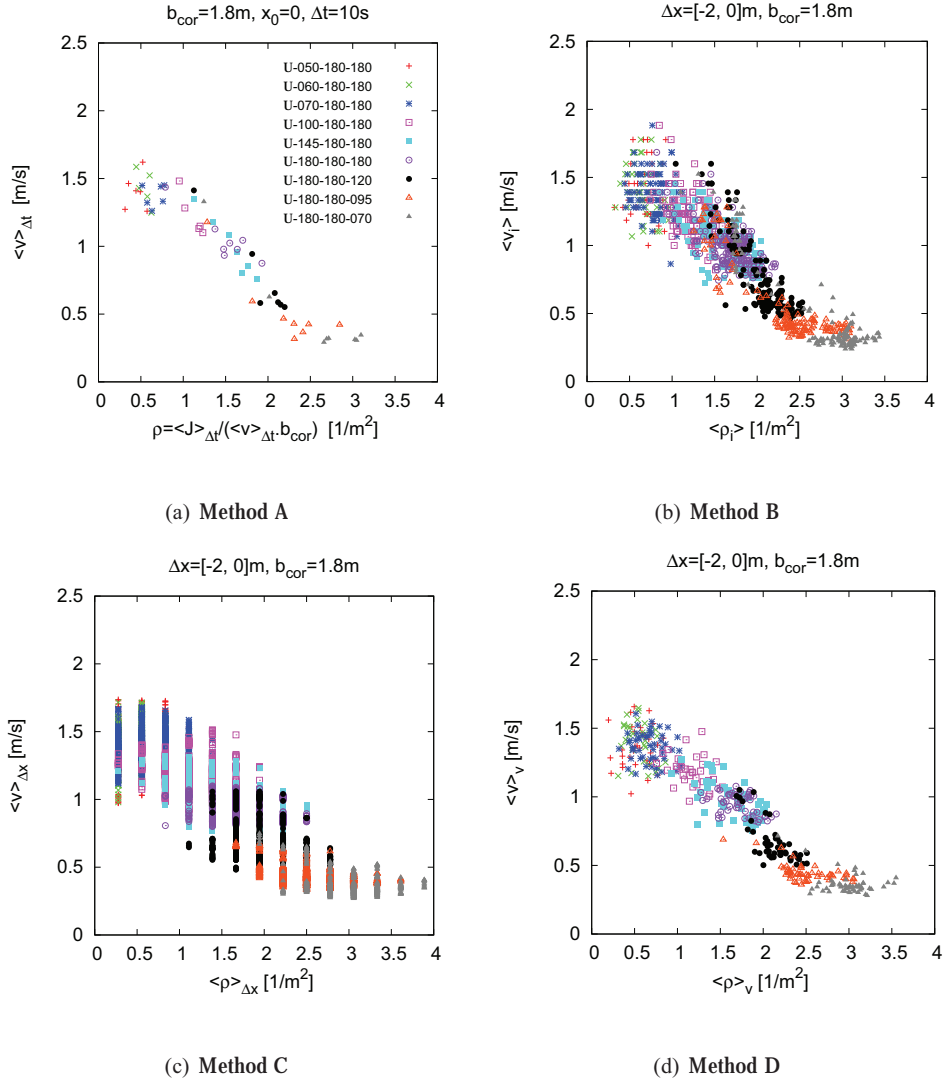


Figure 3.11: The relationships between density and velocity measured on the same set of trajectories but with different methods. Except for the density in (a), which is calculated using  $\rho = \mathbf{J} / (\mathbf{b} \cdot \Delta \mathbf{x})$ , all data are determined directly from the trajectories. The legends in (b), (c) and (d) are the same as in (a).

approaches, the fluctuations in **Method B** and **C** are larger.

Density interval [ $\text{m}^{-2}$ ]	A [ $\text{m/s}$ ]	B [ $\text{m/s}$ ]	C [ $\text{m/s}$ ]	D [ $\text{m/s}$ ]
$\rho \in [0.8, 1.2]$	0.119	0.169	0.175	0.120
$\rho \in [1.6, 2.0]$	0.086	0.144	0.175	0.111

Table 3.6: Standard deviation of velocities in certain density interval for different methods

Another criterion for the quality of the methods is the resolution in time and space. Even if **Method A** provides a smaller standard deviation than **Method D**, the low resolution in time smears the transition at  $\rho = 2\text{m}^{-2}$  clearly visible in Figure 3.11(d). The density in **Method C** has a strong dependence on the size of the measurement area  $A_m = b_{\text{cor}} \cdot \Delta x$ . The interval between two density values is  $1/A_m$ , which indicates that the measurement area should not be too small using this method. But large areas limit the spatial resolution. **Method D** can reduce the density and velocity scatter [61]. The reduced fluctuations of **Method D** are combined with a good resolution in time and space, which reveal a phenomenon that is not observable with **Method A** and **C**. In Figure 3.11(d) it seems that there is a discontinuity of the fundamental diagram when the density is about  $2\text{m}^{-2}$ . This will be analyzed in detail in the next chapter.

Figure 3.12 shows the relationship between the density and the flow obtained from different methods. The pedestrian flow shows small fluctuations at low densities and high fluctuations at high densities. The fluctuations for **Method A** and **Method D** are smaller than that for other methods. However, there is a major difference between the results. While the fundamental diagrams obtained using **Method A** and **Method C** are smooth, fundamental diagrams obtained with **Method B** and **Method D** show a clear discontinuity

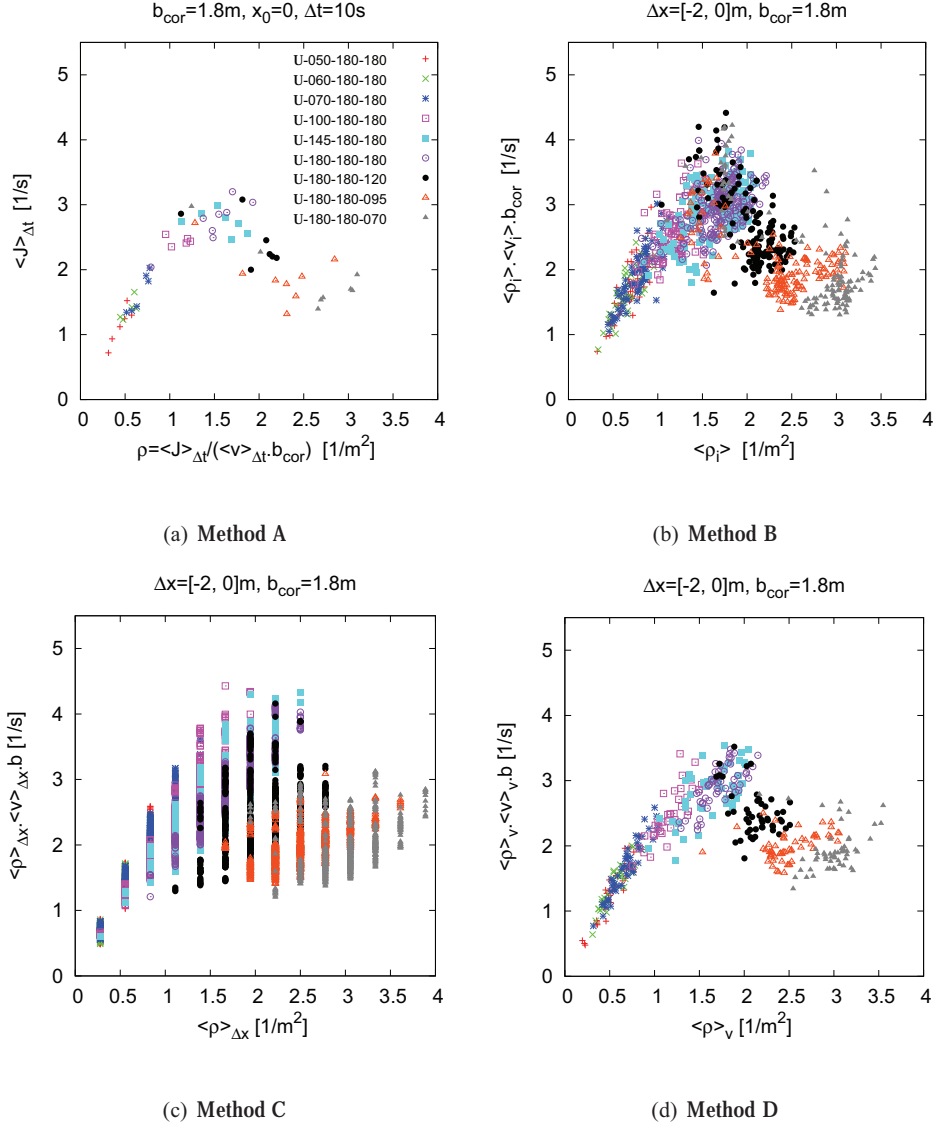


Figure 3.12: The relationships between density and flow measured at the same set of trajectories but with different methods. The density in (a) is calculated indirectly using  $\rho = J / (\mathbf{b} \cdot \Delta \mathbf{x})$ , while the flows in (b), (c) and (d) are obtained by adopting the equation  $\mathbf{J} = \rho \mathbf{v} \mathbf{b}$ . The legends in (b), (c) and (d) are the same as in (a).



at a density of about  $2 \text{ m}^{-2}$ . The average over a time interval of **Method A** and the large scatter of **Method C** blur this discontinuity. In disagreement with the results in [58], no marked differences occur among the fundamental diagrams produced by different methods. Possibly the differences of different methods will be larger in the cases where stop waves occur or when the characteristic of the pedestrian flow is not laminar.

## Chapter 4

### Fundamental diagram analysis

In this chapter, experiments of uni- and bidirectional flows in straight corridors and merging flows in T-junctions are analyzed mainly using the Voronoi method for its high resolution and small fluctuation. Space-resolved measurements for the density, velocity and specific flow profiles are also presented. The fundamental diagrams of these three kinds of pedestrian flow obtained from the experiments are compared after investigating the influence of the size and location of the measurement area on them.

#### 4.1 Unidirectional flow

##### 4.1.1 Spatiotemporal profile

To analyze the spatial dependence of density, velocity and specific flow precisely, we use the Voronoi method to determine these quantities in areas smaller than the size of pedestrians. We calculate the Voronoi density, velocity and specific flow over small regions ( $10\text{ cm} \times 10\text{ cm}$ ) each frame. Then the spatiotemporal profiles of density ( $\bar{\rho}(\mathbf{x}, y)$ ), velocity

## Fundamental diagram analysis

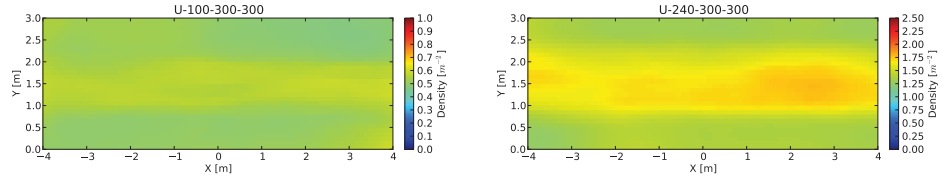
---

$(\bar{\mathbf{v}}(\mathbf{x}, y))$  and specific flow  $(\bar{\mathbf{J}}_s(\mathbf{x}, y))$  can be obtained over the stationary state separately for each run as follows:

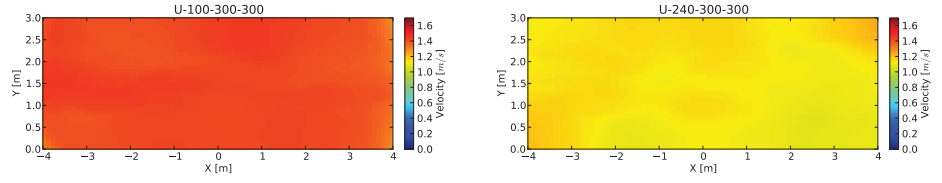
$$\bar{\rho}(\mathbf{x}, y) = \frac{\int_{t_1}^{t_2} \langle \rho \rangle_v(\mathbf{x}, y, t) dt}{t_2 - t_1}, \quad (4.1)$$

$$\bar{\mathbf{v}}(\mathbf{x}, y) = \frac{\int_{t_1}^{t_2} \langle \mathbf{v} \rangle_v(\mathbf{x}, y, t) dt}{t_2 - t_1}, \quad (4.2)$$

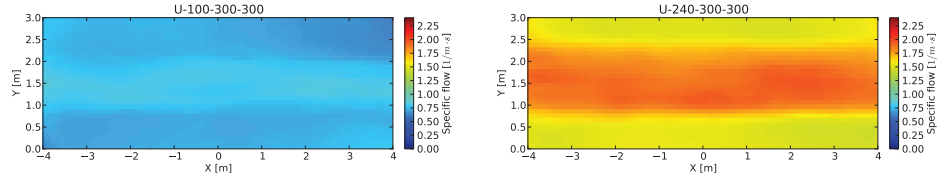
$$\bar{\mathbf{J}}_s(\mathbf{x}, y) = \bar{\rho}(\mathbf{x}, y) \cdot \bar{\mathbf{v}}(\mathbf{x}, y). \quad (4.3)$$



(a) Density profile



(b) Velocity profile



(c) Specific flow profile

Figure 4.1: Spatiotemporal profiles of unidirectional flow for different density interval

These profiles provide new insights into the spatial properties of the motion and the

## Fundamental diagram analysis

---

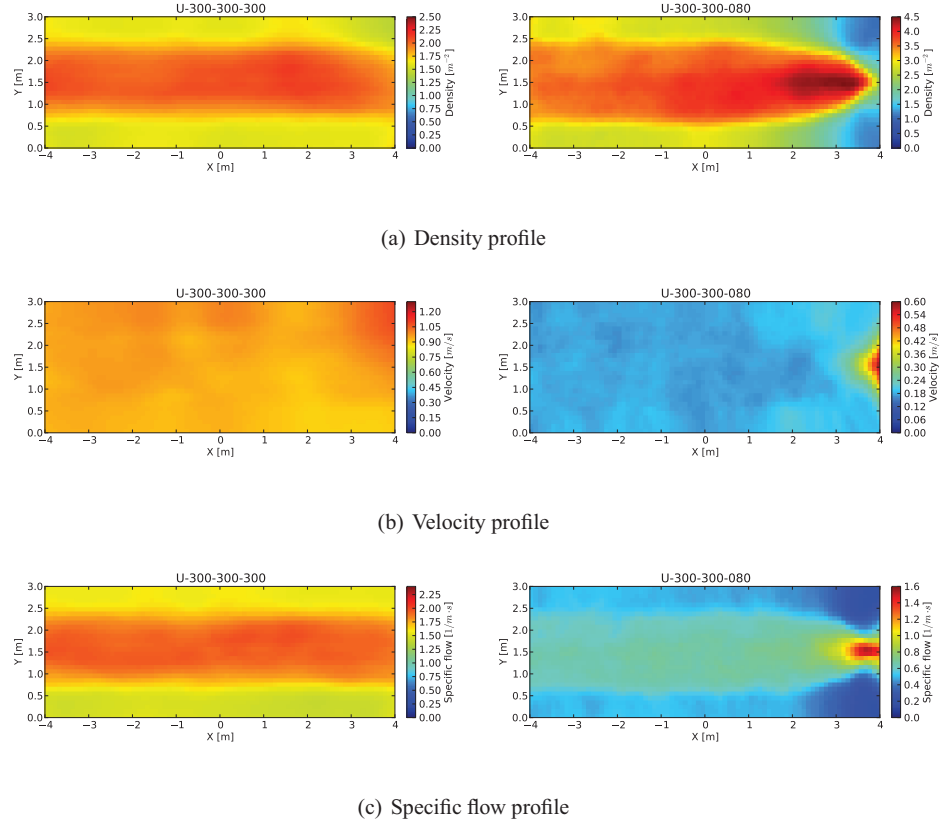


Figure 4.2: Spatiotemporal profiles of unidirectional flow for different exit widths

sensitivity of the quantities to other factors. Figure 4.1 shows the density, velocity and specific flow profiles of unidirectional flow at low and high densities for  $b_{\text{cor}} = 3.0 \text{ m}$ . The mean densities for experiment U-100-300-300 and U-240-300-300 are around  $0.5 \text{ m}^{-2}$  and  $2.0 \text{ m}^{-2}$  respectively.

From the density profile, it can be seen that the walls have strong influence on the density distribution not only for low density but also for high density situation. There are low density zones with width of  $0.5 \text{ m}$  approximately near the both walls. The higher the

density in the corridor is, the clearer the effect is. We call it **boundary effect** since the calculated variable values are influenced by the distribution of measurement points to the boundary of geometries. Somewhat differently, this effect seems to have no influence on the distribution of the velocity which is homogeneous in the corridor along transverse direction in the profiles.

Besides, we study the effects of exit forms on the distribution of density, velocity and specific flow. We compare the profiles from experiment U-300-300-300 and U-300-300-080, as shown in Figure 4.2. For the former, the width of exit is the same with corridor. While for the latter it is smaller than the corridor, which becomes a bottleneck. Besides the boundary effect, the exit effect also displays from this comparison. When the exit is smaller, the density increases gradually along the movement direction to the exit. The distribution of density along this direction is not uniform any more and the high density propagates backward from exit. The details of these phenomena will be studied in Section 4.1.2.

Figure 4.3 compares the profiles obtained from experiments in corridors with different widths ( $b_{\text{cor}} = 1.8 \text{ m}$ ,  $2.4 \text{ m}$  and  $3.0 \text{ m}$ ). The boundary effect exists for all widths. However, its influence seems to depend on the width. The density and velocity distributions along movement direction are not uniform in narrow corridor. In the area near the entrance the densities are higher and the velocities are lower. On the contrary, the specific flow stays uniform along movement direction and exhibits the boundary effect for all widths.

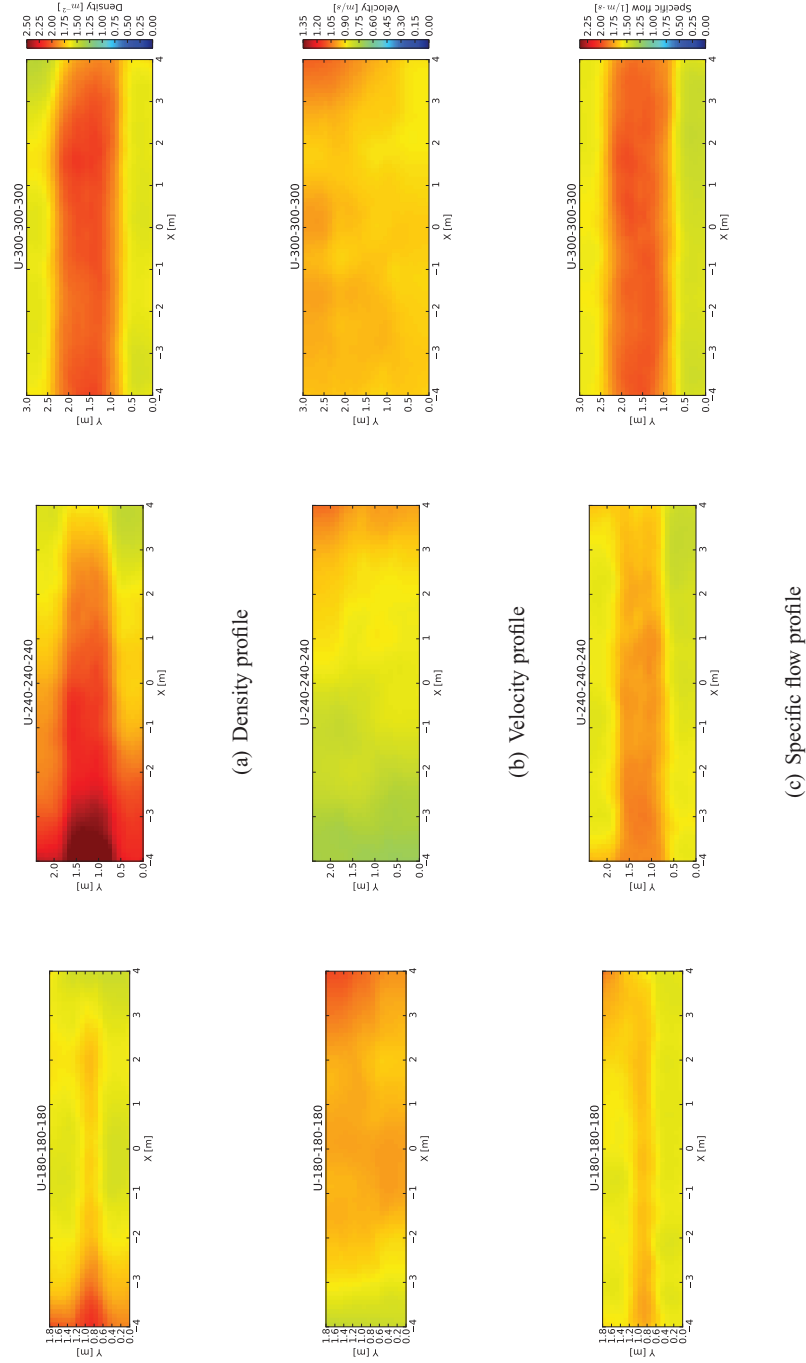


Figure 4.3: Spatiotemporal profiles of unidirectional flow for different corridor widths

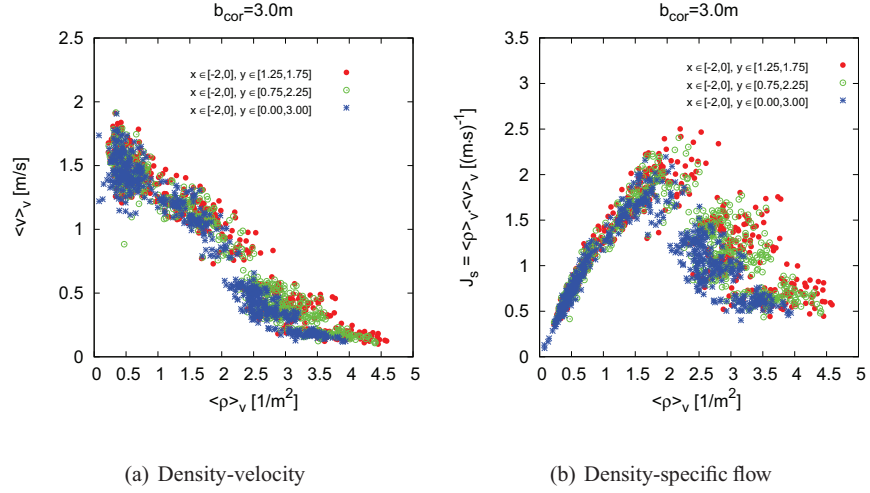


Figure 4.4: Effect of the size of the measurement area on the fundamental diagram.

From the above analysis, the profiles show that the measurements of density and velocity are sensitive to the size and location of the measurement area. In particular, the boundary effect influences the determination of the density obviously. This raises the question whether the size and location influence the relationship between density, velocity and specific flow. If so, it becomes incomparable for different results if the size and position of the measurement area and the geometry are not clearly specified.

#### 4.1.2 Size and position of the measurement area

The analysis in Section 4.1.1 indicates that the size and location of measurement area could influence the quantities of pedestrian dynamics including density, velocity etc.. In this section, we investigate their effect on the fundamental diagram of unidirectional pedestrian flow quantitatively.

As shown in Figure 4.4, we study the influence of the size of the measurement on the

## Fundamental diagram analysis

---

fundamental diagram. Three areas,  $1 \text{ m}^2$ ,  $3 \text{ m}^2$  and  $6 \text{ m}^2$ , located at  $x \in [-2, 0]$  but with different ranges of width  $y$ , are chosen for the experiments in 3.0 m corridor. It is shown that the fundamental diagrams differ especially at high density condition but have no noticeable discrepancies for  $\rho < 2.0 \text{ m}^{-2}$ . For  $\rho > 2.0 \text{ m}^{-2}$ , the spreading of the densities increases with decreasing size of measurement area. The size of measurement area mainly influences the fluctuation of density but not the shape of fundamental diagram. This result can be attributed to the boundary effect which influences not only the mean value and standard deviation but also the shape of the fundamental diagram.

Measurement area	$\langle \rho \rangle_v [\text{m}^{-2}]$	$\langle v \rangle_v [\text{m/s}]$
$x \in [-4, -2], y \in [0.0, 3.0]$	$3.23 \pm 0.33$	$0.18 \pm 0.03$
$x \in [-3, -1], y \in [0.0, 3.0]$	$3.26 \pm 0.30$	$0.18 \pm 0.03$
$x \in [-2, 0], y \in [0.0, 3.0]$	$3.31 \pm 0.30$	$0.18 \pm 0.02$
$x \in [-1, 1], y \in [0.0, 3.0]$	$3.37 \pm 0.25$	$0.18 \pm 0.02$
$x \in [0, 2], y \in [0.0, 3.0]$	$3.31 \pm 0.19$	$0.18 \pm 0.03$
$x \in [1, 3], y \in [0.0, 3.0]$	$3.12 \pm 0.22$	$0.19 \pm 0.03$
$x \in [2, 4], y \in [0.0, 3.0]$	$2.52 \pm 0.19$	$0.22 \pm 0.05$

Table 4.1: Measured density and velocity from different measurement areas along x-direction (U-300-300-080)

Since the boundary effect is larger for higher density, we use experiment U-300-300-080 to study the effect the size and position of measurement area respectively. The ranges of the variation obtained from measurements area with the same size but in different positions are listed in Table 4.1 and 4.2. Along the x-direction, an area of  $2 \text{ m} \times 3 \text{ m} = 6 \text{ m}^2$  is chosen, while an area of  $2 \text{ m} \times 0.5 \text{ m} = 1 \text{ m}^2$  is selected along y-direction. For all the variations of the measurement area along the x and y direction, the velocities show no large change. But the calculated densities differ obvious especially when the location of the measurement



### Fundamental diagram analysis

---

Measurement area	$\langle \rho \rangle_V [\text{m}^{-2}]$	$\langle v \rangle_V [\text{m/s}]$
$x \in [-2, 0], y \in [2.5, 3.0]$	$2.82 \pm 0.31$	$0.18 \pm 0.05$
$x \in [-2, 0], y \in [2.0, 2.5]$	$3.49 \pm 0.32$	$0.18 \pm 0.04$
$x \in [-2, 0], y \in [1.5, 2.0]$	$3.77 \pm 0.33$	$0.18 \pm 0.03$
$x \in [-2, 0], y \in [1.0, 1.5]$	$3.66 \pm 0.49$	$0.18 \pm 0.03$
$x \in [-2, 0], y \in [0.5, 1.0]$	$3.32 \pm 0.66$	$0.18 \pm 0.03$
$x \in [-2, 0], y \in [0.0, 0.5]$	$2.79 \pm 0.50$	$0.18 \pm 0.04$

Table 4.2: Measured density and velocity from different measurement areas along y-direction (U-300-300-080)

area changes along y-direction. To understand this point in detail, we study the density and velocity distribution along transverse direction in the runs U-180-180-095, U-240-240-130 and U-300-300-160, because the mean densities ( $2.47 \pm 0.44 \text{ m}^{-2}$ ,  $2.50 \pm 0.47 \text{ m}^{-2}$ ,  $2.54 \pm 0.44 \text{ m}^{-2}$ ) and velocities ( $0.22 \pm 0.05 \text{ m/s}$ ,  $0.27 \pm 0.05 \text{ m/s}$ ,  $0.33 \pm 0.05 \text{ m/s}$ ) of them in stationary state are nearly the same for the measurement area  $x \in [-2, 0]$  and  $y \in [0, b_{\text{cor}}]$ . However, the results in Figure 4.5 show some other properties if the small measurement area  $0.1 \text{ m} \times 2 \text{ m}$  is chosen. The velocity of the crowd seems to be constant in any place of corridor. While the ranges of densities increase with the increase of corridor width and the density shows a bell-shaped distribution along transverse direction. Further, there exist a constant region where the densities is nearly constant. The range of the region is positively correlated with the corridor width. Even the mean value of densities for a whole corridor is the same, the maximum density is larger and the minimum density for wide corridors is smaller than that of narrow corridors.

Thus, it can be said that the size and position of measurement surely affect the fundamental diagram of pedestrian flow. This influence is obvious especially on crowd density and mainly arises from the boundary effect. To make comparison, we will choose the mea-

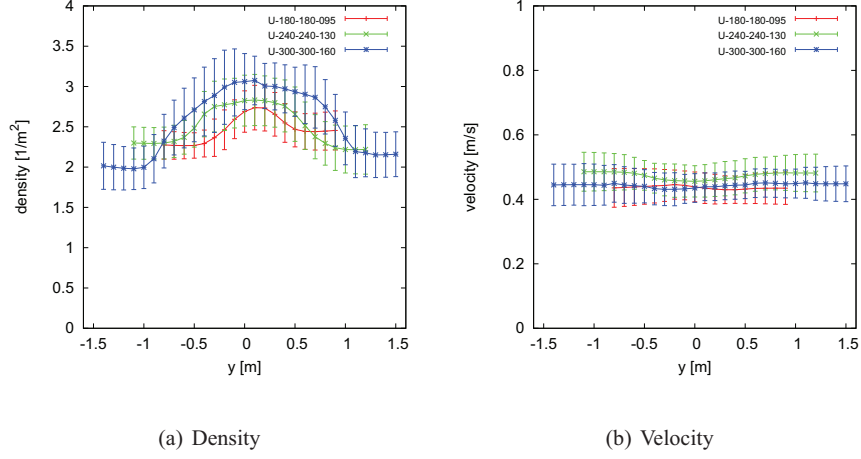


Figure 4.5: Density and velocity distribution along transverse direction in corridor.

surement area by considering the boundary effect in the next studies. That is, the rectangle in corridor with a length of 2 m and the width of the corridor will be selected as measurement area in different runs of experiments.

### 4.1.3 Specific flow concept

In general it is assumed that for a given facility (e.g. corridors, stairs, doors) the specific flow  $J_s$  is independent on width  $b$ . This implies that the fundamental diagrams  $J(\rho)$  for different  $b$  merge into one universal diagram for the specific flow  $J_s$ . We call this the specific flow concept. From the above analysis, however, the boundary effect surely affects the crowd density and specific flow in corridor. Thus, it is necessary to check whether the specific flow concept is applicable or not.

Figure 4.6 shows the relationship between density, velocity and specific flow obtained from the Voronoi method. The fundamental diagrams of unidirectional pedestrian flow in the same type of corridor but with three different widths are compared. It can be seen that

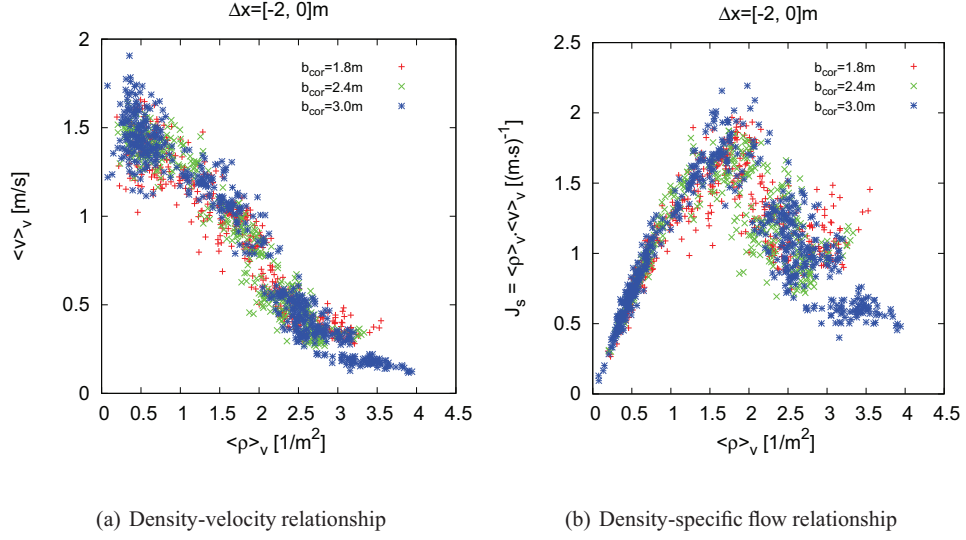


Figure 4.6: Comparison of the fundamental diagram for different corridor widths.

they agree well with each other. The specific flow in the corridors is independent on the corridor width. At about  $\rho = 2.0 \text{ m}^{-2}$ , the specific flow reaches the maximum value which is named the capacity of a facility. This result is in conformance with Hankin's findings [18]. He found that above a certain minimum of about 4 ft (about 1.22 m) the maximum flow in subways is directly proportional to the width of the corridor. Our results seem to support the specific flow concept in the range of densities reached in the experiment.

According to the assumptions in most handbooks, a congestion occurs in corridor when the flow in the corridor exceeds the capacity of exit. Under this situation, the flow rate through exit is either its capacity or  $J_s(D_{\max})$ . We calculate the mean flow rate of pedestrians passing the line  $x = 0 \text{ m}$  ( $J_{\text{cor}}$ ) and  $x = 4.0 \text{ m}$  ( $J_{\text{exit}}$ ) in the corridor over 10 s using **Method A** for the runs of the experiment with  $b_{\text{exit}} < b_{\text{cor}}$ .  $J_{\text{cor}} > J_{\text{exit}}$  seems always correct as shown in Table 4.3 and Figure 4.7.

## Fundamental diagram analysis

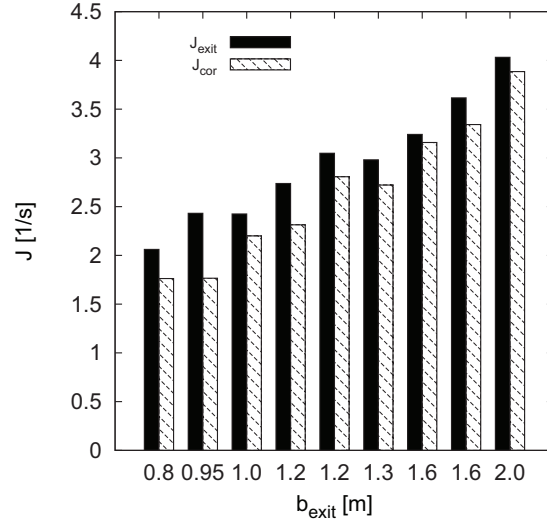


Figure 4.7: Comparison of flow rate through the corridor and the exit under congestion situations.

$b_{\text{cor}}$ [m]	Name	$b_{\text{exit}}$ [m]	$J_{\text{cor}}$ [1/s]	$J_{\text{exit}}$ [1/s]
1.8	U-180-180-070	0.70	1.881	1.626
	U-180-180-095	0.95	2.432	1.766
	U-180-180-120	1.20	2.738	2.314
	U-180-180-180	1.80	2.733	2.683
2.4	U-240-240-100	1.00	2.425	2.200
	U-240-240-130	1.30	2.981	2.722
	U-240-240-160	1.60	3.241	3.158
	U-240-240-240	2.40	3.975	3.791
3.0	U-300-300-080	0.80	2.061	1.762
	U-300-300-120	1.20	3.048	2.807
	U-300-300-160	1.60	3.616	3.342
	U-300-300-200	2.00	4.031	3.885
	U-300-300-300	3.00	4.820	5.035

Table 4.3: Comparison of flow rate for congestion conditions at  $x = 0$  m and  $x = 4$  m

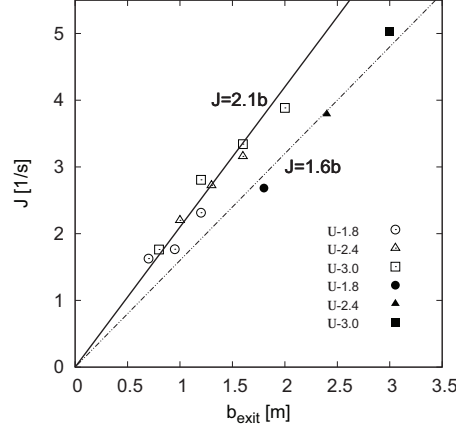


Figure 4.8: Relationship between flow rate  $J_{\text{exit}}$  and width  $b_{\text{exit}}$ . The open points are obtained from the runs for  $b_{\text{cor}} > b_{\text{exit}}$ . While the solid points are the maximum flow rate in corridor observed in the experiments.

We further study the relationship between the flow rate  $J_{\text{exit}}$  and the opening width  $b_{\text{exit}}$ . From Figure 4.8, it shows nearly linear relationships  $J = 2.1 \cdot b$  for opening and  $J = 1.6 \cdot b$  for the corridor exist. Note that the solid points in the figure are the maximum flow rates in the corridor that have been observed in the experiments. The open points are obtained from the runs for  $b_{\text{cor}} > b_{\text{exit}}$ . From the result it seems that the specific flow through the opening is  $2.1 (\text{m} \cdot \text{s})^{-1}$  when congestions occur in front of the opening. The same relationship  $J = 1.9 \cdot b$  is also obtained for the bottleneck in [59]. If all the maximum values of flow we obtained from our experiments are the capacity  $C$  of the facilities, we could conclude that it should be  $C_{\text{opening}} > C_{\text{bottleneck}} > C_{\text{corridor}}$ . This does not agree with most handbooks like SFPE which do not distinguish between the fundamental diagrams of these three types of facilities. However, with the current setup of the experiments we cannot decide whether it

is the capacity of the opening or  $J_s(D_{\max})$ . Besides, we even could not check whether the capacity of the opening is larger than that of the corridor or not. That is because we do not know whether higher specific flow can be observed in the condition of  $b_{\text{cor}} = b_{\text{exit}}$ .

#### 4.1.4 Interpretation in terms of boundary-induced phase transitions

From Figure 3.12(b) and 3.12(d), we can see that a discontinuity of the fundamental diagram occurs at  $\rho \approx 2 \text{ m}^{-2}$ , separating the function  $J_s(\rho)$  in a region  $\rho < 2 \text{ m}^{-2}$  with negative curvature and a region  $\rho > 2 \text{ m}^{-2}$  with positive curvature. Moreover, for **Method D** a gap occurs around  $v = 0.7 \text{ m/s}$ . This transition is also found in the experiments with  $b_{\text{cor}} = 2.4 \text{ m}$  and  $b_{\text{cor}} = 3.0 \text{ m}$ . The fundamental diagram changes qualitatively when the width of the exit  $b_{\text{exit}}$  is modified. The modification of the exit width was necessary to achieve high densities. However, it seems that this change in the setup of the experiment causes a significant change in the flow-density relation. This point becomes obvious in the velocity-density relation, especially in Figure 3.11(d) which is obtained from **Method D**. Although the measurement area in the corridor is 4 m away from the exit, the influence of the variation of the exit on the fundamental diagram is observable. The decrease of  $b_{\text{exit}}$  will increase the density in the corridor and limit the outflow of pedestrians. However, it also leads to a discontinuity in the fundamental diagram.

This can be interpreted in terms of the well-established theory of boundary-induced phase transitions [36, 54]. In nonequilibrium systems phase transitions (in the bulk) can be induced by changing the boundary conditions, generically input and output rates in case of transport systems. A mesoscopic theory has been developed which allows to derive the phase diagram of an open system (allowing input and output of particles at the boundaries,

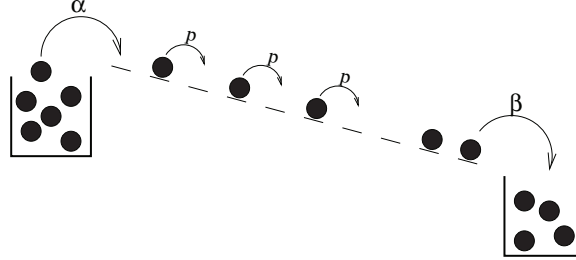


Figure 4.9: Open system with particle input at the left boundary with rate  $\alpha$  and particle output at the right boundary with rate  $\beta$ .

see Figure 4.9) from the fundamental diagram of the periodic system [33]. This theory even makes quantitative predictions on the basis of an extremal principle [49].

The phase diagram as function of the boundary rates  $\alpha$  and  $\beta$  has a generic structure. The number of phases observed depends only on the number of local maxima in the fundamental diagram. For generic traffic systems it has only one maximum and the  $\alpha$ - $\beta$ -phase diagram consists of three phases, the high-density phase (HD), the low-density phase (LD) and the maximum current phase (MC), see Figure 4.10. When the supply rate  $\alpha$  of the particles is larger than the removal rate  $\beta$  and  $\beta < \beta_c$ , the particle extraction is the limiting process resulting in a high density phase where the current is independent of  $\alpha$ . When the particles are supplied not too fast,  $\alpha < \alpha_c$  and  $\beta > \alpha$ , a low density phase is formed which is limited by the particle supply. Here the current is independent of  $\alpha$ . There is a discontinuous phase transition along the line  $\alpha = \beta < \alpha_c$ . When particles are supplied and removed sufficiently rapidly,  $\alpha > \alpha_c$  and  $\beta > \beta_c$ , a continuous phase transition into a maximum-current phase for which transport is bulk dominated [36] occurs where the current is independent of both  $\alpha$  and  $\beta$ .

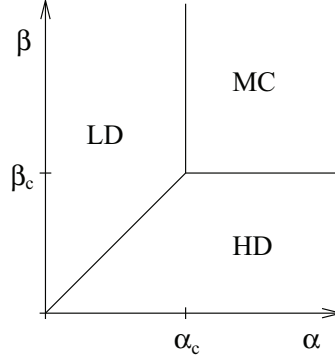


Figure 4.10: Generic form of the phase diagram for an open system with input rate  $\alpha$  and output rate  $\beta$ . In the LD phase the current has the form  $J = J(\alpha; \mathbf{p})$  and in the HD phase  $J = J(\beta; \mathbf{p})$ . In the MC phase, the current is independent of  $\alpha$  and  $\beta$  and corresponds to the maximum of the fundamental diagram:  $J = J_{\max}(\mathbf{p})$ .

The experiments in the corridor geometry can effectively be described by such a scenario. The input rate  $\alpha$  into the corridor is controlled by the width  $\mathbf{b}_{\text{entrance}}$  of the entrance whereas the output rate  $\beta$  is controlled by the width  $\mathbf{b}_{\text{exit}}$  of the exit. Therefore the  $\alpha$ - $\beta$ -phase diagram corresponds in our case to a  $\mathbf{b}_{\text{entrance}}$ - $\mathbf{b}_{\text{exit}}$ -diagram. The width  $\mathbf{b}_{\text{cor}}$  of the corridor, on the other hand, controls the maximal possible bulk flow in the system, given by the maximal flow  $J_{\max}$  in the fundamental diagram.

For the experiments with  $\mathbf{b}_{\text{exit}} = \mathbf{b}_{\text{cor}}$  the flow through the system is not limited by the exit (see Figure 3.12), corresponding to the case  $\beta > \beta_c$ . The system is then in the low-density phase. Here the flow is controlled by the inflow into the system, i.e. effectively by  $\mathbf{b}_{\text{entrance}}$ . At  $\mathbf{b}_{\text{entrance}} \approx 1.45$  m a transition into the maximum current phase can be observed (see especially Figure 3.12(a)). For  $\mathbf{b}_{\text{entrance}} = \mathbf{b}_{\text{cor}}$  and  $\mathbf{b}_{\text{exit}} < \mathbf{b}_{\text{cor}}$  the system is in the high-density phase.



## Fundamental diagram analysis

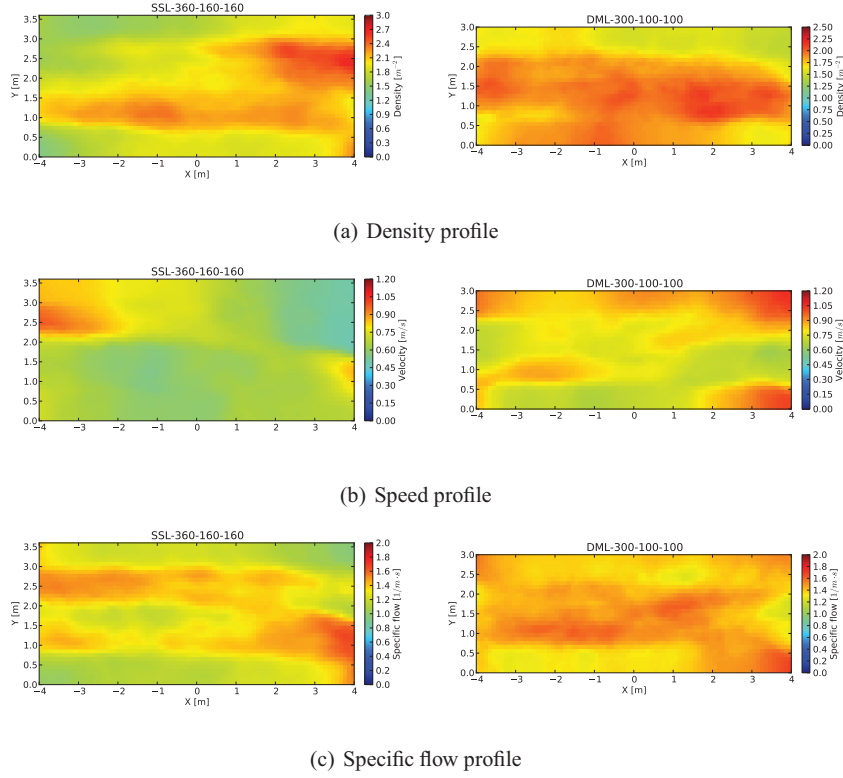


Figure 4.11: Spatiotemporal profiles of bidirectional flow

## 4.2 Bidirectional flow

In this section, the characteristics of bidirectional pedestrian flows are analyzed using the Voronoi method. As in the last section, we choose a rectangle with length of 2 m from  $x = -1$  m to  $x = 1$  m and the width of the corridor as the measurement area. The methods for the selection of the data points are the same with last section.

#### 4.2.1 Spatiotemporal profile

Figure 4.11 shows the density, speed and specific flow profile of **Stable Separated Lanes (SSL)** and **Dynamical Multi-Lanes (DML)** flow in our experiment. The space is divided into  $10\text{ cm} \times 10\text{ cm}$  small cells to measure the Voronoi density and speed. These quantities are calculated in each cell frame by frame. Note that we calculate the speed (absolute value of velocity) but not the velocity. For these profiles the average over the stationary state is calculated.

For flow with stable separated lanes, the density, speed and specific flow profiles are obviously not homogeneous. Boundary effect occurs also at the interface of the opposing streams. The densities and specific flow at the interface are smaller than that in other place. While for flow with dynamical multi-lanes, we don't observe this effect. The density and specific flow at the middle of the corridor seems larger than that near the boundary. The self-organized dynamical lanes in space and time seems to weaken the effect of the interface on pedestrian movement. The profiles of this kind of flow are not homogenous anymore either. The influence of dynamical lanes on the profile can be seen clearly.

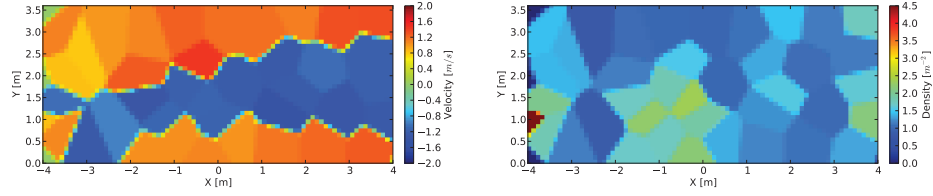
#### 4.2.2 Lane formation

Lane formation, as one of the most important phenomena in bidirectional flows, occurs because pedestrians follow other persons moving in the same direction to minimize conflicts with persons moving in the opposite direction. Lanes that emerge in this way could be stable (**SSL**) and unstable (**DML**) in time.

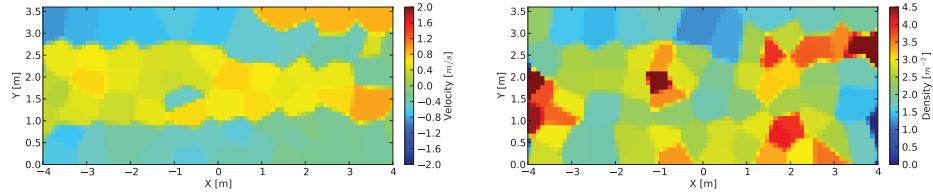
The recognition and representation of the lanes has been investigated in different ways, e.g. the cluster analysis method introduced by Hoogendoorn [23], the bond index method

## Fundamental diagram analysis

---



(a)  $t = 222$  frame = 13.875 sec



(b)  $t = 822$  frame = 51.375 sec

Figure 4.12: Representation of lane formation using profile. These four profiles are from experiment BFR-DML-360-160-160 at different frames (times).

of Yamori [70] et al. as well as the laning order parameter used to detect lanes in driven colloidal systems [52]. Using the Voronoi method, we are able to calculate the integrated velocity over small measurement regions ( $10 \text{ cm} \times 10 \text{ cm}$ ). In this way, the velocity distribution over the whole space can be obtained. Figure 4.12 shows the velocity and density profiles of BFR-DML-360-160-160 for two different times. We use different colors to indicate the value of the velocity and density and thus to determine the number of lanes in the corridor from the velocity profiles. The velocity profiles seem to be a good way to display the lane formation in bidirectional streams. In comparison, density profiles don't have such ability to show the lanes clearly. However, it is possible for density profiles to show some other information such as crowded and dangerous spots.

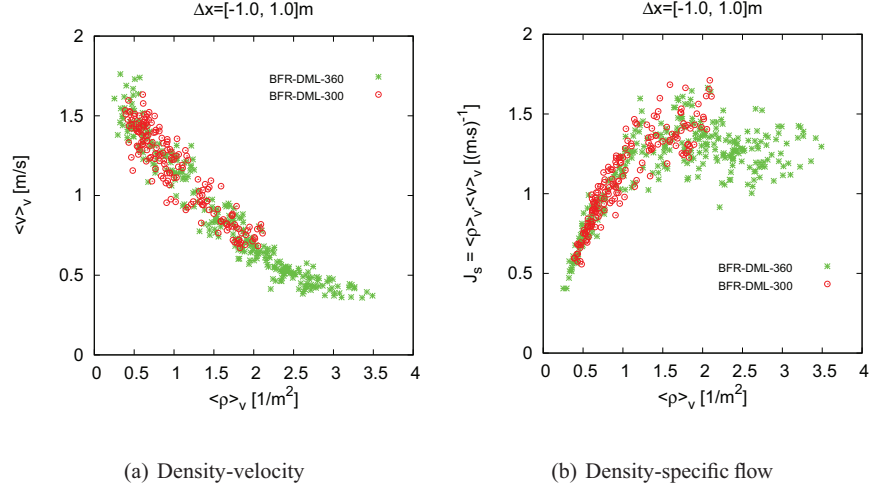


Figure 4.13: Comparison of fundamental diagram of DML flow at different width of corridors

### 4.2.3 Specific flow concept

The formation of lanes decreases the number of conflicts among the opposing moving pedestrians. The dynamical lanes however are likely to increase the boundary effect, which is larger in bidirectional flow than that in unidirectional flow. It is not sure whether the specific flow concept is applicable to bidirectional pedestrian flow. For this reason, we study the influence of the corridor width on the fundamental diagram. The BFR-DML flow experiments were carried out for two widths  $b_{\text{cor}} = 3.0$  m and  $b_{\text{cor}} = 3.6$  m respectively. By comparing the fundamental diagram from these experiments in Figure 4.13, it is found that they are in good agreement in the observed range of density. From Figure 4.13(b), it can be seen that the specific flow reaches its maximum of  $1.5 \text{ (m} \cdot \text{s)}^{-1}$  at a density of  $\rho = 2.0 \text{ m}^{-2}$  and then is nearly constant until  $\rho = 3.5 \text{ m}^{-2}$ .

The results show that the specific flow concept is also applicable to bidirectional flow

at least for  $\rho < 2.0 \text{ m}^{-2}$ , due to the limitation of the time resources during the experiments only densities  $\rho < 2.0 \text{ m}^{-2}$  are realized for  $b_{\text{cor}} = 3.0 \text{ m}$ .

#### 4.2.4 Comparison of SSL and DML flow

In bidirectional pedestrian flow, especially for **DML** type, head-on conflicts and cross-directional conflicts occur from time to time. These conflicts could be less in **SSL** flow than in **DML** flow. It would be interesting to know whether they have positive, negative or no influence on the flow rate in bidirectional flow. To investigate this effect we compare the fundamental diagram of **SSL** and **DML** flow for  $b_{\text{cor}} = 3.6 \text{ m}$ . As shown in Figure 4.14, it can be seen that the fundamental diagrams of these two types of bidirectional flow are consistent at least for densities  $\rho < 2.0 \text{ m}^{-2}$ . The lower degree of ordering in dynamical multi-lanes (**DML**) has no effect on the fundamental diagram which agrees with the findings of Older [48]. This might be taken as an indication that head-on conflicts in multi-lanes have the same influence as the conflicts at the borders in stable separated lane flow on the fundamental diagram. On the other hand, the self-organized lanes increase the order and make pedestrian movement smoother. Whether the degree of ordering has an influence on the fundamental diagram at higher densities can not be decided from our data.

#### 4.2.5 Comparison of BFR and UFR flow

The flow ratio of the opposing pedestrian streams is another factor that is worth studying. Under unbalanced conditions (**UFR**), pedestrians from the direction with high flow ratio may dominate and restrain the movement of pedestrians from the opposing direction. To study the influence of this interaction, we compare the fundamental diagrams of **BFR**– and

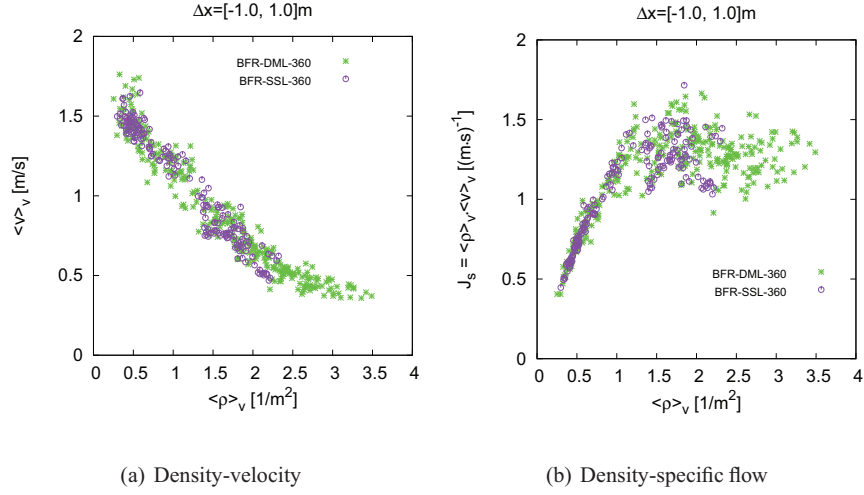


Figure 4.14: Comparison of the fundamental diagram of SSL and DML flow.

UFR – DML flow in the corridor with width  $b_{\text{cor}} = 3.0$  m. Due to the limitation of the number of runs, only data for  $\rho < 2.0$  m<sup>-2</sup> have been obtained. As shown in Figure 4.15, the asymmetry of bidirectional flow does not affect the fundamental diagrams, at least for DML flows and densities  $\rho < 2.0$  m<sup>-2</sup>. Although it can not be excluded that a higher flow ratio will dominate the whole movement, for the flow ratios in our experiments it does not affect the total flow rate in the corridor.

### 4.3 Merging flow

T-junction is a common but complex geometry in building. In this kind of structure, bottleneck flow, merging flow or split flow could take place. In this section, we will analyze merging of pedestrian stream at a T-junction experimentally. As in the other sections, we use the Voronoi method and apply the same approach for the selection of the measurement area and data points.

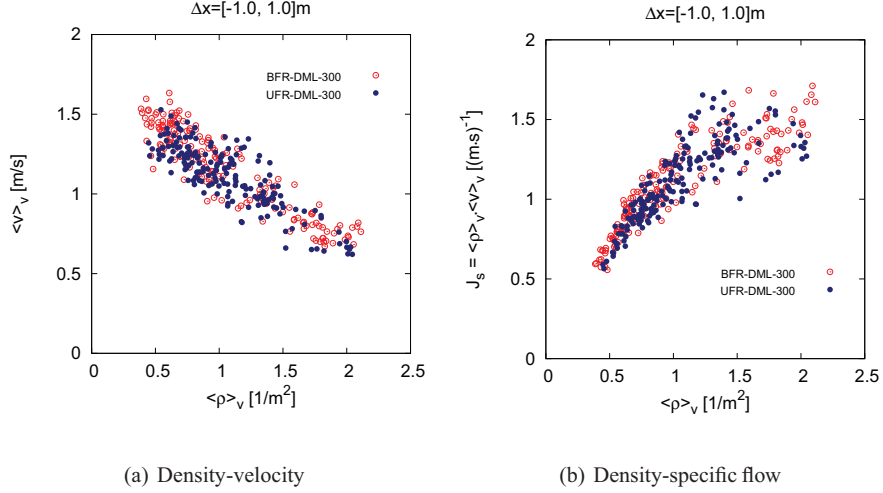
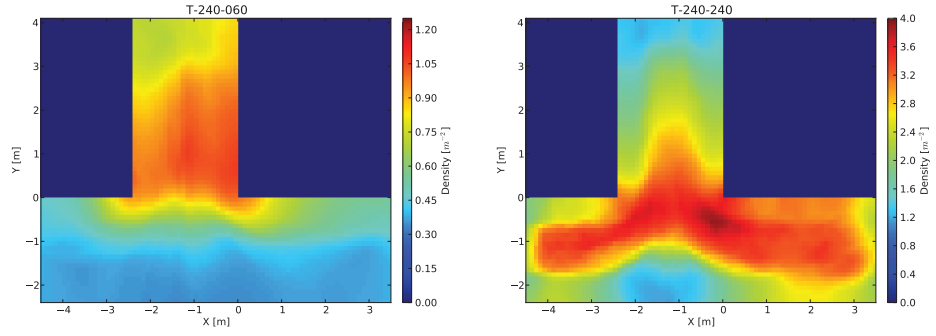


Figure 4.15: Comparison of the fundamental diagram of BFR and UFR flow.

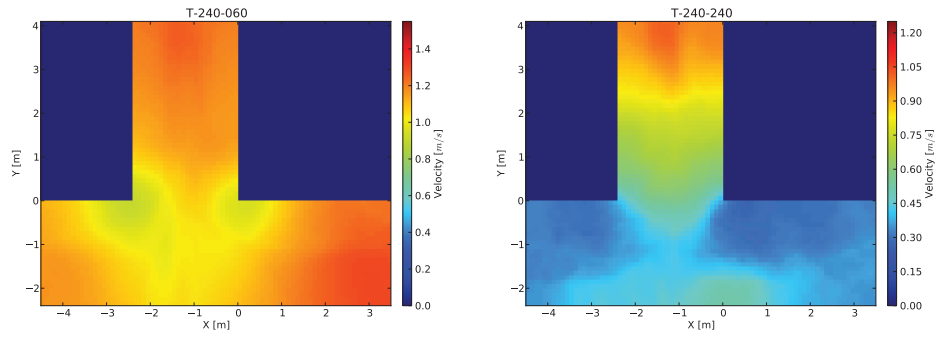
### 4.3.1 Spatiotemporal profile

Figure 4.16 shows the profiles for two runs of the experiments under the situations of low density (T-240-060) and high density (T-240-240), respectively. These profiles provide new insights into the spatiotemporal dynamics of the motion and the sensitivity of the quantities to other potential factors. The density distribution in a T-junction is not homogeneous both for low and high density situations. For the former, the higher density region is located in the main stream after merging. For the latter, the higher density region appears near the junction and the lowest density region locates at a small triangle area, where the left and right branches begin to merge. For both of the two situations, the densities in the branches are not uniform and are higher over the inner side, especially near the corners. In other words, pedestrians prefer to move along the shorter and smoother path. Moreover the density profile shows obvious boundary effects at high density situations. The spatiotemporal variation of the velocity is different. At low density situations, the velocity profile is

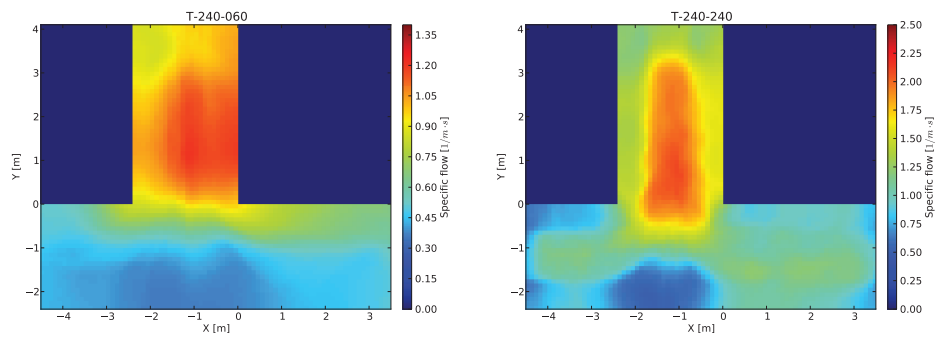
## Fundamental diagram analysis



(a) Density profile



(b) Velocity profile



(c) Specific flow profile

Figure 4.16: Spatiotemporal profiles of T-junction flow



nearly homogeneous all over the T-junction except close to the corners. Pedestrians move at free velocity and slow down round the corners. For high densities condition, the velocity distribution is no longer uniform. The velocity of main stream is obviously higher than that in the branches. Boundary effects do not occur and the velocities after merging increase along the movement direction persistently. By comparison of the specific flow profiles in the two different situations, the highest flow regions in both cases are observed at the center of the main stream after the merging. The region extends further into the area where the two branches start to merge. This indicates that the merging process in front of the exit corridor leads to a flow restriction. Causes for the restriction of the flow must be located outside the region of highest flow.

These profiles demonstrate that density and velocity measurements are sensitive to the size and location of the measurement area. For the comparison of measurements (e.g. for model validation or calibration) it is necessary to specify precisely the size and position of the measurement area.

### 4.3.2 Branch and main stream

In Figure 4.17, we compare the fundamental diagrams of pedestrian merging flow in T-junction with corridor width  $b_{\text{cor}} = 2.4 \text{ m}$ . The data assigned with 'T-left' and 'T-right' are measured in the areas where the streams prepare to merge, while the data assigned with 'T-front' are measured in the region where the streams have already merged. The locations of these measurement areas are documented in Table 4.4. For easing of comparison, we choose these measurement areas with the same size ( $4.8 \text{ m}^2$ ). One finds that the fundamental diagrams of the left and right branches match well. It means that the right or left

## Fundamental diagram analysis

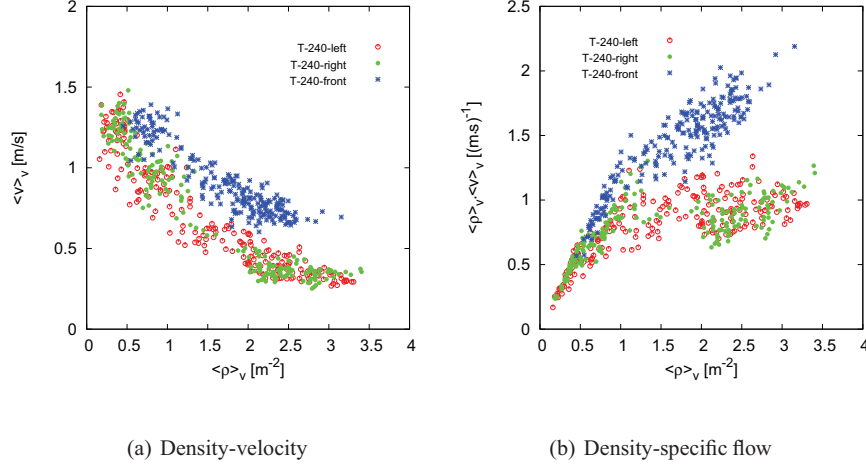


Figure 4.17: Comparison of the fundamental diagram of merging flow in different parts of T-junction

turning of the stream dose not have influence on the fundamental diagram. However, for densities  $\rho > 0.5 \text{ m}^{-2}$  the velocities in the 'right' and 'left' part of the T-junction (T-left and T-right) are significantly lower than the velocities measured after the merging of the streams (T-front). This discrepancy becomes more distinct in the relation between density and specific flow. In the main stream (T-front), the specific flow increases with the density  $\rho$  up to  $2.5 \text{ m}^{-2}$ . While in the branches, the specific flow nearly remains constant for density  $\rho$  between  $1.5 \text{ m}^{-2}$  and  $3.5 \text{ m}^{-2}$ . Thus, there seems to be no unique fundamental diagram which describes the relation between velocity and density for the complete system.

For this difference we can only offer speculate about the causes. One is based on behavior of pedestrians. Congestions occur at the end of the branches where the region of maximum density appears. Pedestrians stand in a jam in front of the merging and can not perceive where the congestion disperse or whether the jam lasts after the merging. In such a situation it is questionable whether an urge or a push will lead to a benefit. Thus an optimal

Measurement area	Range
T-240-Left	$x \in [-4.5, -2.5], y \in [-2.4, 0]$
T-240-Right	$x \in [1.0, 3.0], y \in [-2.4, 0]$
T-240-Front	$x \in [-2.4, 0], y \in [1.0, 3.0]$
T-300-Right	$x \in [0.5, 2.5], y \in [-3.0, 0]$
T-300-Front	$x \in [-3.0, 0], y \in [1.0, 3.0]$

Table 4.4: The location of measurement area in T-junction.

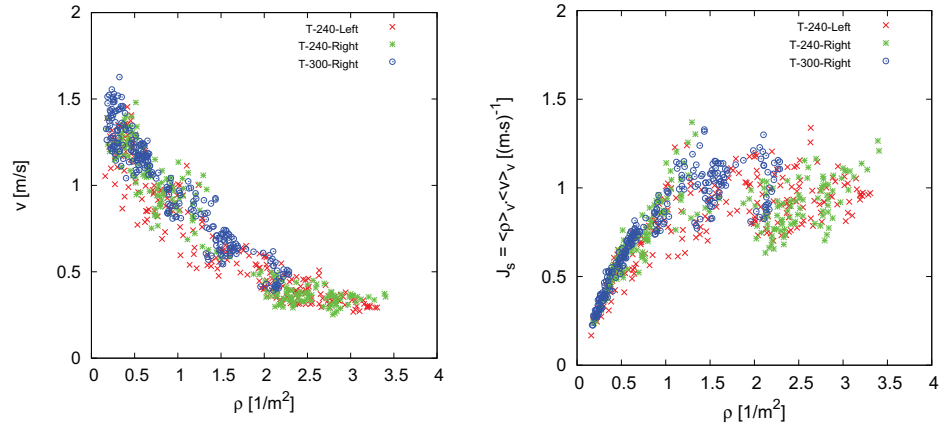
usage of the available space becomes unimportant. Otherwise, the situation totally changes if the location of dissolution becomes apparent. Then a certain urge or an optimal usage of the available space makes sense and could lead to a benefit. In this situation, pedestrians would prefer to move in a relatively active way and pick up their pace. This might be the reason why the velocities after merging are higher than that in front of merging at the same density. Whether this explanation is plausible could be answered by a comparison of these data with experimental data at a corner without the merging.

### 4.3.3 Specific flow concept

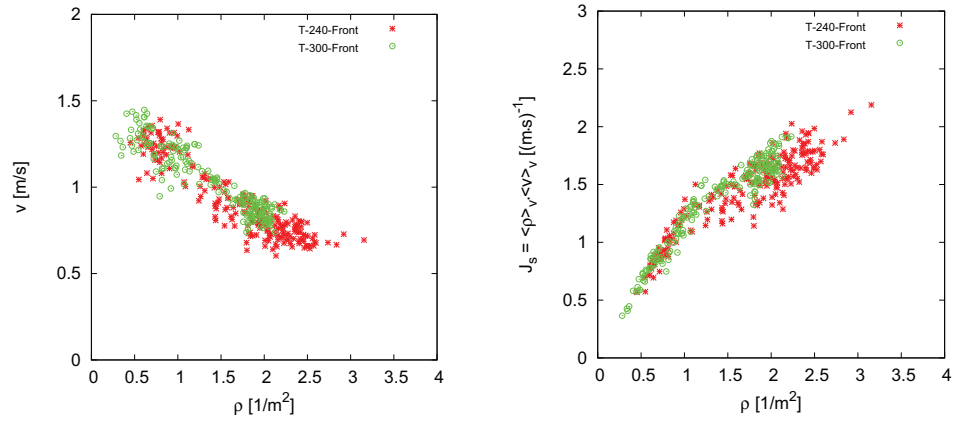
In this section, we will check whether the specific flow concept holds also for merging flows in T-junctions. The fundamental diagrams of merging flows in different corridor widths with  $b_{\text{cor}} = 2.4 \text{ m}$  and  $b_{\text{cor}} = 3.0 \text{ m}$  are calculated. We compare the results before and after merging separately. Because of the symmetry of the geometry, only the fundamental diagram of the right branch is considered for the runs with  $b_{\text{cor}} = 3.0 \text{ m}$ .

Figure 4.18 shows the results from the experiments. In the branches, the obtained maximum densities are about  $3.5 \text{ m}^{-2}$  for  $b_{\text{cor}} = 2.4 \text{ m}$  and  $2.2 \text{ m}^{-2}$  for  $b_{\text{cor}} = 3.0 \text{ m}$ . While behind merging, the maximum densities are  $3.3 \text{ m}^{-2}$  for  $b_{\text{cor}} = 2.4 \text{ m}$  and  $2.2 \text{ m}^{-2}$  for

## Fundamental diagram analysis



(a) In front of merging



(b) Behind merging

Figure 4.18: Comparison of the fundamental diagram of T-junction with different corridor width

$b_{\text{cor}} = 3.0 \text{ m}$ . Thus, only the results for  $\rho < 2.2 \text{ m}^{-2}$  can be compared. From the plots it can be seen that not only in front of merging but also behind merging the specific flow concept works well in the observed ranges of density. The specific flow in T-junction is directly proportional to the width of the corridor in corresponding places, although the maximum specific flows before and after the merging are different.

## 4.4 Comparison of different types of flows

In previous sections, we have analyzed three different types of pedestrian flow in straight corridors and T-junctions. Some characteristics of uni-, bidirectional and merging pedestrian flow have been obtained. With these data it is possible to determine the difference between them.

### 4.4.1 Uni- and bidirectional flows

In Figure 4.19, we compare the fundamental diagram of uni- and bidirectional flows. Since the corridor width and the forms of bidirectional flow have little influence on the fundamental diagram, we are free to choose the experiments with a larger range of density (experiment U-300 and BFR-DML-360), to compare the characteristics of them. One of the remarkable things is that the data of the unidirectional flow for  $\rho > 2.0 \text{ m}^{-2}$  are obtained by slight change of the experiment setup. To reach densities  $\rho > 2.0 \text{ m}^{-2}$  in an unidirectional experiment, a bottleneck at the end of the corridor is formed. We discussed in section 4.1.4 that the decrease of the outflow is induced by changing the boundary conditions. This may limit the comparability of fundamental diagrams for  $\rho > 2.0 \text{ m}^{-2}$ .

Figure 4.19(a) shows the relationship between density and velocity for these two kinds

## Fundamental diagram analysis

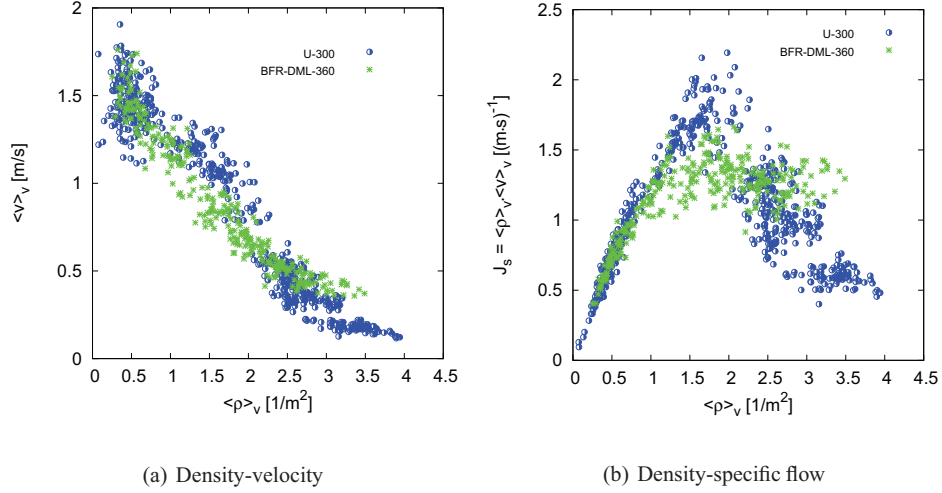


Figure 4.19: Comparison of the fundamental diagrams of unidirectional flow and bidirectional flow

of flow. At densities of  $\rho < 1.0 \text{ m}^{-2}$ , no significant difference exists. For  $\rho > 1.0 \text{ m}^{-2}$ , however, the velocities for unidirectional flows are larger than that of bidirectional flows. The difference between the two cases becomes more apparent in the flow-density diagram (Figure 4.19(b)) where a qualitative difference can be observed. In the bidirectional case a plateau is formed starting at a density  $\rho \approx 1.0 \text{ m}^{-2}$  and the flow becomes almost independent of the density. Such plateaus are typical for systems which contain 'defects' which limit the flow and have been observed e.g. on bidirectional ant trails [28] where they are a consequence of the interaction of the ants. In our experiments the defects are conflicts of persons moving in the opposite direction. These conflicts only happen between two persons but the reduction of the velocity influences those following.

This difference in the fundamental diagrams implies that a SSL flow should not be interpreted as two unidirectional flows. Although the self-organized lanes can decrease the

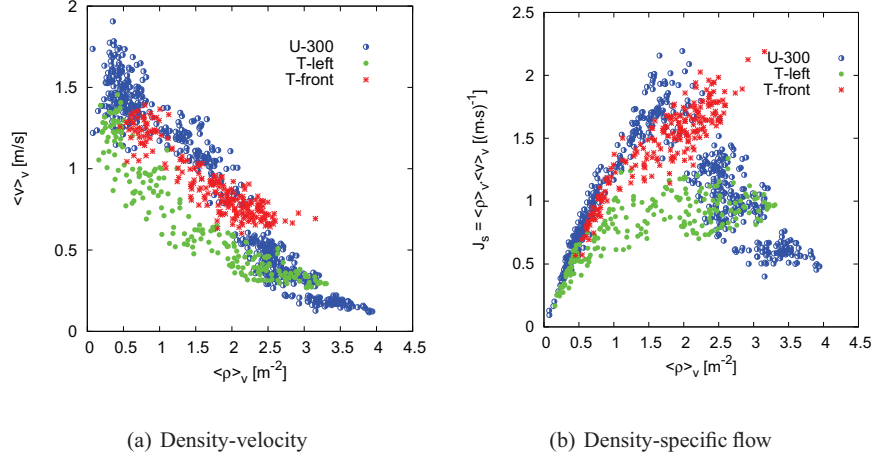


Figure 4.20: Comparison of the fundamental diagram between unidirectional and merging flow.

head-on conflicts, interactions between the opposing streams are still relevant.

#### 4.4.2 Unidirectional and merging flows

In this section, we compare the fundamental diagrams for unidirectional flow in straight corridor and merging flow in a T-junction. Due to the availability of the specific flow concept, we choose the data (T-240 and U-300) with a large range of the density to compare.

Figure 4.20 shows the results obtained from the experiments using the Voronoi method. The data of T-front and U-300 seem comparable, while they are obviously different from that of T-left. In section 4.3.2 the difference between branch and main stream has been discussed. Thus we mainly analyze the similarities and differences between T-front and U-300. No matter in the relation of density-velocity or density-specific flow, the data points of T-front are a little bit lower than that of U-300 for the density of  $\rho < 2.0 \text{ m}^{-2}$ . This difference becomes clearer with the increase of density. Actually, pedestrian flow after the

merging in the T-junction can be considered as unidirectional flow in an open corridor. Specifically pedestrian movement in T-junction includes right or left turn action around the corner in T-junction. As shown in Figure 4.16, the velocities at the corner is obviously slower than in other area. The turning action could restrict the moving speed of pedestrians. Behind the corner, pedestrian starts to accelerate and the speed increases along the movement direction. Due to the setup of the experiments, the measurement areas are located in the acceleration area but not in stability area. While the acceleration is density-dependent which is also reflected in Figure 4.16. Thus, the difference becomes easy to understand.

Besides, another point is also worth mentioning. The velocities in T-front are higher than that obtained from U-300 obviously for  $2.0 \text{ m}^{-2} < \rho < 3.0 \text{ m}^{-2}$ . Without considering the data of U-300, the specific flow of T-front seems increasing consistently with the density until  $2.5 \text{ m}^{-2}$  or  $3.0 \text{ m}^{-2}$  in the observed range of density. If so, it indicates that the density where the specific flow reaches maximum could be larger than  $2.0 \text{ m}^{-2}$  obtained in U-300. On the other hand, these data points could also be considered to agree with the jamming phase of the fundamental diagram of U-300. To know which statement is correct, the data at higher density are necessary for straight corridors without exit narrowing.



# **Chapter 5**

## **Conclusion and outlook**

This study is aimed to investigate the factors that influence the fundamental diagram of pedestrian flows and to supply a more reliable database for facility design and model calibration. To achieve this goal, uni- and bidirectional flow in straight corridors and merging flow in T-junctions are analyzed from well-controlled laboratory experiments. The main results and limitations as well as possible directions for future research are provided in this chapter.

### **5.1 Conclusion**

As a first step of the analysis, the influences of different measurement methods on the fundamental diagram are studied. With the highly precise pedestrian trajectories obtained from video recordings of the experiments, detailed analysis on pedestrian characteristics are possible. Four different measurement methods are used in the thesis to calculate crowd density, velocity and flow and thereby to obtain the fundamental diagram. The empirical data from unidirectional flow in a corridor are used to test their effects on the fundamental

## Conclusion and outlook

---

diagram. Surprisingly, only minor differences between these four methods are found in the range of the density observed in our experiments. However, the Voronoi method is able to resolve a finer structure of the fundamental diagram compared with the other three ones. It can reduce the scatter of density and velocity and has the advantage of small fluctuation and high resolution in time and space. This enhanced measurement method permits observing the occurrence of a boundary-induced transition and are mainly used in this study.

Boundary effects are observed in the spatiotemporal profiles of uni-, bidirectional and merging flows. The specific flow concept works well for all these three types of flows at the observed density ranges in the experiments respectively. At the same density, the specific flows for different width of corridors agree fairly well with each other. The value of flow is proportional to the facility width. Especially for the bidirectional flow, different movement patterns (BFR-SSL, BFR-DML and UFR-DML flows) are observed from the experiments. No marked differences are observed from their fundamental diagram at least for density  $\rho < 2.0 \text{ m}^{-2}$ . It seems that the coordination ability of pedestrians decreases the effect of the potential head-on conflicts in multi-lanes condition. Although the fundamental diagrams are not the same in main stream and branches for merging flow in T-junction, they obey the specific flow concept well respectively.

The fundamental diagram of uni-, bidirectional and merging flow are compared with each other. It is found that the velocities in unidirectional streams are larger than that of bidirectional streams for  $\rho > 1.0 \text{ m}^{-2}$ . Correspondingly, the maximum specific flow of unidirectional streams is larger than that of bidirectional streams, where a plateau in fundamental diagram is formed starting at a density of  $\rho \approx 1.0 \text{ m}^{-2}$  and the flow becomes almost independent on the density. It indicates that the pedestrian stream with stable separated lanes cannot be treated as two unidirectional flows. The self-organized lanes can decrease

head-on conflicts but cannot wipe off its influence on the total flow. For  $\rho < 2.0 \text{ m}^{-2}$  the fundamental diagram of the merging flow in the main stream is comparable with that of unidirectional flow. Whereas when  $\rho > 2.0 \text{ m}^{-2}$ , differences appear and it's not easy to draw conclusion with the existing data in these experiments.

A discontinuous trend of the fundamental diagram is observed in case of jams in unidirectional flow in corridor. It has been interpreted in terms of the well-established theory of boundary-induced phase transitions. However, for the difference of the fundamental diagram of merging flow in main stream and branches, only speculations are offered based on the perception behavior of pedestrians.

## 5.2 Outlook

This thesis focus on the fundamental diagrams of different types of pedestrian flows and also the influence of measurement methodologies on them. In view of the time constraint and also experiment limitations for the study, it is hard to solve all the problems concerning the fundamental diagram. At least the following issues should be considered in future works:

As for the measurement methodologies, no marked influences were found for them on the pedestrian fundamental diagram. This disagrees with the result in [58] for 1D movement, in which stop-and-go waves are observed. Thus it is necessary to check whether discrepancies also occur in the case that stop-and-go waves appear in 2D movement.

For the analysis, only the data points belonging to stationary states, which were solely selected manually, were adopted. By observing the time series of density and velocity, the stationary states could be different and could not be fixed for different observer. Different

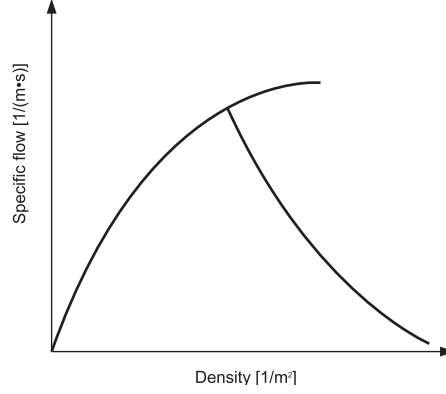


Figure 5.1: The probable fundamental diagram of unidirectional flow in corridor.

selections would influence the stability of the fundamental diagram. Whereas large scatters could hide or blur some important information such as phase transition. Thus, it is necessary to give a reasonable definition for the stationary state and an uniform method to detect the time interval of it precisely.

For all of the experiments used in this study, the specific flow concept worked well. However, the maximum density in this study is only about  $4.0 \text{ m}^{-2}$ , which is smaller than the maximum densities given in literature. It keeps an open question if  $J_s$  is dependent on  $b$  for higher densities.

In unidirectional flow, a discontinuity of the fundamental diagram was observed. However, it was not sure whether this phenomenon arised from the change of the experiment setup. When the density is larger than  $2.0 \text{ m}^{-2}$ , the specific flow in the corridor start to decrease in the fundamental diagram of unidirectional flow. The maximum flow rate obtained from the experiment is  $J = 1.6 \cdot b$  in a corridor, while the flow rate passing through the exit is  $J = 2.1 \cdot b$  when congestion occurs in front of the exit. If  $1.6 (\text{m} \cdot \text{s})^{-1}$  is the

## Conclusion and outlook

---

capacity of the corridor, it does not agree with handbooks. The flow rate passing through a transition is never larger than the capacity of corridor almost in all the handbooks. On the other side, the specific flow in main corridor of T-junction seems increasing persistently for  $\rho > 2.0 \text{ m}^{-2}$ . As a result, it is not clear whether higher specific flow can be obtained in straight corridor at high density. If the second doubt is true and  $1.6 (\text{m} \cdot \text{s})^{-1}$  is not the capacity of straight corridor, then it could be assumed that the fundamental diagram of uni-directional flow should look like the diagram shown in Figure 5.1. For pedestrian flow in a corridor two different phases could exist in certain density intervals. However, this is only an assumption that needs to be confirmed further in the future.

For different types of bidirectional flow in straight corridor, no any difference were found in the fundamental diagram at the density ranges observed in the experiments. However, they are different types of movement after all. The interaction mode among pedestrians are clearly different. How do these interactions affect the pedestrian flow? In which way or state, the effect of these differences could be found. These problems also need to be investigated deeply.

For merging flow in T-junctions, it is found that the fundamental diagrams of the main stream and branches are totally different. The velocities of pedestrians in branches are smaller than that in the main stream nearly at all densities. It seems that the merging behavior of pedestrian streams has something to do with it. And the perception ability of pedestrian is assumed as a reason for this discrepancy. However, it is not sure whether the turning behavior around the corner is another factor for this difference. All of these doubts and assumptions need to be answered and addressed in further studies.

# Bibliography

- [1] Code of design on building fire protection and prevention (GB50016-2006).
- [2] <http://www2.fz-juelich.de/jsc/hermes>.
- [3] <http://www.jxcn.cn/525/2010-12-15/30079@824075.htm>.
- [4] <http://www.stern.de/panorama/jahrestag-loveparade-unglueck-gefangen-im-hexenkessel-1706033.html>.
- [5] **Simulex User Guide, Virtual Environment 5.9.** [www.ies4d.com](http://www.ies4d.com).
- [6] **Human factors of means of egress: History, Current Problems and Implications for the Future**, 2007. 2007 World Safety Conference & Exposition, Boston.
- [7] C. Appert-Rolland, F. Chevoir, P. Gondret, S. Lassarre, J.-P. Lebacque, and M. Schreckenberg, editors. **Traffic and Granular Flow '07**. Springer, Berlin Heidelberg, 2009.
- [8] S. Bandini, S. Manzoni, H. Umeo, and G. Vizzari, editors. **Lecture Notes in Computer Science**. 9th International Conference on Cellular Automata for Research and Industry, ACRI 2010 Ascoli Piceno, Italy, September 2010, Springer-Verlag Berlin Heidelberg, 2010.

## BIBLIOGRAPHY

---

- [9] M. Boltes, A. Seyfried, B. Steffen, and A. Schadschneider. Automatic Extraction of Pedestrian Trajectories from Video Recordings. In **Pedestrian and Evacuation Dynamics 2008**, pages 43–54. Springer-Verlag Berlin Heidelberg, 2010.
- [10] C. Burstedde, K. Klauck, A. Schadschneider, and J. Zittartz. Simulation of pedestrian dynamics using a two-dimensional cellular automaton. **Physica A**, 295:507–525, 2001.
- [11] U. Chattaraj, A. Seyfried, and P. Chakroborty. Comparison of Pedestrian Fundamental Diagram Across Cultures. **Advances in Complex Systems (ACS)**, 12(3):393–405, 2009.
- [12] M. Chraïbi, A. Seyfried, and A. Schadschneider. Generalized centrifugal force model for pedestrian dynamics. **Physical Review E**, 82:046111, 2010.
- [13] E. Christiani, B. Piccoli, and A. Tosin. Macroscopic and microscopic self-organization by nonlocal anisotropic interactions. arXiv:0906.4702.
- [14] M. Davidich and G. Köster. Towards automatic and robust adjustment of human behavioral parameters in a pedestrian stream model to measured data. **Safety Science**, 50(5):1253 – 1260, 2012.
- [15] P. J. DiNenno. **SFPE Handbook of Fire Protection Engineering**. National Fire Protection Association, Quincy MA, third edition, 2002.
- [16] I. J. Farkas and T. Vicsek. Patterns in the collective behavior of humans. In P. L. G. et. al., editor, **Modeling Cooperative Behavior in the Social Sciences**. AIP, New York, 2005. Proceedings of the eighth Granada Lectures 2005, Spain.

## BIBLIOGRAPHY

---

- [17] J. J. Fruin. **Pedestrian Planning and Design**. Elevator World, New York, 1971.
- [18] B. D. Hankin and R. A. Wright. Passenger Flow in Subways. **Operational Research Quarterly**, 9:81–88, 1958.
- [19] D. Helbing, L. Buzna, A. Johansson, and T. Werner. Self-Organized Pedestrian Crowd Dynamics: Experiments, Simulations, and Design Solutions. **Transportation Science**, 39:1–24, 2005.
- [20] D. Helbing, I. Farkas, and T. Vicsek. Simulating dynamical features of escape panic. **Nature**, 407:487–490, 2000.
- [21] D. Helbing, A. Johansson, and H. Z. Al-Abideen. Dynamics of Crowd Disasters: An Empirical Study. **Physical Review E**, 75:046109, 2007.
- [22] D. Helbing, A. Johansson, J. Mathiesen, M. H. Jensen, and A. Hansen. Analytical Approach to Continuous and Intermittent Bottleneck Flows. **Physical Review Letters**, 97:168001, 2006.
- [23] S. P. Hoogendoorn and W. Daamen. Self-organization in walker experiments. In **Proceedings of the 5th Symposium on Traffic and Granular Flow, Delft, The Netherlands**, pages 121–132, 2004.
- [24] S. P. Hoogendoorn and W. Daamen. Pedestrian Behavior at Bottlenecks. **Transportation Science**, 39(2):147–159, 2005.
- [25] M. Jian, S. Weiguo, Z. Jun, L. Siuming, and L. Guangxuan. k-Nearest-Neighbor interaction induced self-organized pedestrian counter flow. **Physica A: Statistical Mechanics and its Applications**, 389(10):2101–2117, 2010.



## BIBLIOGRAPHY

---

- [26] A. Johansson. Constant-net-time headway as a key mechanism behind pedestrian flow dynamics. **Phys. Rev. E**, 80:026120–1 – 026120–5, 2009.
- [27] A. Johansson and D. Helbing. From crowd dynamics to crowd safety: a video-based analysis. **Advances in Complex Systems (ACS)**, 4(4):497–527, 2008.
- [28] A. John, A. Schadschneider, D. Chowdhury, and K. Nishinari. Collective effects in traffic on bi-directional ant trails. **J. Theor. Biol.**, 231:279, 2004.
- [29] B. S. Kerner. **The Physics Of Traffic: Empirical Freeway Pattern Features, Engineering Applications, and Theory**. Springer, 1 edition, 2004.
- [30] A. Kirchner and A. Schadschneider. Simulation of evacuation processes using a bionics-inspired cellular automaton model for pedestrian dynamics. **Physica A**, 312:260–276, 2002.
- [31] W. Klingsch, C. Rogsch, A. Schadschneider, and M. Schreckenberg, editors. **Pedestrian and Evacuation Dynamics 2008**. Springer-Verlag Berlin Heidelberg, 2010.
- [32] R. L. Knoblauch, M. T. P. Ietrucha, and M. Nitzburg. Field studies of pedestrian walking speed and start-up time. **Transportation Research Record**, 1538:27–38, 1996.
- [33] A. B. Kolomeisky, G. M. Schütz, E. B. Kolomeisky, and J. P. Straley. Phase diagram of one-dimensional driven lattice gases with open boundaries. **J. Phys. A: Math. Gen.**, 31:6911–6919, 1998.
- [34] T. Kretz, A. Grünebohm, M. Kaufman, F. Mazur, and M. Schreckenberg. Experimental study of pedestrian counterflow in a corridor. **J. Stat. Mech.**, 10:P10001, 2006.

## BIBLIOGRAPHY

---

- [35] T. Kretz, A. Grünebohm, and M. Schreckenberg. Experimental study of pedestrian flow through a bottleneck. **J. Stat. Mech.**, 10:P10014, 2006.
- [36] J. Krug. Boundary-Induced Phase Transition in Driven Diffusive Systems. **Phys. Rev. Lett.**, 67(14):1882–1885, sep 1991.
- [37] W. H. K. Lam, J. Y. S. Lee, K. S. Chan, and P. K. Goh. A generalised function for modeling bi-directional flow effects on indoor walkways in Hong Kong. **Transportation Research Part A: Policy and Practice**, 37:789–810, 2003.
- [38] W. H. K. Lam, J. Y. S. Lee, and C. Y. Cheung. A study of the bi-directional pedestrian flow characteristics at Hong Kong signalized crosswalk facilities. **Transportation**, 29:169–192, 2002.
- [39] W. Leutzbach. **Introduction to the Theory of Traffic Flow**. Springer, 1988.
- [40] X. Liu, W. Song, and J. Zhang. Extraction and quantitative analysis of microscopic evacuation characteristics based on digital image processing. **Physica A: Statistical Mechanics and its Applications**, 388(13):2717–2726, 2009.
- [41] S. J. Melinek and S. Booth. An Analysis of Evacuation Times and the Movement of Crowds in Buildings. report BRE Current Paper CP 96/75 FRS, Building Research Establishment, 1975.
- [42] M. Mori and H. Tsukaguchi. A new method for evaluation of level of service in pedestrian facilities. **Transp. Res.**, 21A(3):223–234, 1987.

## BIBLIOGRAPHY

---

- [43] M. Moussaïd, D. Helbing, S. Garnier, A. Johansson, M. Combe, and G. Theraulaz. Experimental study of the behavioural mechanisms underlying self-organization in human crowds. *Proc. R. Soc. B*, 276(1668):2755–2762, 2009.
- [44] M. Muramatsu and T. Nagatani. Jamming transition in two-dimensional pedestrian traffic. *Physica A*, 275:281–291, 2000.
- [45] T. Nagatani. Dynamical transition in merging pedestrian flow without bottleneck. *Physica A*, 307:505–515, 2002.
- [46] F. D. Navin and R. J. Wheeler. Pedestrian flow characteristics. *Traffic Engineering*, 39:31–36, 1969.
- [47] S. Okazaki and S. Matsushita. A study of simulation model for pedestrian movement with evacuation and queuing. *Engineering for Crowd Safety: Proceedings of the International Conference on Engineering for Crowd Safety*. London, UK, Elsevier Science Publishing Co Inc., 1993.
- [48] S. Older. Movement of Pedestrians on Footways in Shopping Streets. *Traffic Engineering and Control*, 10:160–163, 1968.
- [49] V. Popkov and G. Schütz. Steady-state selection in driven diffusive systems with open boundaries. *Europhys. Lett.*, 48(3):257–263, 1999.
- [50] V. M. Predtechenskii and A. I. Milinskii. *Planning for Foot Traffic Flow in Buildings*. Amerind Publishing, New Dehli, 1978. Translation of: Proekttirovanie Zh-danii s Uchetom Organizatsii Dvizheniya Lyuddskikh Potokov, Stroiizdat Publishers, Moscow, 1969.

## BIBLIOGRAPHY

---

- [51] B. Pushkarev and J. M. Zupan. Capacity of Walkways. **Transportation Research Record**, 538:1–15, 1975.
- [52] M. Rex and H. Löwen. Lane formation in oppositely charged colloids driven by an electric field: Chaining and two-dimensional crystallization. **Phys. Rev. E**, 75:051402, 2007.
- [53] C. Rogsch and W. Klingsch. Risk Analysis with Evacuation Software - How Should We Interpret Calculated Results? vfdb International Fire Protection Symposium 2010, 2010.
- [54] A. Schadschneider, D. Chowdhury, and K. Nishinari. **Stochastic Transport in Complex Systems - From Molecules to Vehicles**. Elsevier, 2010.
- [55] A. Schadschneider, W. Klingsch, H. Kluepfel, T. Kretz, C. Rogsch, and A. Seyfried. **Encyclopedia of Complexity and System Science**, volume 5, chapter Evacuation Dynamics: Empirical Results, Modeling and Applications, pages 3142–3176. Springer, Berlin, Heidelberg, 2009.
- [56] A. Schadschneider, H. Klüpfel, T. Kretz, and A. Rogsch, C.and Seyfried. Fundamentals of Pedestrian and Evacuation Dynamics. In A. Bazzan and F. Klügl, editors, **Multi-Agent Systems for Traffic and Transportation Engineering**, chapter 6, pages 124–154. IGI Global, Hershey, Pennsylvania, USA, 2009.
- [57] A. Schadschneider and A. Seyfried. Empirical Results for Pedestrian Dynamics and their Implications for Cellular Automata Models. **Pedestrian Behavior: Data Collection and Applications**, chapter 2, pages 27–43. Emerald Group Publishing Limited, 1 edition, 2009.

## BIBLIOGRAPHY

---

- [58] A. Seyfried, M. Boltes, J. Kähler, W. Klingsch, A. Portz, T. Rupperecht, A. Schadschneider, B. Steffen, and A. Winkens. Enhanced empirical data for the fundamental diagram and the flow through bottlenecks. **Pedestrian and Evacuation Dynamics 2008**, pages 145–156. Springer-Verlag Berlin Heidelberg, 2010.
- [59] A. Seyfried, O. Passon, B. Steffen, M. Boltes, T. Rupperecht, and W. Klingsch. New insights into pedestrian flow through bottlenecks. **Transportation Science**, 43(3):395–406, 2009.
- [60] W. Song, X. Xu, B.-H. Wang, and S. Ni. Simulation of evacuation processes using a multi-grid model for pedestrian dynamics. **Physica A**, 363:492–500, 2006.
- [61] B. Steffen and A. Seyfried. Methods for measuring pedestrian density, flow, speed and direction with minimal scatter. **Physica A**, 389(9):1902–1910, 2010.
- [62] P. Stucki. Obstacles in Pedestrian Simulations. Master’s thesis, ETH Zürich, sep 2003.
- [63] Y. Tajima and T. Nagatani. Clogging transition of pedestrian flow in T-shaped channel. **Physica A**, 303:239–250, 2002.
- [64] Y. Tajima, K. Takimoto, and T. Nagatani. Scaling of pedestrian channel flow with a bottleneck. **Physica A**, 294:257–268, 2001.
- [65] R. M. Tavares. Prescriptive codes vs. performance-based codes: which one is the best fire safety code for the brazilian context. **Safety Science monitor**, 12, 2008.
- [66] M. Thomas. Personenströme auf tribünen - vergleichende untersuchung mit makroskopischen und mikroskopischen modellen. Master’s thesis, Bergische Universität Wuppertal, 2011.

## BIBLIOGRAPHY

---

- [67] M. R. Virkler and S. Elayadath. Pedestrian Speed-Flow-Density Relationships. **Transportation Research Record**, 1438:51–58, 1994.
- [68] G. M. Voronoi. Nouvelles applications des paramètres continus à la théorie des formes quadratiques. **Journal für die reine und angewandte Mathematik**, 133:198–287, 1908.
- [69] U. Weidmann. Transporttechnik der Fussgänger. Technical Report Schriftenreihe des IVT Nr. 90, Institut für Verkehrsplanung, Transporttechnik, Strassen- und Eisenbahnbau, ETH Zürich, ETH Zürich, 1993. Zweite, ergänzte Auflage.
- [70] K. Yamori. Going with the Flow: Micro-Macro Dynamics in the Macrobehavioral Patterns of Pedestrian Crowds. **Psychological Review**, 105(3):530–557, 1998.
- [71] S. B. Young. Evaluation of Pedestrian Walking Speeds in Airport Terminals. **Transportation Research Record**, 1674:20–26, 1999.
- [72] Q. Zhang, G. Zhao, and J. Liu. Performance-Based Design for Large Crowd Venue Control Using a Multi-Agent Model. **Tsinghua Science & Technology**, 14(3):352–359, 2009.

## Publications during PhD study

- **J. Zhang**, W. Klingsch, A. Schadschneider, and A. Seyfried, "Ordering in bidirectional pedestrian flows and its influence on the fundamental diagram", Journal of Statistical Mechanics: Theory and Experiment, vol. P02002, 2012
- **J. Zhang**, W. Klingsch, A. Schadschneider, and A. Seyfried, "Transitions in pedestrian fundamental diagrams of straight corridors and T-junctions", Journal of Statistical Mechanics: Theory and Experiment, vol. P06004, 2011
- **J. Zhang**, W. Klingsch, T. Rupprecht, A. Schadschneider, A. Seyfried, "Empirical study of turning and merging of pedestrians streams in T-junction", Fourth International Symposium on Agent-Based Modeling and Simulation, 2012, Vienna, Austria
- **J. Zhang**, W. Klingsch, A. Schadschneider, A. Seyfried, "Experimental study of pedestrian flow through a T-junction", TGF'11, 28 Sep.-1th Oct. 2011, Moscow, Russia
- M. Boltes, **J. Zhang**, A. Seyfried, B. Steffen, "T-Junction: Experiments, Trajectory Collection, and Analysis", 1st IEEE Workshop on Modeling, Simulation and Visual Analysis of Large Crowds, 7th Nov. 2011, Barcelona, Spain
- **J. Zhang**, W. Klingsch, A. Seyfried, "High precision analysis of unidirectional pedestrian flow within the Hermes Project". The Fifth Performance-based Fire Protection and Fire Protection Engineering Seminars. 6th-9th. Dec. 2010, Guangzhou, China

# Curriculum Vitae

## Personal information

**Name:** Jun Zhang  
**Gender:** Male  
**Date of Birth:** 14. July 1984  
**Place of Birth:** Gansu, China

## Education

<b>1990-1995</b>	Baowen primary school, Gansu, China
<b>1995-1998</b>	Mapaoquan Middle school, Gansu, China
<b>1998-2002</b>	No. 2 High School in Tianshui City
<b>2002-2006</b>	B.E, Safety Engineering  Xi'an University of Architecture and Technology, Shaanxi, China  Thesis: Risk analysis and fire safety design of a gas station  Supervisor: Prof. Xuzhang Zhu
<b>2006-2009</b>	M.E, Safety Technology and Engineering  University of Science and Technology of China, Anhui, China  Thesis: Evacuation dynamics simulation using discrete models with uncertainty factors  Supervisors: Prof. Weiguo Song and Prof. Jianjun Zhou
<b>2009-</b>	PhD candidate, Civil Engineering  University of Wuppertal, Wuppertal, Germany





1. **Three-dimensional modelling of soil-plant interactions: Consistent coupling of soil and plant root systems**  
by T. Schröder (2009), VIII, 72 pages  
ISBN: 978-3-89336-576-0  
URN: urn:nbn:de:0001-00505
2. **Large-Scale Simulations of Error-Prone Quantum Computation Devices**  
by D. B. Trieu (2009), VI, 173 pages  
ISBN: 978-3-89336-601-9  
URN: urn:nbn:de:0001-00552
3. **NIC Symposium 2010**  
Proceedings, 24 – 25 February 2010 | Jülich, Germany  
edited by G. Münster, D. Wolf, M. Kremer (2010), V, 395 pages  
ISBN: 978-3-89336-606-4  
URN: urn:nbn:de:0001-2010020108
4. **Timestamp Synchronization of Concurrent Events**  
by D. Becker (2010), XVIII, 116 pages  
ISBN: 978-3-89336-625-5  
URN: urn:nbn:de:0001-2010051916
5. **UNICORE Summit 2010**  
Proceedings, 18 – 19 May 2010 | Jülich, Germany  
edited by A. Streit, M. Romberg, D. Mallmann (2010), iv, 123 pages  
ISBN: 978-3-89336-661-3  
URN: urn:nbn:de:0001-2010082304
6. **Fast Methods for Long-Range Interactions in Complex Systems**  
Lecture Notes, Summer School, 6 – 10 September 2010, Jülich, Germany  
edited by P. Gibbon, T. Lippert, G. Sutmann (2011), ii, 167 pages  
ISBN: 978-3-89336-714-6  
URN: urn:nbn:de:0001-2011051907
7. **Generalized Algebraic Kernels and Multipole Expansions for Massively Parallel Vortex Particle Methods**  
by R. Speck (2011), iv, 125 pages  
ISBN: 978-3-89336-733-7  
URN: urn:nbn:de:0001-2011083003
8. **From Computational Biophysics to Systems Biology (CBSB11)**  
Proceedings, 20 - 22 July 2011 | Jülich, Germany  
edited by P. Carloni, U. H. E. Hansmann, T. Lippert, J. H. Meinke, S. Mohanty, W. Nadler, O. Zimmermann (2011), v, 255 pages  
ISBN: 978-3-89336-748-1  
URN: urn:nbn:de:0001-2011112819

9.    **UNICORE Summit 2011**  
Proceedings, 7 - 8 July 2011 | Toruń, Poland  
edited by M. Romberg, P. Bała, R. Müller-Pfefferkorn, D. Mallmann (2011), iv,  
150 pages  
ISBN: 978-3-89336-750-4  
URN: urn:nbn:de:0001-2011120103
  
10.   **Hierarchical Methods for Dynamics in Complex Molecular Systems**  
Lecture Notes, IAS Winter School, 5 – 9 March 2012, Jülich, Germany  
edited by J. Grotendorst, G. Sutmann, G. Gompfer, D. Marx (2012), vi,  
540 pages  
ISBN: 978-3-89336-768-9  
URN: urn:nbn:de:0001-2012020208
  
11.   **Periodic Boundary Conditions and the Error-Controlled Fast Multipole  
Method**  
by I. Kabadshow (2012), v, 126 pages  
ISBN: 978-3-89336-770-2  
URN: urn:nbn:de:0001-2012020810
  
12.   **Capturing Parallel Performance Dynamics**  
by Z. P. Szebenyi (2012), xxi, 192 pages  
ISBN: 978-3-89336-798-6  
URN: urn:nbn:de:0001-2012062204
  
13.   **Validated force-based modeling of pedestrian dynamics**  
by M. Chraïbi (2012), xiv, 112 pages  
ISBN: 978-3-89336-799-3  
URN: urn:nbn:de:0001-2012062608
  
14.   **Pedestrian fundamental diagrams: Comparative analysis of experiments  
in different geometries**  
by J. Zhang (2012), xiii, 103 pages  
ISBN: 978-3-89336-825-9  
URN: urn:nbn:de:0001-2012102405



This dissertation mainly analyzes the fundamental diagram describing the relation between crowd density, velocity and flow based on series of well-controlled laboratory experiments. The commonly used fundamental diagrams in handbooks are reviewed especially for uni- and bidirectional pedestrian streams. The differences and influence of them on facility designs are compared.

Four different measurement methods are taken to calculate the crowd density, velocity and specific flow. Their influences on the fundamental diagram are tested with the data obtained from the experiment of unidirectional flow.

Pedestrian experiments of uni-, bidirectional and merging flow are analyzed based on the Voronoi method for its high precision. The topographical information for density, velocity and specific flow, from which the boundary effect are observed, are extracted. The specific flow concept is applicable to all types of flows in the density ranges observed in the experiments. Surprisingly, no difference is found for the fundamental diagrams of bidirectional flow with different modes of ordering.

A sharp distinction is observed between the fundamental diagrams of uni- and bidirectional flow. For the merging flow in T-junction, the fundamental diagrams measured in front of and behind the merging show also significant differences.